2014

Development and modelling of an advanced solar-assisted liquid desiccant dehumidification air-conditioning system

Aqeel Kareem Mohaisen
University of Wollongong

UNIVERSITY OF WOLLONGONG

Development and modelling of an advanced solar-assisted liquid desiccant dehumidification air-conditioning system

By

Aqeel Kareem Mohaisen

This thesis is presented as part of the requirements for the award of the Degree of

Master of Engineering (Mechanical)

From

University of Wollongong

Sustainable Buildings Research Centre (SBRC)

Faculty of Engineering and Information Sciences

September 2014

Abstract

Advanced liquid desiccant air-conditioning systems driven by solar energy may offer alternative answers for better indoor thermal comfort and enhanced energy efficiency in the built environment.

This thesis presents the development, modelling and simulation of an advanced solar-assisted liquid desiccant dehumidification air-conditioning system for energy efficiency and sustainability. The proposed system includes a counter-flow packed bed absorber, a counter-flow packed bed regenerator and a solar water heating system which consists of an array of flat plate solar collectors integrated with a thermal storage tank and an electric heater. It is designed to benefit from the low cost evaporative cooling technique in cooling the dehumidified processed air and the strong desiccant solution. Heat exchangers are used to improve the thermal performance of the system or prevent the direct contact between the liquid desiccant and water.

Various aspects such as proper system design, selection of appropriate types of dehumidifiers and liquid desiccants, and modelling of the different system components are addressed in this study. Lithium chloride solution is utilised as the working fluid owing to its excellent dehumidification performance and low regeneration energy requirements. A simplified approach has been developed to predict the size and the pressure drop of the absorber and regenerator at the design stage. A parametric study has been carried out to investigate the effects of various design and operational variables on the overall system performance, especially on the performance of the absorber and regenerator.

A thorough simulation platform for the proposed system has been developed using the Matlab Simulink integrating the models of the individual components developed and selected. The results revealed that enormous free solar energy for Sydney location could be used to reduce the electricity consumption in re-concentrating the liquid desiccant. The simulation results indicated that the proposed system has an average daily thermal coefficient of performance of 0.5-0.55. It was also shown that 73.4% of thermal energy required by the system for thermal regeneration was provided by the solar collectors while the rest was matched by the auxiliary electric heater. It is worthwhile to mention that, at the mid sunny days, the system is expected to consume less energy by the auxiliary heater when less cooling is required.

Acknowledgements

At first, praise be to God, the Compassionate, the Merciful for everything.

I owe my deepest gratitude and appreciation to my supervisors Dr Zhenjun Ma, and Prof Paul Cooper for their valuable supervision, kind assistance, guidance and encouragement throughout the journey of this research.

I would like to express special thanks and dedicate this work to my parents for their limitless love, support, kindness and forbearance during this study.

Last but not least, I would like to convey special thanks to all of my brothers, sisters and friends who performed assistance wherever needed.

Aqeel Kareem Mohaisen

Table of contents

List of figures

List of tables

List of publications from this study

Mohaisen AK, Ma Z and Copper P (2013), 'Modelling and investigation of a solar-assisted liquid desiccant dehumidification air-conditioning system', 12th International Conference on Sustainable Energy technologies (SET-2013) 26-29th August, 2013, Hong Kong.

Mohaisen AK and Ma Z (2014), 'Development and modelling of a solar assisted liquid desiccant dehumidification (SA-LDD) air-conditioning system', *Building Simulation, Accepted*.

Nomenclature

List of symbols

Δp	pressure drop (kPa)
$a_{0\text{-}2}$	coefficients used in Equation (3.5)
$a'_{1\text{-}6}$	coefficients used in Equation (3.23)
a_t	dry specific surface area of packings (m^2/m^3)
a_w	wetted specific surface area of packings (m^2/m^3)
A	area (m^2)
A_1	coefficient used in Equation (3.1)
A_2	coefficient used in Equation (3.6)
A_3	coefficient used in Equation (3.12)
A_c	solar collector area (m^2)
A_e	elevation (km)
$b_{0\text{-}2}$	coefficients used in Equation (3.5)
B_1	coefficient used in Equation (3.1)
B_2	coefficient used in Equation (3.6)
B_3	coefficient used in Equation (3.12)
B'_{0-5}	coefficients used in Equation (3.14)
$c_{0\text{-}2}$	coefficients used in Equation (3.5)
c_p	specific heat capacity (J/kg.K)
C	heat capacity rate (W/K)
C_1	coefficient used in Equation (3.1)
C_2	coefficient used in Equation (3.6)
C_3	coefficient used in Equation (3.12) or constant in Equation (4.21)
C_4	constant used in Equation (4.21)
C_{af}	fictitious heat capacity rate of air (W/K)
C_r	heat capacity rate ratio
COP	coefficient of performance
CP	capacity parameter
D	diameter of the absorber or regenerator (m)
D_3	coefficient used in Equation (3.12)
D_f	diffusion coefficient (m/s)
D_h	hydraulic diameter (m)

d_p particle diameter (m)

e_a actual air vapour pressure (kPa)

e_{sa} air saturation vapour pressure (kPa)

e_{sw} air vapour pressure at the wet-bulb temperature (kPa)

E equation of time (min)

F_f flooding factor (%)

F_{LG} flow parameter

F_p packing factor (m^{-1})

F_{pd} dry packing factor (m^{-1})

g acceleration of gravity (9.81 m/s^2)

G air specific flow rate ($kg/m^2.s$)

G_{bn} normal beam radiation (W/m^2)

G_f gas loading factor ($kg/m^2.s$)

G_{inc} incident beam radiation (W/m^2)

G_{on} normal extraterrestrial radiation (W/m^2)

h enthalpy (kJ/kg.K)

H_2O water

HOG height of transfer units (m)

I_b direct beam irradiance on a horizontal surface (W/m^2)

I_d diffuse beam irradiance (W/m^2)

k constant value used in Equation (3.37)

k' coefficient used in Equation (3.72)

K correlation factor used in Equation (3.66)

K_{OG} gas mass transfer coefficient ($\frac{g.mol}{hr.m^2.Pa}$)

l characteristic length (m)

L liquid specific flow rate ($kg/m^2.s$)

L_f liquid loading factor ($kg/m^2.s$)

$LiCl$ lithium chloride

L_{loc} local longitude (degree)

L_{st} local standard longitude (degree)

m mass flow rate (kg/s) or coefficient

m_{cond} water condensation rate (kg/s)

m_{evap} water evaporation rate (kg/s)

M_a air flow rate of the cooling tower (kg/s)

M_w water flow rate of the cooling tower (kg/s)

n coefficient or day of the year or nominal

N_p number of packings

NTU number of transfer units

p vapour pressure (kPa)

p_w water vapour pressure (kPa)

P power (W)

q heat transfer rate (W)

Q heating load (W)

Q_G gas volumetric flow rate (m^3/s)

Q_p quantity of packings per m^3

r_o factor used in Equation (3.68)

r_1 factor used in Equation (3.69)

r_k factor used in Equation (3.70)

Re Reynolds number

RH relative humidity (%)

Sc Schmidt number

SDT solar time (min)

Sh Sherwood number

ST standard time

t temperature (°C)

T absolute temperature (K)

U superficial velocity (m/s)

UA overall heat transfer coefficient (W/K)

$UA_{fic,dry,n}$ fictitious heat transfer coefficient (W/K)

V volume (m^3)

w air moisture-content (kg/kg) or hour angle (degree)

w_t weight of the dry column (kg)

x variable

X solution concentration (%)

y variable

y_1 inlet mole fraction

y_2 outlet mole fraction

y_{eq} equilibrium mole fraction

Z packing height (m)

Greek letters

β surface tilt angle (degree)

γ surface tension (kg/s^2)

γ_{H2O} surface tension of water (kg/s^2)

δ declination angle (degree)

ε effectiveness (%) or void fraction (%)

η_{1-4} coefficients used in Equation (3.10)

η_c solar collector efficiency

θ incident angle (degree)

θ_z zenith angle of the sun (degree)

μ dynamic viscosity (Pa.s)

π vapour pressure difference (unit less)

ρ density (kg/m^3)

ρ_{H2O} density of water (kg/m^3)

τ coefficient used in Equation (3.23)

φ latitude angle (degree)

ω speed (rad/s)

Subscripts

a air

atm atmospheric

aux,h auxiliary heater

c critical or cold

d dehumidification

eq equilibrium

ex exit

f flooding

G gas

h heat or hot

i	inlet
L	liquid
lam	laminar
m	mean
max	maximum
mf	minimum fluidisation
min	minimum
o	outlet
opt	operation
r	ratio or refrigerant
reg	regeneration
s	solution
su	supply
sol	solar
tank	thermal storage tank
th	thermal
turb	turbulent
w	water
wb	wet-bulb

1 Introduction

1.1 Background

The continuously growing demand on energy production, in conjunction with global warming due to greenhouse-gas emissions from the use of fossil fuels, has led to the rapid development of environmentally friendly and energy-efficient air-conditioning systems for building heating and cooling applications (Ma and Wang 2009; Seghouani and Galanis 2009; Thomas and Andre 2012). It has become crucial to find alternatives that address the needs of reducing the use of fossil-fuels, and cut down the increased carbon emissions when generating electricity owing to global warming deterioration in recent years (Fong *et al.* 2010). Recent developments in this area have heightened the tremendous amount of power consumption resulting from the widespread use of the conventional air-conditioning systems, and motivated researchers to develop new generations of heating, ventilation and air-conditioning (HVAC) systems to replace conventional air-conditioning systems significantly to reduce CO_2 emission footprint.

Fig. 1.1 shows the projected total energy consumption in the Australian residential sector in 2020 (AGDI 2008). It is clearly shown that an enormous amount of electricity will be required for space heating (15.6 PJ) and space cooling (17.7 PJ), respectively.

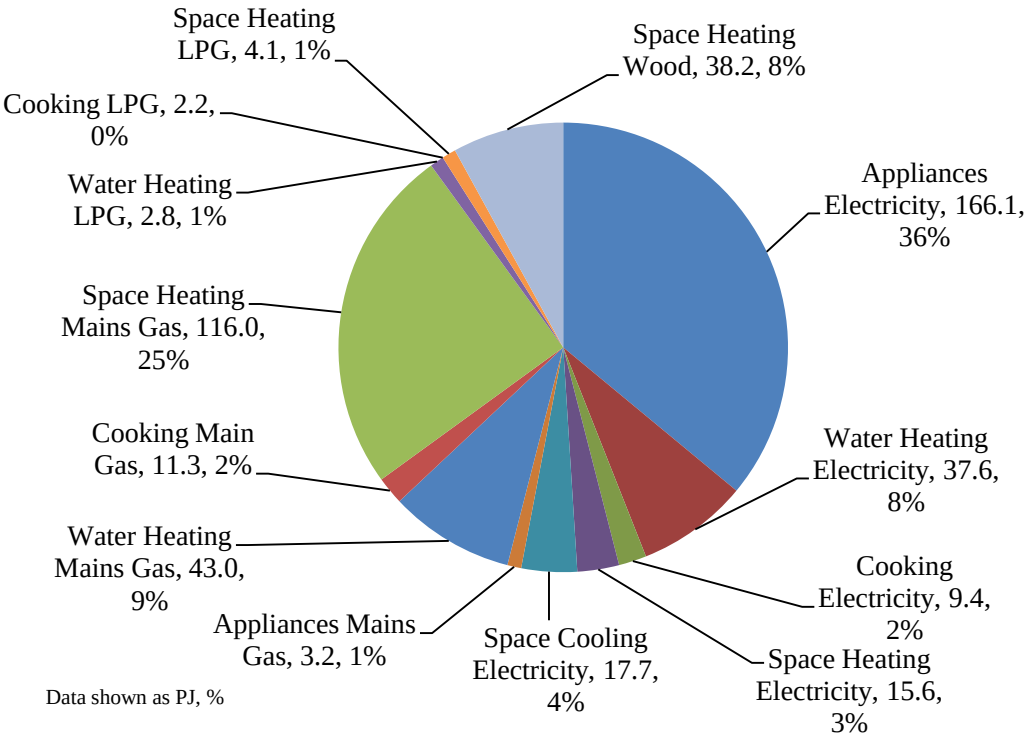

Fig. 1.1 Projected energy consumption in the Australian residential sector in 2020 (Source: AGDI 2008).

Desiccant dehumidification systems have been developed based on a process called sorption. Sorption is the process of attracting or holding one substance by another, and sorbents are materials that have the ability to attract liquids or gases. One category of sorbents is desiccant, which has a special affinity for water (ASHRAE 2009). Desiccant materials are classified as either adsorbents or absorbents when linked to the adsorption and absorption processes. The difference is that the absorption process depends on the chemical properties of the material while the adsorption process is dependent on the physical properties of the material. Most absorbents are liquids, whereas adsorbents are solids. By incorporating the unique characteristics of desiccant materials, some researchers have started to develop alternatives for conventional air-conditioning systems. Solar-assisted desiccant air-conditioning systems might be one of the possible solutions in reducing large amounts of greenhouse-gas emissions, providing energy efficient systems and

enhanced indoor air quality. One of the most important benefits offered by desiccant air-conditioning systems is that the dehumidification process occurs separately from the cooling process. This gives more flexibility in controlling the humidity level in the conditioned space, and hence provides better indoor thermal comfort. Compared with solid desiccant systems, liquid desiccant systems offer many advantages such as the low regeneration temperature to re-concentrate the liquid desiccant after attracting the moisture from the processed air (Kessling *et al.* 1998), the flexibility in designing the liquid desiccant system due to the ability of pumping the liquid desiccant between the different units in the system (Pesaran *et al.* 1992), and the low pressure drop. They also can work as a steriliser of the processed air (Abdul-Wahab *et al.* 2004).

Liquid desiccant dehumidification as one of advanced energy technologies has been receiving increasing attention and wide concern due to its high efficient utilisation of low grade energy, effectiveness in dehumidification, low energy consumption, low or no effect on the ozone layer, low dehumidification cost and improved indoor air equality (Yin *et al.* 2014). Liquid desiccant technologies are starting to shift how people think about cooling and dehumidification (Farese 2012).

Fig. 1.2 shows an example of a liquid desiccant dehumidification system which mainly consists of an absorber, a heat exchanger, a desiccant heater, a regenerator, a desiccant cooler and fluid pumps. In the liquid desiccant dehumidification systems, the processed air passes through an absorber to reduce the humidity level. In the absorber, an absorption process occurs such that the air is in contact with the liquid desiccant directly. Due to the pressure difference, the moisture in the processed air transfers to the liquid desiccant. The liquid desiccant then passes through the regenerator to release the absorbed moisture to a scavenging air stream. To ensure

the continual absorption and regeneration processes, a variety of techniques can be used to cool and heat the liquid desiccant before entering the absorber and regenerator, respectively.

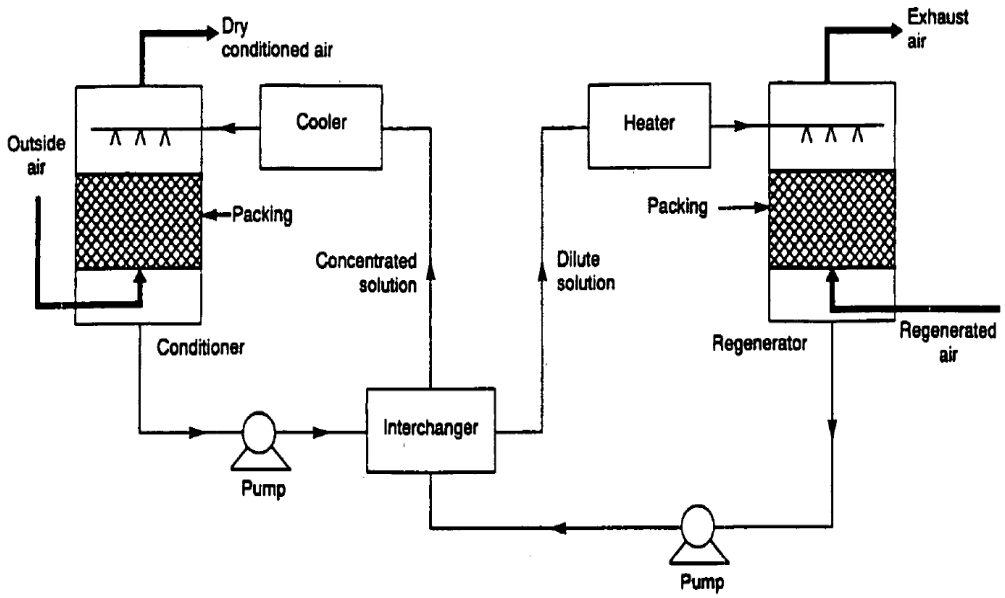

Fig. 1.2 Illustration of a typical liquid desiccant dehumidification system (Pesaran *et al.* 1992).

Although different liquid desiccant dehumidification systems have been proposed, and various modelling techniques have been used to analyse the heat and mass transfer performance of absorbers and regenerators, few studies have used whole system simulation systematically to evaluate and analyse the performance of liquid desiccant dehumidification air-conditioning systems. As liquid desiccant systems are highly nonlinear and interactive, whole system simulation might be essential to help fully understand the system-level and subsystem-level interactions and characteristics. Appropriate sizing of key components such as the absorber and regenerator in the liquid desiccant air-conditioning system is quite important at the design stage.

1.2 Aim and objectives

This research aims to develop an advanced solar-assisted liquid desiccant dehumidification air-conditioning system, and use whole system simulation to investigate system interactions and overall performance. The aim of this research will be achieved through addressing the following objectives:

- Configuration design of a solar-assisted desiccant dehumidification air-conditioning system.
- Development and selection of appropriate components models for system simulation.
- Sizing of system components by taking into account the interactions among different subsystems.
- Identification of key variables that will influence system performance.
- Systematic evaluation of the performance of the proposed solar-assisted liquid desiccant air-conditioning system under different operational conditions.

1.3 Structure of the thesis

The thesis has been organised in the following way. Chapter 1, as previously seen, presents the background and introduction to the liquid desiccant systems and outlines the main objectives of this study. Chapter 2 provides a literature review on the liquid desiccant air-conditioning systems, and explores the research problems and the contributions of this thesis. Chapter 3 presents the development and modelling of the proposed solar-assisted liquid desiccant dehumidification air-conditioning system. The key components models are validated by using experimental data published in previous studies. Chapter 4 describes a simplified approach developed for the

absorber and regenerator to predict the diameter, height and pressure drop of both components. Chapter 5 presents a parametric study to examine the effects of the key operational and design parameters of the absorber and regenerator on the system performance. In Chapter 6, the performance of the proposed system is tested and evaluated on the basis of a full-scale simulation platform developed, and the test results are reported. Chapter 7 summarises the work reported in this thesis, and gives some recommendations for further research in this field.

2 Literature review

2.1 Introduction

The design of the ventilation systems has thrived and been used in many countries since the late 1880s. In parallel, by 1880s, refrigeration machines were available for industrial use, and mainly for meat freezing and ice making until the early 1990s, such that there was the first invention for building cooling comfort, which was called air-conditioning. Since then, air-conditioning systems have undergone many enhancements until they have reached its current state (McDowall 2006). Although air-conditioning systems have been developed to provide high levels of thermal comfort, serious problems have thrived due to the widespread of these systems. This chapter will highlight such problems, possible solutions, and since this study mainly focuses on the development and modelling of a novel solar-assisted liquid desiccant dehumidification air-conditioning system, a review of the research and development as well as application of desiccant air-conditioning systems, in particular, liquid desiccant air-conditioning systems, is essential to assist in identifying research gaps in this field and avoiding major pitfalls. Fig. 2.1 outlines the structure of the literature review.

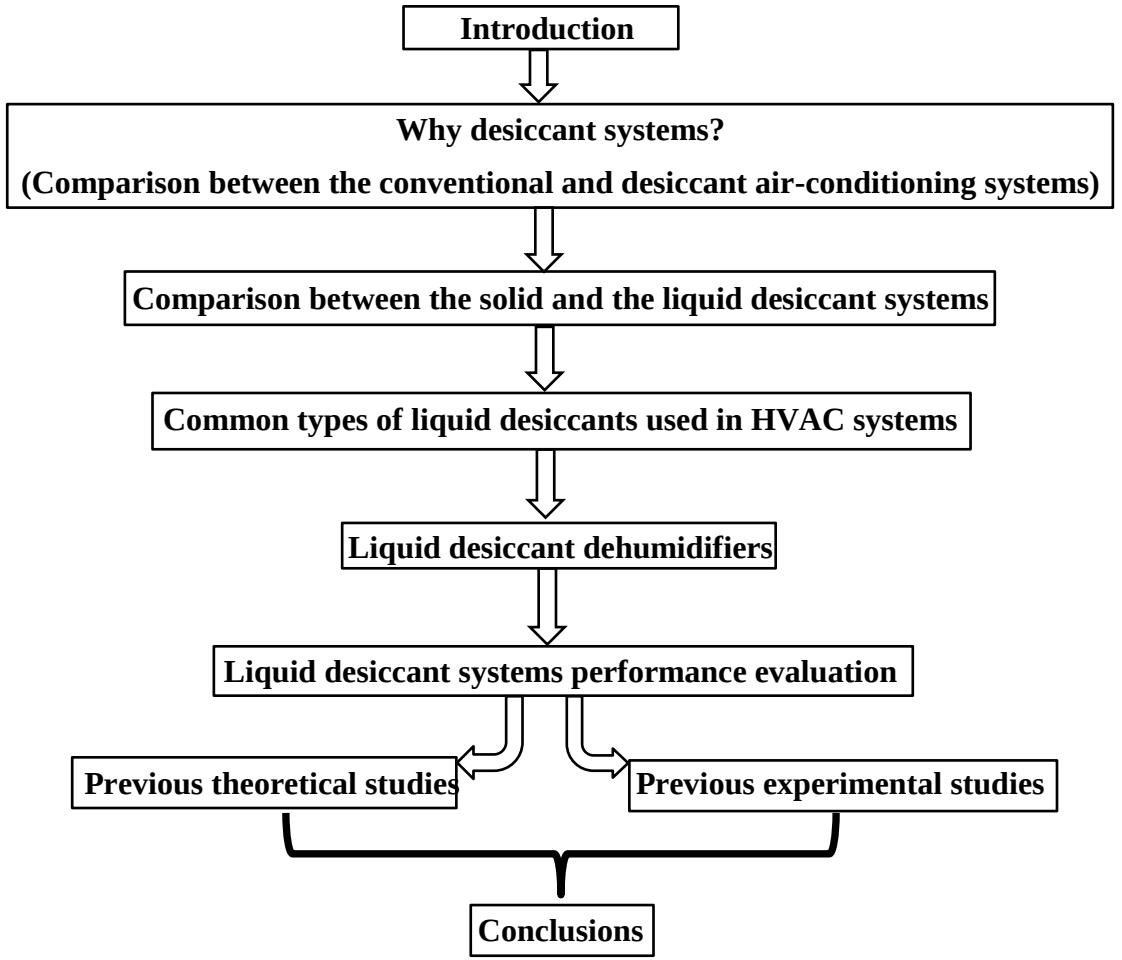

Fig. 2.1 Structure of the literature review.

2.2 Comparison between the desiccant and conventional vapour compression air-conditioning systems

Desiccant air-conditioning systems offer many advantages over vapour compression air-conditioning systems such as eradicating or reducing the depleting of the ozone layer, providing better indoor air quality, and consuming less electricity (Davanagere *et al.* 1999). Desiccant air-conditioning systems not only have the ability to attract the humidity, but can also filter the processed air from airborne pollutants, organic vapours and microbiological pollutants (Buffalo Testing Laboratory 1974; Battle 1991 cited in ASHRAE 2009). Desiccants are particularly useful when the sensible load is smaller than the latent load, and the regeneration cost of the desiccant is lower than dehumidifying the air by cooling below the dew-point temperature and then reheat it, as well as when the moisture in the space is required to be controlled at a certain level by cooling the air to a subfreezing dew-point (ASHRAE 2009).

The main aim of using desiccant air-conditioning systems is to control the humidity level inside the conditioned space to achieve a certain level of thermal comfort to suit occupants with minimised energy consumption. In addition, they do not impact the occupants' health negatively or cause any damage to the environment (i.e. maintaining healthy and environmentally friendly air-conditioning system). Fig. 2.2 shows the health and environmental problems that can be caused by humid air, and the optimum thermal comfort zone that should be targeted. It can be seen that, it is necessary to control the relative humidity (RH) of a conditioned space in the range of 30%-60% for thermal comfort requirement. Otherwise, serious problems can arise, causing different types of health implications such as rhinitis and flu (Arundel *et al.* 1986; Baughman and Arens 1996) and damaging to the environment.

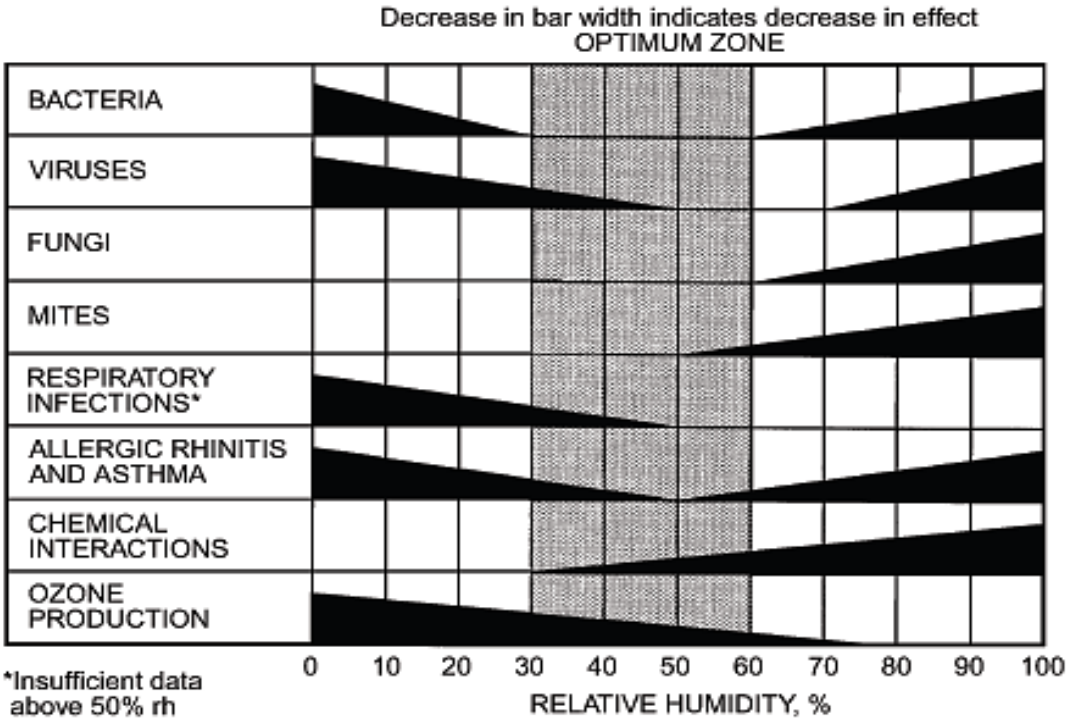

Fig. 2.2 Unhealthy and optimum relative humidity for thermal comfort (Sterling *et al.* 1985 cited in ASHRAE 2008).

2.3 Comparison between the liquid and the solid desiccant systems

Many advantages can be achieved by using liquid desiccant systems as follows.

- The different components of liquid desiccant systems can be installed in different positions owing to the possibility of pumping the liquid desiccant between each other, and hence, offering flexibility in the system design (Pesaran *et al.* 1992).
- Efficient dehumidification can be achieved with a low regeneration temperature of about 50-80°C, while 80-100°C regeneration temperature is required to regenerate solid desiccants for sufficient dehumidification (Kessling *et al.* 1998).
- Liquid desiccant systems offer low pressure drop, adaptability and flexibility in pumping the diluted solution to a storage unit as well as sterilising the processed air (Abdul-Wahab *et al.* 2004).

However, compared with liquid desiccant systems, solid desiccant systems are more compact and do not have the problems of liquid desiccant systems such as the desiccants carryover or material corrosion (Agrarwal 2001). Many companies have already manufactured solid desiccant dehumidification systems while the liquid desiccant dehumidification systems are still in the development phase, and far few companies have manufactured such a type of air-conditioning systems.

2.4 Types of desiccants used in HVAC applications

There are two types of desiccants, namely absorbent desiccants and adsorbent desiccants. Most of the absorbent desiccants are liquids, and chemically can attract the humidity from the processed air. These desiccants are subject to physical and chemical changes when absorbing moisture (Davanagere *et al.* 1999). Adsorbent materials are solid, and physically can attract the humidity from the processed air. Silica gel and molecular sieve are examples of adsorbents that are commonly used in solid desiccant dehumidification systems. It is worthwhile to mention that the water absorbing capacity of liquid desiccants is higher than solid desiccants (ASHRAE 2009). The key liquid desiccants used in HVAC systems are summarised below.

Lithium chloride solution

Lowenstein *et al.* (1998) reported that lithium chloride solution ($LiCl\text{-}H_2O$) is an excellent liquid desiccant because of its essential zero vapor pressure and the ability of regenerating the solution at high temperatures without losing or evaporating the desiccant into the scavenging air. Lithium chloride solution can work as an excellent liquid desiccant, and does not evaporate at natural ambient conditions (Fumo and Goswami 2002).

Lithium chloride (LiCl) is found as a dry material if it absorbs just two molecules of water (H_2O), but it turns into liquid when continuing to absorb water. For example, one dry molecule of LiCl can absorb two molecules of water, but LiCl turns into liquid when absorbing more than two molecules of water. It can absorb a maximum of 26 water molecules, which means that its capacity to absorb moisture is more than 1000% (ASHRAE 2009). These characteristics make it suitable to be used as an active desiccant salt. Fig. 2.3 shows the relationship of the dew-point temperature and the surface vapor pressure with the solution temperature of lithium chloride solution. It can be observed that lithium chloride will be at equilibrium with an airstream at dew-point temperature of 26ºC if the temperature and the concentration of the solution are 40ºC and 25%, respectively.

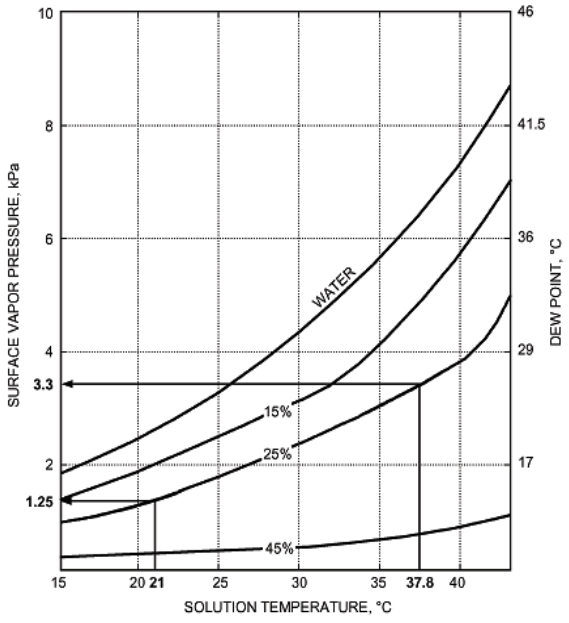

Fig. 2.3 Surface vapour pressure of LiCl solution at different solution temperatures (Foote Mineral 1988 cited in ASHRAE 2009).

Lithium bromide solution

A saturated solution of lithium bromide (LiBr-H_2O) can dehumidify the air down to 6% relative humidity (Lowenstein 2008), which means that lithium bromide solution

works excellently if it is utilised in air dehumidification systems. However, lithium chloride solution offers several advantages over lithium bromide solution as follows.

- The cost of lithium bromide solution per pound is about double that for lithium chloride solution (Lowenstein *et al.* 1998).
- The regeneration temperature required for LiBr solution is around 70-88ºC (Ward *et al.* 1979 cited in Mittal *et al.* 2005). This high regeneration temperature means higher energy consumption, and hence higher dehumidification cost when compared with lithium chloride solution.
- Liu *et al.* (2011) concluded that similar COP could be achieved when using LiCl and LiBr solutions.

Glycols

Glycols (triethylene and propylene) solutions are classified as a second candidate of liquid desiccants, and have been examined in liquid desiccant dehumidification systems due to their low toxicity and compatibility with many metals (Oberg and Goswami 1998; Elsarrag 2006). However, these solutions can cause problems that are not acceptable in HVAC applications as follows.

- Glycols evaporate easily into the air stream due to their low vapor pressure (Oberg and Goswami 1998).
- The expense of pumping may be high due to the high viscosity of Triethylene Glycol solution (TEG-H_2O) (Chung and Luo 1999), such that its concentration might be higher than 90% to provide acceptable dehumidification.
- Glycols can transport and condense on the windows of the conditioned space (Abdul-Wahab *et al.* 2004), causing economic problems due to the continual loss of the desiccant.

Lowenstein (2008) reported that these desiccants have an unfavorable volatile characteristic, and the dehumidification capacity of triethylene glycol solution with a concentration of 96% can be achieved by using 42% LiCl solution down to the same air dew-point.

Fig. 2.4 shows the relationship of the dew-point temperature and the surface vapor pressure with the solution temperature of TEG solution. It can be observed that TEG solution will be at equilibrium with an airstream at dew-point temperature of 29ºC if the temperature and the concentration of the solution are 32ºC and 50%, respectively.

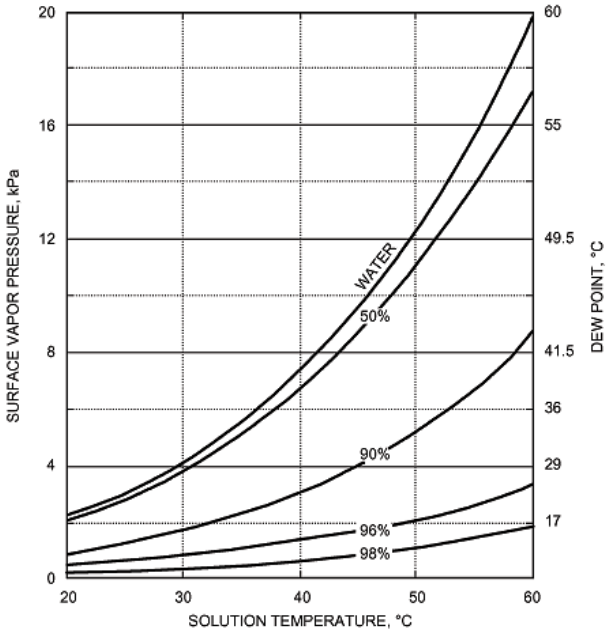

Fig. 2.4 Surface vapour pressure of TEG solution at different solution temperatures (Dow 1981 cited in ASHRAE 2009).

Based on the above, the following factors should be taken into account when using a liquid desiccant for HVAC purposes:

- Crystallisation, corrosion and volatile problems;
- Desiccant carryover and evaporation problems;
- Regeneration temperature;
- Desiccant and pumping costs; and

- Desiccant affinity to attract water vapour.

2.5 Desiccant dehumidifiers

Fig. 2.5 shows different types of dehumidifiers that are currently considered in HVAC applications. This section will review some types of desiccant dehumidifiers that are used in liquid desiccant dehumidification systems including the packed bed dehumidifiers and flat plate heat exchanger dehumidifier.

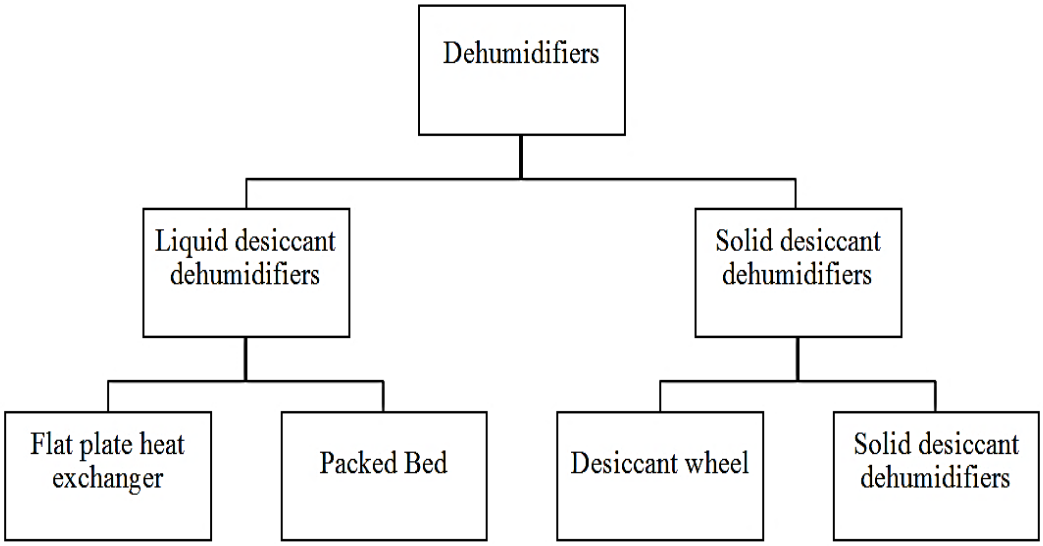

Fig. 2.5 Types of dehumidifiers used in HVAC applications.

Desiccant wheel and solid desiccant dehumidifiers are commonly used in solid desiccant air-conditioning systems. Detailed information about the working mechanisms of these dehumidifiers is available in Harriman (2002) and Munters (2012).

2.5.1 Packed bed dehumidifier

Packed bed dehumidifiers (i.e. absorbers) can be classified into counter-current, co-current or cross-current structured or randomly filled packed bed dehumidifiers according to the flow and the packings filling method within the dehumidifiers. Fig.

2.6 shows three types of absorbers, which are named according to the flow of both the gas and the solution.

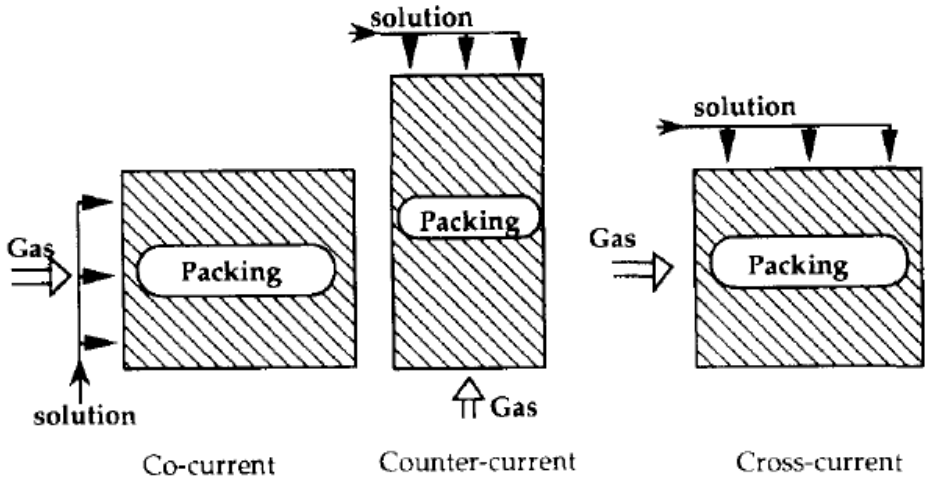

Fig. 2.6 Three types of packed bed absorbers (Westerlund and Dahl 1994).

The flow type can significantly impact the pressure drop across the absorber. For instance, the pressure drop of cross-current packed bed absorber is proportional to 1/4-1/2 of counter-current packed bed absorber at equivalent flow rates (Westerlund and Dahl 1994). In general, packed bed dehumidifiers contain packing layers that assist in widening the contact area between the gas and the liquid desiccant. Many types of packing media can be used in the production of packed bed dehumidifiers. Fig. 2.7 shows some types of dumped type packings. The packed bed dehumidifier is called random packed bed dehumidifier if it is filled with such types of packings. However, if the packings are structurally self-supporting, it is called structured packed bed dehumidifier (Schifftner 2002).

The dehumidification process of a packed bed dehumidifier is caused by a liquid desiccant which is sprayed on a contact media (i.e. packings), and the processed air then comes over this media; the consequence is dry air such that the desiccant absorbs the moisture from the processed air, and heat is launched due to this process.

However, the relatively high-flow rate of the liquid desiccant limits the increase in the desiccant temperature into few degrees (Lowenstein 2008). Useful hydraulic properties of different types of structured and random packings can be found in Kister *et al.* (2008).

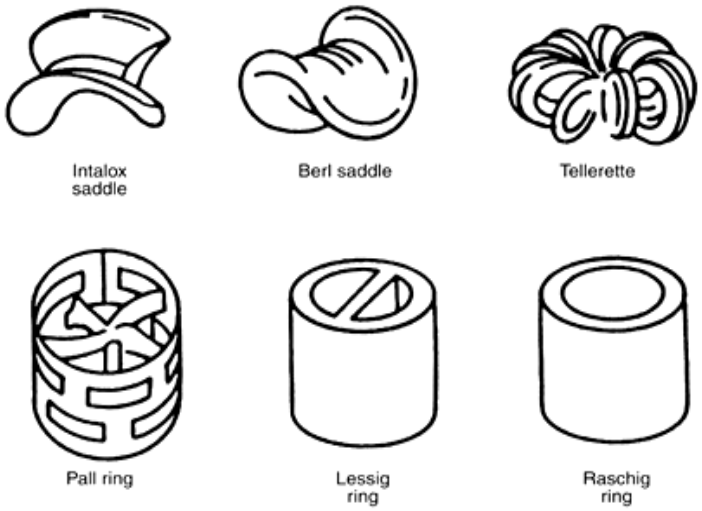

Fig. 2.7 Some types of dumped type packings (Schifftner 2002).

Structured packings can be manufactured by using many materials such as Carbon Steel, Stainless Steel alloys, Aluminum, Titanium, Nickel alloys, Copper alloys, and Zirconium (koch-glitsch 2013).

Many studies have been carried out using different types of packings, flow and liquid desiccants to test and evaluate the performance of the packed bed dehumidifiers. Oberg and Goswami (1998), for example, experimentally analysed a random packing counter-flow dehumidifier using polypropylene Rauschert Hiflow packings. Triethylene glycol solution was used as the liquid desiccant. Many design variables of the packed bed dehumidifier were tested. The results indicated that the height of the packed bed, concentration and temperature of the desiccant, air flow rate and humidity ratio have high impacts on the performance of the dehumidifier. Lazzrin *et al.* (1999) examined and analysed a cross-flow random packed bed dehumidifier

using plastic Pall Rings packings. $CaCl_2$ and LiBr solutions were used as liquid desiccants. Fig. 2.8 compares the reduction of the humidity ratio achieved by each liquid desiccant at different inlet temperatures and concentrations. It can be found that the humidity reduction achieved by LiBr solution is higher than that of $CaCl_2$ solution. However, the inlet solution concentration of LiBr solution is higher than the $CaCl_2$ solution, and may result in higher pumping cost.

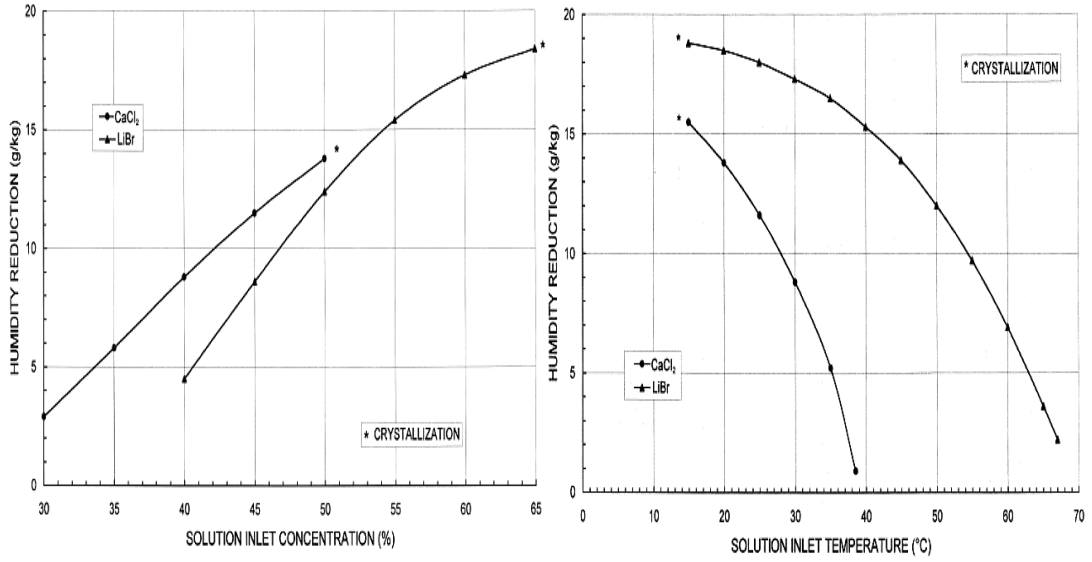

Fig. 2.8 Dehumidification behaviour of LiBr and $CaCl_2$ solutions across a random packed bed dehumidifier (Lazzarin *et al.* 1999).

Zurigat *et al.* (2004) experimentally examined the effects of a number of parameters, including the air flow rate, the solution concentration, the humidity and the temperature of the inlet air, on the performance of the air dehumidification using a structured packed bed dehumidifier. Wood and aluminum structured packings were used. It was found that the moisture removal performance of the dehumidifier can be enhanced through increasing the concentration of triethylene glycol solution and the flow rate of both inlet liquid desiccant and inlet air. Longo and Gasparella (2005) experimentally tested and theoretically analysed the performance of a counter-flow random packed bed column using Rauschert Hiflow Rings packings. Three types of

liquid desiccants, namely LiCl, LiBr and KCOOH solutions, were used. Fig. 2.9 shows the dehumidification behaviour of each liquid desiccant.

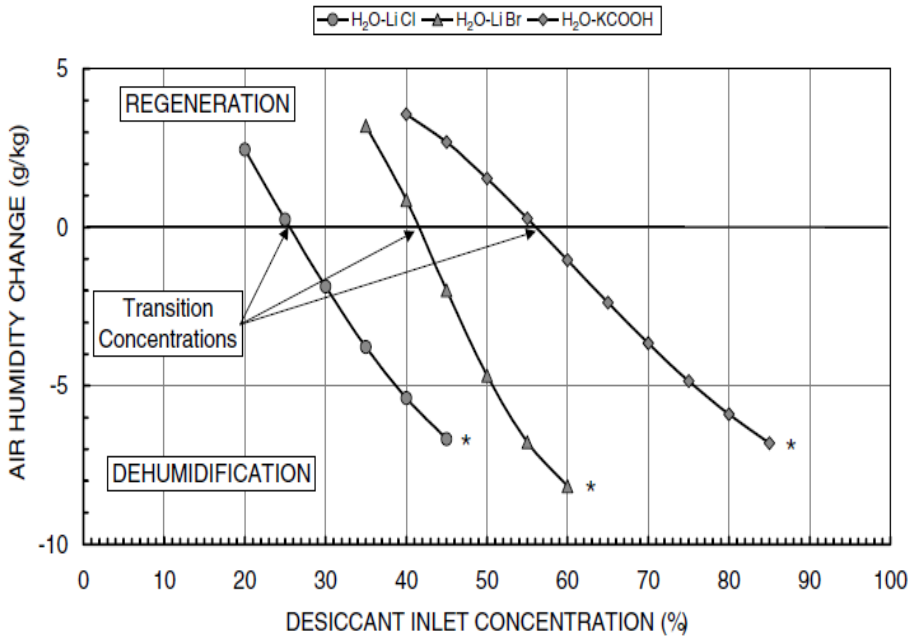

Fig. 2.9 Dehumidification behaviour of three different liquid desiccant solutions (Longo and Gasparella 2005).

As illustrated in Fig. 2.9, the maximum air humidity reduction can be achieved when the LiCl, LiBr and KCOOH solutions at the concentrations of 44%, 60% and 85%, respectively. LiBr solution has the highest dehumidification performance. However, the concentration of the LiBr solution is higher than LiCl solution, which means that extra pumping cost will be required. It is also shown that LiCl solution has excellent dehumidification behaviour when the inlet concentration is in the range of 34-45%, so that the dehumidification system can operate in this range efficiently.

2.5.2 Cross-flow plate heat exchanger

Cross-flow plate heat exchanger is another type of liquid desiccant dehumidifiers. This type of dehumidifiers was proposed and mathematically modelled by Saman and Alizadeh (2001) for air dehumidification and cooling at the same time. Saman and Alizadeh (2002) experimentally tested the cross-flow plate heat exchanger

dehumidifier. A good agreement was achieved between the modelled data and experimental data. It was concluded that this system is suitable for the tropic Brisbane city in Australia. Kakac *et al.* (2012) reported that the summer performance of the plate heat exchanger materials does not specify the comfort standards of Brisbane.

Fig. 2.10 shows a schematic diagram of a cross-flow heat exchanger dehumidifier. In this dehumidifier, the moisture from the processed air (i.e. primary air stream) is absorbed when it contacts with the solution while the evaporative cooling that occurs between the secondary air stream and water, assists in eliminating the launched heat due to absorption, and even cooling the processed air at the same time. The schematic diagram (Fig. 2.10) illustrates the flow of the different liquid desiccant, air and water streams in this dehumidifier.

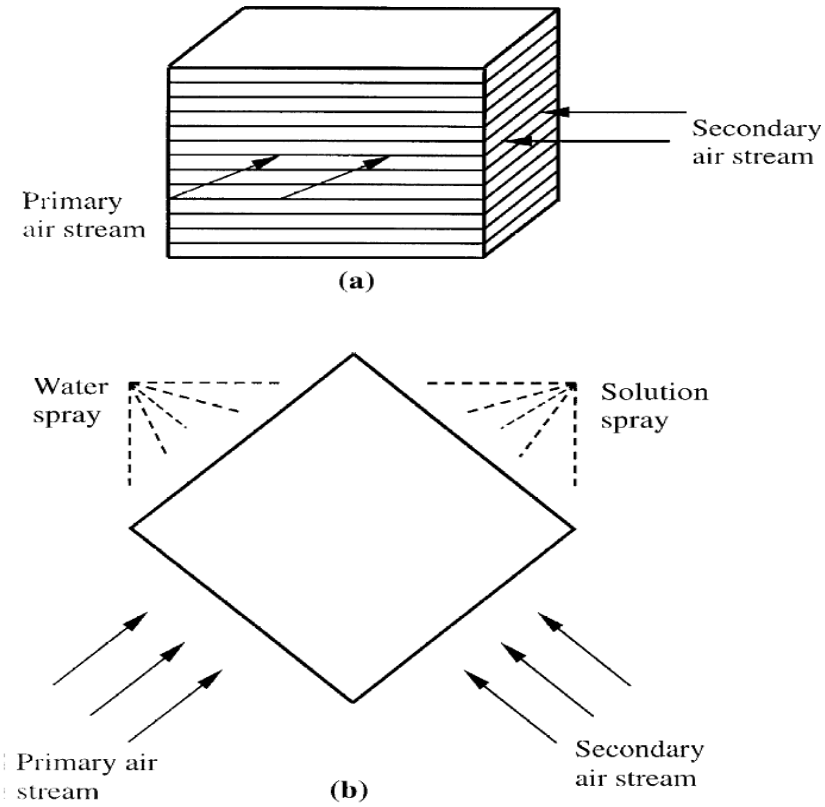

Fig. 2.10 Schematic diagram of a cross-flow heat exchanger dehumidifier (Saman and Alizadeh 2002).

In addition to the packed bed and plate heat exchanger dehumidifiers, researchers in this field are still developing other types of dehumidifiers to provide cooling and dehumidification at the same time with minimised energy requirements. Table 2.1 summarises the key findings from previous studies on the liquid desiccant dehumidification systems. It is worthwhile to mention that there are many factors, such as air flow rate, desiccant flow rate, inlet air temperature, inlet desiccant temperature, desiccant type, packing height, packing type, etc., can influence the dehumidification effectiveness of absorbers. Usually, the random packing provides a higher contact area than the structured packing (Babakhani and Soleymani 2010). Table 2.2 shows examples of the effectiveness variations under different factors and operational conditions.

Table 2.1 Summary of key findings from previous studies.

Reference	Liquid desiccant used	Absorber Type	Packings Type	Concentration (%)	Max. dehumidification effectiveness (%)	Max. humidity Reduction (kg/kg or kg/s)	Key Findings
Öberg and Goswani (1998)	TEG	Counter-flow random packed bed	2.54cm polypropylene Rauschert Hiflow rings	94-96	90	≈0.0007.2 kg/s	Design variables, including air flow rate, desiccant temperature, desiccant concentration and packed bed height have the highest impact on the dehumidification performance.
Lazzarin et al. (1999)	LiBr	Cross-flow, random packed bed	2.5cm plastic Pall Rings	53-57	87	≈0.0 132	Good design of the absorber, selecting appropriate flow ratios and packing media can significantly impact the performance of the packed tower absorber
Fumo and Goswami (2002)	LiCl[1]	Counter-flow random packed bed	2.54 cm polypropylene Rauschert Hiflow rings	33.1-34.9	84	0.0095	Design variables such as desiccant temperature, desiccant concentration, air flow rate and air humidity ratio have the highest impact on the performance of the absorber
Saman and Alizadah (2002)	$CaCl_2$[5]	Cross-flow heat exchanger	0.2 mm (thick) plates	40	90	≈0.0005 kg/s	The angle of the plate heat exchanger has a significant impact on the dehumidification performance
Zurigat et al. (2004)	TEG[4]	Counter flow Structured packed bed	0.48 m height aluminum and wood structured packing	93-98 (wood Packing)	43.1	0.233×10^{-3} kg/s	Owing to the use of structured packing, it is possible to work with low flows with good packings wettability
				93-98 (aluminum Packing)	46.3	0.256×10^{-3} kg/s	
Longo and Gasparella (2005)	LiCl	Counter flow random packed bed	2.5cm plastic Pall Rings	39.2-40.6	90	0.0 17	Better dehumidification performance can be obtained by using LiCl and LiBr solutions than that using KCOOH solution. LiCl and LiBr solutions have higher humidification reduction while KCOOH solution has the advantageous as a non-corrosive material
	KCOOH[2]			72.8-74	90	0.0135	
	LiBr[3]			51.9-53.9	90	0.0 18	
Lowenstein et al. (2006)	LiCl	Internally cooled absorber (plastic-plate heat exchanger)	Plastic plates	36-44	–	≈ 0.0123	Low flow internally cooled liquid dehumidification air-conditioning has advantages such as lower pressure drop, higher COP, more dryness of the air as comparing with other technologies.
Liu et al. (2006)	LiBr	Cross-flow, structured packed bed	0.55m height Celdek structured packings	42.8-54.8	69	–	Rising the dehumidification effectiveness is in conjunction with decreasing the air flow rate and increasing the desiccant flow rate
Chau and Worek (2009)	TEG	Counter-flow random packed bed	1.588cm Polypropylene Flexi rings	90-100	98	≈ 0.0045 kg/s	High liquid to gas flow rate can lead to high removal rate and efficiency f the absorber

[1] lithium chloride, [2] potassium formate, [3] lithium bromide, [4] triethylene glycol, [5] $CaCl_2$ calcium chlorideo

Table 2.2 Experimental effectiveness variations under different operational conditions from previous studies.

Study	Packing type	Desiccant used	L_i[1] (kg/m^2.s)	X_{si}[2] (%)	T_{si}[3] (°C)	G[4] (kg/m^2.s)	T_{ai}[5] (°C)	w_{ai}[6] (g/kg)	Effectiveness (%)
Öberg and Goswani (1998)	random packing	TEG	4.5-6.5	94-96	25-35	0.5-2	25-35	11-22	72-90
Lazzarin et al. (1999)	Random packing	LiBr	0.0183-0.1297	53-57	16.1-34.1	61.11 (m^3/s)	23.6-35.4	10.4-18.7	26-87
Fumo and Goswami (2002)	Random packing	LiCl	5.019-7.42	33.1-34.9	25-35.52	0.89-1.92	29.9-40.1	14.2-21.5	75-84
Zurigat et al. (2004)	Structured packing (wood)	TEG	0.13-0.82	93-98	28.2-45.5	1.5-2.61	25.4-44	16.2-20.7	19-43.1
	Structured packing (aluminium)	TEG	0.13-0.82	93-98	25-43.2	1.5-2.61	25.6-40.7	16-21.8	18.7-46.3
Longo and Gasparella (2005)	Random packing	LiCl	0.10-1.17	39.2-40.6	23.4-24.0	0.43-0.47	24.3-37.6	7.3-23.3	30-90
		LiBr	0.16-1.39	53.9-51.9	23.7	0.44-0.47	23.6-36.7	8.2-22.8	30-90
		KCOOH	0.09-1.23	72.8-74.0	21.9-24.8	0.48-0.52	22.6-35.8	8.8-20.7	30-90
Liu et al. (2006)	Structured packing	LiBr	0.3-0.64	42.8-54.8	20.1-29.5	0.31-0.47 (kg/s)	24.7-33.9	10-21	38-69

[1] desiccant flow, [2] desiccant concentration, [3] solution temperature, [4] air flow, [5] air temperature, [6] air moisture-content

2.6 Performance evaluation of liquid desiccant systems

Recently, significant efforts have been made on the development and application of liquid desiccant dehumidification technology in building applications, and a number of review papers specifically pertaining to liquid desiccant dehumidification are now in the public domain (Cheng and Zhang 2013; Huang and Zhang 2013; Mohammad *et al.* 2013; Yin *et al.* 2014). These review articles have addressed various issues such as system modelling, design and operational optimisation, performance evaluation, development of dehumidifiers and regenerators, the use of different regeneration methods, etc. Jain and Bansal (2007), for example, reviewed the recent studies on the use of the liquid desiccant technology in HVAC systems. A comprehensive analysis among different types of desiccant liquids and absorbers was provided. A number of studies presented the characterisation and parametric studies to identify the system-level and subsystem-level interactions and evaluate the performance of liquid desiccant systems under different operational conditions (Mohan *et al.* 2008; Patanwar and Shukla 2012; Das *et al.* 2012).

This section can be divided into two groups based on the methods used to evaluate the performance of liquid desiccant systems: (1) theoretical studies, (2) experimental studies.

2.6.1 Previous theoretical studies

Gandhidasan (1994) proposed and numerically simulated an open-cycle solar-driven liquid desiccant cooling system. An open solar regenerator was used to re-concentrate the weak liquid desiccant after leaving the absorber. It was found that the performance of the cooling system is highly affected by several factors, including the inlet air temperature, the cooling water temperature (i.e. water comes from the

cooling tower to cool the hot strong solution) and the desiccant concentration. Jain *et al.* (2000) developed an optimisation procedure by implementing an algorithm called Modified Box's complex method to solve the objective function defined. The results indicated that the utilisation of waste heat leads to reduced initial and subsequent running costs when compared with conventional air-conditioning systems.

Oliveira *et al.* (2000) examined the thermal performance of a novel liquid desiccant air-conditioning system integrated with a needle impeller rotor to improve the heat and mass transfer in some system components (i.e. evaporators and absorber). A numerical model was developed to simulate the system with the assistance of experimental data obtained from the absorber and the evaporators. It was found that without recirculation of the indoor air, the coefficient of performance (COP) was always higher than 0.7. Abdalla and Abdalla (2006) proposed and investigated a radiant air-conditioning system combined with a solar-driven liquid desiccant and an evaporative cooler. The study was accomplished using Matlab, and the main results indicated that dehumidification rate of about 1.6 kg/s could be achieved at the design conditions with the dry-bulb temperature of 30.1°C and humidity ratio of 6.6×10^{-3} kg/kg. Li and Yang (2008) numerically simulated an open-cycle solar liquid desiccant dehumidification system and concluded that this system could achieve energy savings of 25-50% compared with the traditional vapour compression system.

Audah *et al.* (2011) conducted a feasibility study on the use of a solar liquid desiccant system to supply cooling and fresh water to the building, and concluded that the heat sink (desiccant cooler) temperature is the key optimisation parameter that affects the regeneration temperature and system power consumption. Li *et al.* (2011) proposed a new liquid desiccant dehumidification system using photovoltaic-

electrodialysis for regeneration. The results showed that the photovoltaic-electrodialysis regeneration can reduce the system energy consumption and avoid adding additional heat to the liquid desiccant, which negatively impacts the dehumidification process. Zhang *et al.* (2012) developed a heat pump-driven liquid desiccant dehumidification system. The key results showed that the system integrated with a water-cooled condenser can achieve a higher COP (i.e. 35%) than the basic heat pump liquid desiccant system.

2.6.2 Previous experimental studies

Many studies have used different approaches to testing and evaluating the performance of liquid desiccant air-conditioning systems. Patnaik *et al.* (1990), for example, designed and experimentally tested the performance of a solar open-cycle liquid desiccant air dehumidification system with a nominal capacity of 10.5 kW. Two types of liquid desiccant distribution systems, namely gravity tray distributor and spray nozzle distributor, were evaluated within the regenerator. It was found that 40-50% higher capacity and 30-40% lower pressure drop across the regenerator could be obtained when using the spray distribution system. The main experimental results indicated that the water condensation rate across the absorber was ranging between 9.6×10^{-4} and 5.62×10^{-3} kg/s. Lazzarin *et al.* (1999) presented a mathematical model and experimental study to evaluate the heat and mass transfer across a packed bed absorber using lithium bromide and calcium chloride solutions to verify their effectiveness. Fumo and Goswami (2002) examined the effects of the operative design conditions on the performance of the absorber and regenerator. Chau and Worek (2009) investigated the effects of different design parameters on a packed bed dehumidifier, and Triethylene Glycol solution (TEG-H_2O) was used as the liquid desiccant.

Lazzarin and D'Ascanio (2006) presented an experimental study of an open-cycle liquid desiccant air-conditioning system. The experimental tests were carried out for both winter and summer cases, and the main results revealed that Primary Energy Ratio (PER) of 1.11 for winter, and 0.72 for summer could be achieved. It was concluded that more energy savings can be achived if the system design is optimised by employing the benefits offered by the liquid desiccant dehumidification technology. Gommed and Grossman (2007) experimentally investigated a solar liquid desiccant system for air-conditioning offices. The results showed that a thermal coefficient of performance of around 0.8 can be achieved. Liu *et al.* (2008) performed an analytical study to examine the heat and mass transfer performance of a cross-flow packed bed absorber. It was indicated that the developed analytical solutions are useful to optimise the absorber. A reduction in the size (from 0.5 m × 0.5 m × 1.2 m to 0.6 m × 0.35 m × 0.83 m) and packing volume (up to 58% reduction) could be achieved without significantly affecting the key performance indicators such as pressure drops and heat and mass transfer efficiencies.

Wang *et al.* (2009) designed a liquid desiccant air-conditioning system to handle the required sensible and latent loads by integrating the desiccant dehumidification system with two humidifiers. It was shown that, with a heat source of 70ºC, a COP of 0.8 could be achieved. It was claimed that the system can be driven by low grade energy sources such as waste heat and solar energy to provide the required regeneration heat. Nayak *et al.* (2009) experimentally investigated the performance characterisation of a gas engine generator combined with a liquid desiccant dehumidification system.The combined heat and power system was integrated to provide electricity and regeneration heat for the liquid desiccant. The combined heat and power system and the liquid desiccant system were separate units, which mainly

used to assist a rooftop unit that supplies the cooling loads. It was found that the average COP of the liquid desiccant system was 0.5 while the processed air could be dehumidified to 7×10^{-3} kg/kg.

Lychnos (2010) conducted a study on the feasibility of using a solar liquid desiccant air-conditioning system to cool a commercial greenhouse, and to evaluate the performance of the regenerator. Magnesium chloride solution was used as the liquid desiccant when running the experimental tests. The proposed system was found to be able to improve the cooling by 2.3-5.6ºC. Liang *et al.* (2011) examined the performance of a liquid desiccant air-conditioning system integrated with a combined cooling, heating and power (CHP) system. Through effectively utilising the high-temperature of the exhaust gas and recycling waste hot water of the combined CHP system, the cooling capacity of the proposed system can be increased from 464 to 537 kWt, and the total energy utilisation efficiency can be improved to 94.81%. The aforementioned studies showed that liquid desiccant dehumidification systems can achieve better performance through integrating with other advanced energy technologies.

2.7 Conclusions

Based on the above review, some useful conclusions can be summarised, and a few recommendations for future work in this direction are presented.

- Liquid desiccant systems have many advantages as compared to other systems such as the low energy consumption, enhanced thermal comfort, low or no negative impact on the ozone layer, and low dehumidification cost.
- Many studies have demonstrated that liquid desiccant dehumidification is a promising technology for developing energy efficient buildings.

- Among the different types of liquid desiccant solutions, LiCl solution has demonstrated excellent dehumidification behaviour with low regeneration temperature requirements.
- Many types of dehumidifiers (i.e. absorbers) can be utilised in liquid desiccant systems. The counter-flow random packed bed dehumidifier exhibits excellent performance.
- Parametric study is still of importance to be performed to evaluate the effects of the design and operational parameters on the performance of the absorber and regenerators.

The ultimate objective of any technique development comes to a point, i.e., its application. The key issues for the development and application of liquid desiccant dehumidification system for building applications may include:

- Selection of appropriate types of dehumidifiers and liquid desiccants.
- Proper system design and optimal control.
- Whole system simulation to understand system-level and subsystem-level interactions.

3 Development and modelling of an advanced solar-assisted liquid desiccant dehumidification air-conditioning system

3.1 Introduction

This chapter presents the development and modelling of an advanced solar-assisted liquid desiccant dehumidification air-conditioning system to control the humidity level and maintain satisfactory indoor thermal comfort with minimised energy consumption. The mathematical models for each component are described, and the key models are validated against experimental data published in the literature.

3.2 Description of the proposed system

Fig. 3.1 illustrates the schematic of the proposed solar-assisted liquid desiccant dehumidification air-conditioning system. It consists of an absorber, a regenerator, three counter-current heat exchangers, an evaporative cooler, a cooling tower, a solar water heating system, five fluid pumps and two air fans. The liquid desiccant used is lithium chloride solution ($LiCl\text{-}H_2O$) due to its excellent performance as a working fluid in liquid desiccant dehumidification systems as illustrated in Chapter 2.

The absorber and regenerator used are random packed bed columns. The packings used are 2.56 cm plastic Pall Rings type. The absorbent desiccant absorbs the moisture from the air when passing through the absorber, and its concentration will be decreased (i.e. process 1-2 in Fig. 3.1). Owing to the absorption process, the air temperature might increase, and its humidity ratio decreases (i.e. process 3-4), leading to warm dry air. The warm dry air then passes through the evaporative cooler (i.e. process 4-4'), where the air will be cooled to the desired condition. The weak solution from the absorber will then pass through the regenerator in order to be re-concentrated (i.e. process 6-7).

In thermal regeneration systems, the temperature of the liquid desiccant should be high enough in order to release the absorbed moisture into the scavenging air stream flowing through the regenerator (i.e. process 8-9). In this proposed system, a solar water heating system, which consists of an array of flat plate solar collectors, an auxiliary electric heater, and a thermal storage tank, is used to provide the necessary heat required for thermal regeneration. The auxiliary electric heater is only used when solar irradiance is not strong enough and cannot provide sufficient heat for the regeneration. The heat exchanger *I* is used to assist in improving the system efficiency by utilising the high temperature of the strong solution from the regenerator to increase the temperature of the weak solution from the absorber (i.e. processes 7-10 and 2-5). The cooling tower and the heat exchanger *III* are used to further decrease the temperature of the strong desiccant to ensure the best performance of the absorber. The heat exchanger *II* is used to increase the temperature of the weak desiccant before entering the regenerator to avoid the direct contact between the liquid desiccant and circulated water in the solar water heating system.

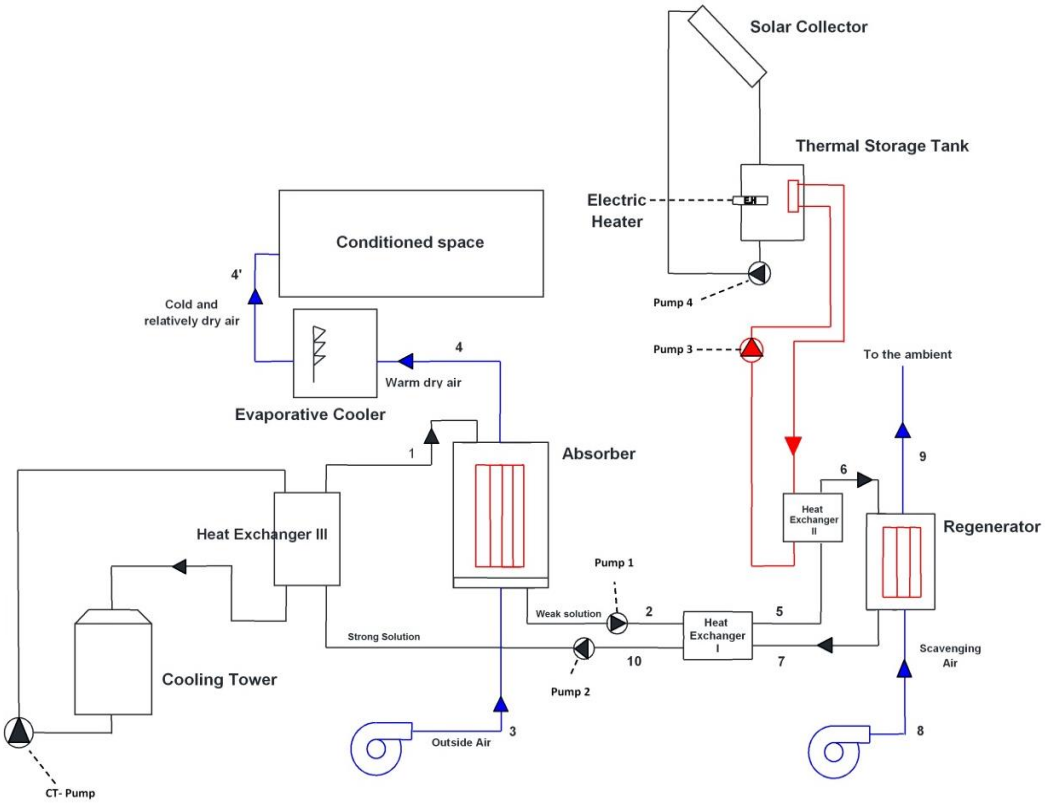

Fig. 3.1 Proposed solar-assisted liquid desiccant dehumidification air-conditioning system.

3.3 Development and selection of components models

3.3.1 Calculation of lithium chloride solution properties

As lithium chloride solution (LiCl-H_2O) is used as the working fluid, determination of its thermal properties is essential for modelling the performance of key system components such as the regenerator and absorber.

The enthalpy of lithium chloride solution can be calculated by using Equation (3.1) (Chaudhari and Patil 2002).

$$h = A_1 + B_1 t + C_1 t^2 \tag{3.1}$$

where, h is the enthalpy, t is the temperature. A_1, B_1 and C_1 are coefficients, which can be determined by Equations (3.2), (3.3) and (3.4), respectively.

$$A_1 = -66.2324 + 11.2711X - 0.79853X^2 + (2.1534 \times 10^{-2})X^3 - (1.66352 \times 10^{-4})X^4 \quad (3.2)$$

$$B_1 = 4.5751 - 0.146924X + (6.307226 \times 10^{-3})X^2 - (1.38054 \times 10^{-4})X^3 + (1.06690 \times 10^{-6})X^4 \quad (3.3)$$

$$C_1 = -8.09689 \times 10^{-4} + (2.18145 \times 10^{-4})X - (1.36194 \times 10^{-5})X^2 + (3.20998 \times 10^{-7})X^3 - (2.64266 \times 10^{-9})X^4 \quad (3.4)$$

where, X is the solution concentration.

The above equations are applicable within the bounds outlined in Table 3.1. Special care should be taken when using the above enthalpy equation outside the bounds specified in Table 3.1, especially at low temperature conditions.

Table 3.1 Limitation of the enthalpy Equation (3.1).

Desiccant	**Min X (%)**	**Max X (%)**	**Min t (^{o}C)**	**Max t (^{o}C)**
LiCl-H_2O	20	35	20	120

The vapour pressure of LiCl solution at the absorption process is calculated using Equation (3.5), and the coefficients in the equation are presented in Table 3.2 (Fumo and Goswami 2002).

$$p = (a_o + a_1 t + a_2 t^2) + (b_o + b_1 t + b_2 t^2)X + (c_o + c_1 t + c_2 t^2)X^2 \quad (3.5)$$

where, p is the vapour pressure, t is the temperature, a_o-a_2, b_o-b_2 and c_o-c_2 are coefficients provided in Table 3.2, and X is the solution concentration.

Table 3.2 Coefficients in Equation (3.5).

Coefficient	**Values (Dehumidification process)**		
	i=0	i=1	i=2
a_i	4.58208	-0.159174	0.0072594
b_i	-18.3816	0.5661	-0.019314
c_i	21.312	-0.666	0.010332

The vapour pressure of lithium chloride solution at the regeneration process is calculated by using Equation (3.6) (Chaudhari and Patil 2002).

$$\log p = A_2 + \frac{B_2}{T} + \frac{C_2}{T} \tag{3.6}$$

where, T is the solution absolute temperature, and A_2, B_2, and C_2 are coefficients, which can be determined by Equations (3.7), (3.8) and (3.9), respectively.

$$A_2 = 8.202988 - 0.1353801X + 0.0179222X^2 - 0.0005292X^3 \tag{3.7}$$

$$B_2 = -1727.8 + 58.3845X - 10.208X^2 + 0.3125X^3 \tag{3.8}$$

$$C_2 = -95014 - 4701.526X + 929.081X^2 - 31.766X^3 \tag{3.9}$$

where, X is the concentration of the LiCl solution.

The dynamic viscosity of LiCl solution is given by Equation (3.10) (Conde-Petit 2009).

$$\mu = \mu_{H_2O}.exp\left(\eta_1.\zeta^{3.6} + \eta_2.\zeta + \eta_3.\frac{\zeta}{\theta} + \eta_4.\zeta^2\right) \tag{3.10}$$

where, ζ is a parameter defined in Equation (3.11), and the parameters η_1 to η_4 are given in Table 3.3.

$$\zeta = \frac{x}{(1-x)^{\frac{1}{0.6}}} \tag{3.11}$$

Table 3.3 Parameters in Equation (3.10).

Desiccant	η_1	η_2	η_3	η_4
LiCl-H_2O	0.090481	1.390262	0.675875	-0.583517

In Equation (3.10), μ_{H_2O} is the water dynamic viscosity at the saturation conditions, which can be obtained by Equation (3.12) (Crabtree and Siman-Tov 1993).

$$\mu_{H_2O} = exp[\frac{A_3+C_3t}{1+B_3t+D_3t^2}] \tag{3.12}$$

where, A_3 = -6.325203964, B_3 = 8.705317×10^{-3}, C_3 = -0.088832314, and D_3 = -9.657×10^{-7}.

The density of LiCl solution is given by Equation (3.13) (Conde-Petit 2009).

$$\rho(x,T) = \rho_{H_2O}(T)\sum_{i=0}^{3}\rho_i\left(\frac{x}{1-x}\right)^i \tag{3.13}$$

where, ρ_{H_2O} is the water density, and given by Equation (3.14).

$$\rho_{H_2O} = \rho_{c,H_2O}\left[1 + \mathrm{B}_0'\tau^{\frac{1}{3}} + \mathrm{B}_1'\tau^{\frac{2}{3}} + \mathrm{B}_2'\tau^{\frac{5}{3}} + \mathrm{B}_3'\tau^{\frac{16}{3}} + \mathrm{B}_4'\tau^{\frac{43}{3}} + \mathrm{B}_5'\tau^{\frac{110}{3}}\right] \tag{3.14}$$

Where, ρ_{c,H_2O} is the critical water density (322 kg/m^3), ρ_i and B_i' are coefficients which can be interpolated from Table 3.4 (Conde-Petit 2009).

Table 3.4 Coefficients in Equations (3.13) and (3.14).

i	ρ_i	B_i'
0	1.0	1.993
1	0.54	1.098
2	-0.303	-0.509
3	0.1	-1.761
4		-45.9
5		-723692.261

The surface tension of LiCl solution is given by Equation (3.15) (Conde-Petit 2009).

$$\gamma(x,\theta) = \gamma_{H_2O}(\theta)[1 + \sigma_1 x + \sigma_2 x\theta + \sigma_3 x\theta^2 + \sigma_4 x^2 + \sigma_5 x^3] \quad (3.15)$$

where, γ_{H_2O} is the surface tension of water, and given by Equation (3.16).

$$\gamma_{H_2O}(\theta) = \sigma_0[1 - b(1-\theta)](1-\theta)^{\mu} \quad (3.16)$$

where, μ, b, and σ_o are coefficients with values of 1.256, -0.625, and 235.8 mN/m (IAPWS cited in Conde-Petit 2009), respectively, the parameter (σ_i) is given in Table 3.5 (Conde-Petit 2009), and θ is given by the following equation.

$$\theta = \frac{t+273.15}{647.29} \quad (3.17)$$

Table 3.5 Values of the parameters in Equation (3.15).

$\boldsymbol{i}$	1	2	3	4	5
$\boldsymbol{\sigma_i}$	2.757115	-12.011299	14.751818	2.443204	-3.147739

3.3.2 Modelling of the absorber and regenerator

The absorber and the regenerator are the key components in the proposed solar-assisted liquid desiccant dehumidification air-conditioning system. In this study, the models used have been developed based on thermodynamics fundamentals and key correlations presented by other researchers. The key assumptions used are:

- The air flow and liquid desiccant flow are assumed to be in a steady state.
- The desiccant solution is evenly distributed into the packings of the absorber and the regenerator.
- The absorber and regenerator are assumed to be adiabatic.
- There is no change of the air specific mass flow rate when passing through the absorber and regenerator.

In this particular system, the absorber and regenerator columns are assumed to be made of stainless-steel, and randomly filled with plastic packings. Since the dehumidification effectiveness, and the moisture removing rate are high when using random packings, it has been decided to utilise such packings in the proposed system. Fig. 3.2 shows the schematic diagram of the absorber and regenerator.

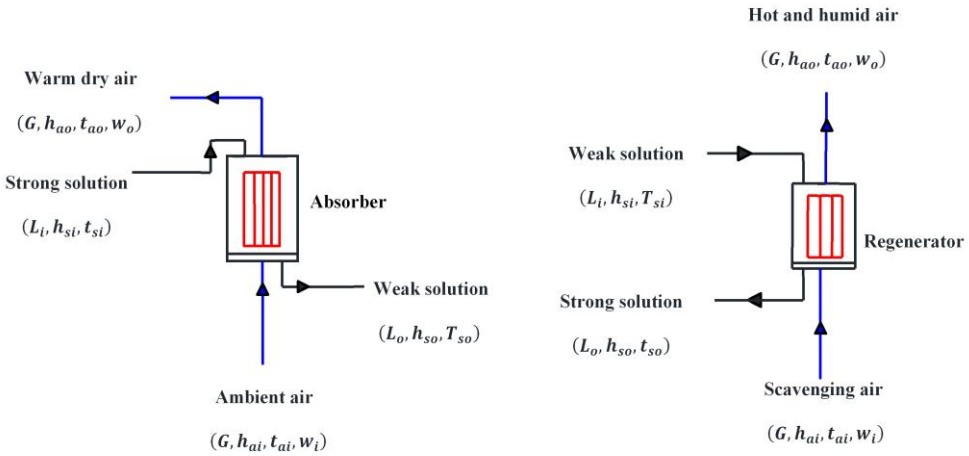

Fig. 3.2 Schematic diagram of the absorber and the regenerator.

The models of the absorber and regenerator have two sides to be considered, i.e. the air side and the liquid desiccant side. The outlet mass flow rate of the liquid desiccant and the change in the desiccant concentration are computed using Equations (3.18) and (3.19), respectively. The energy balance across the absorber and regenerator can be simulated using Equation (3.20). The dehumidification effectiveness (ε_d) is simulated by Equation (3.21) (Chung and Luo 1999). Equation (3.21) can be applied with an average error of ±10% (Chung and Luo 1999; Jain and Bansal 2007).

$$L_o = L_i + G \cdot (w_i - w_o) \tag{3.18}$$

$$X_o = X_i + (G/L_i)X_i\,(w_o - w_i) \tag{3.19}$$

$$Gh_{ai} + L_i\,h_{si} = Gh_{ao} + L_o h_{so} \tag{3.20}$$

$$\varepsilon_d = \left(1 - \frac{0.024\left(\frac{G_i}{L_i}\right)^{0.6}\exp(1.057\,\frac{t_{ai}}{t_{si}})}{(aZ)^{-0.185}\pi^{0.638}}\right) \Big/ \left(1 - \frac{0.192\exp(0.615\frac{t_{ai}}{t_{si}})}{\pi^{-21.498}}\right) \quad (3.21)$$

where, L is the solution specific mass flow rate, G is the air specific mass flow rate, w is the air moisture content, X is the solution concentration, h is the enthalpy, t is the temperature, Z is the column height. The subscripts a, s, i and o represent air, solution, inlet, and outlet, respectively. π is the pressure difference ratio which is given by Equation (3.22).

$$\pi = \frac{p_w - p}{p_w} \quad (3.22)$$

where, p is the desiccant vapour pressure, and p_w is the water vapour pressure at the desiccant's temperature which can be obtained by Equation (3.23) (Wanger and Pruss 1993).

$$ln(\frac{p_w}{p_c}) = \frac{T_c}{T}\,(a'_1\tau + a'_2\tau^{1.5} + a'_3\tau^3 + a'_4\tau^{3.5} + a'_5\tau^4 + a'_6\tau^{7.5}) \quad (3.23)$$

where, the parameter τ is given by Equation (3.24), T is the temperature, and a'_{1-6} are coefficients which are given in Table 3.6.

$$\tau = 1 - \frac{T}{T_c} \quad (3.24)$$

Table 3.6 Values of the coefficients in Equation (3.23).

i	1	2	3	4	5	6
a'_i	-7.85951783	1.84408259	-11.7866497	22.6807411	-15.9618719	1.80122502

where, T_c and p_c are the critical temperature and pressure of water, and can be taken as 647.29 K and 22064 kPa, respectively. Fig. 3.3 shows the variation of the water vapour pressure with the changes of the temperature. It can be seen clearly that the water vapour pressure increases if the temperature increases. It is important to

mention that the absorption process will transform into regeneration process if the solution pressure is higher than the air vapour pressure. Therefore, the solution temperature must be low enough before entering the absorber to ensure good dehumidification performance.

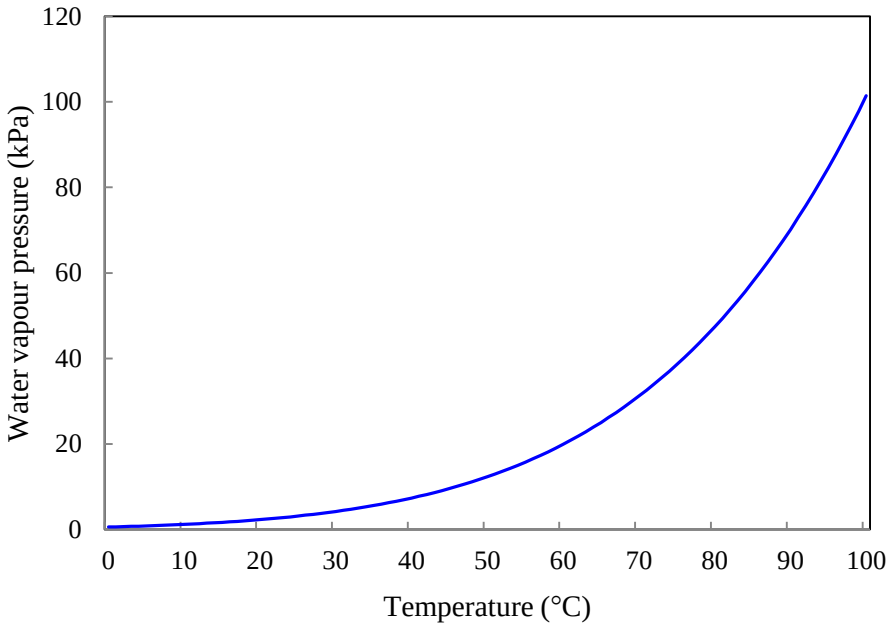

Fig. 3.3 Water vapour pressure versus temperature.

In Equation (3.21), a is the wet specific surface area of the packing (m^2/m^3), and can be calculated by the following equation (Onda *et al.* 1968 cited in Fumo and Goswami 2002):

$$a = a_t[1 - \exp\ ((-1.45) * (\gamma_c/\gamma_L)^{0.75}(L/a_t \cdot \mu_L)^{0.1}(L^2 \cdot a_t/\rho_L^2 \cdot g)^{-0.05}(L^2/\rho_L \cdot \gamma_L \cdot a_t)^{0.2})] \quad (3.25)$$

where, a_t is the dry specific surface area of the packing, γ_L is the solution surface tension, γ_c is the critical surface tension, g is the acceleration of gravity, μ_L is the solution dynamic viscosity, and ρ_L is the solution density.

The absorber and regenerator outlet air moisture contents can be calculated by using Equations (3.26) and (3.27), respectively.

$$w_o = w_i - \varepsilon_d(w_i - w_{min}) \quad (3.26)$$

$$w_o = w_i + \varepsilon_d(w_{max} - w_i) \tag{3.27}$$

where, w_{min} is the minimum moisture-content across the absorber, and w_{max} is the maximum moisture-content across the regenerator. w_{min} and w_{max} can be achieved when the outlet air is in equilibrium with the liquid desiccant at the inlet of the absorber and regenerator (i.e. the outlet air vapour pressure equals to the inlet desiccant vapour pressure).

The water condensation rate from the processed air across the absorber, and the water evaporation rate from the desiccant across the regenerator can be calculated by Equations (3.28) and (3.29), respectively.

$$m_{cond} = m_a(w_i - w_o) \tag{3.28}$$

$$m_{evap} = m_a(w_o - w_i) \tag{3.29}$$

where, m_a is the air flow rate.

The heat effectiveness (ε_h) of the absorber and regenerator is calculated by using Equation (3.30).

$$\varepsilon_h = \frac{|h_{in} - h_{ao}|}{|h_{in} - h_{max;min}|} \tag{3.30}$$

where, h_{min} is the minimum enthalpy across the absorber, and h_{max} is the maximum enthalpy across the regenerator, which can be obtained when the processed air is in equilibrium with the inlet desiccant's concentration and temperature. An iteration method may be used to obtain the value of ε_h. In the whole simulation model, a correlation equation developed by Martin and Goswami (2000) is used to calculate the heat transfer effectiveness of the absorber in order to avoid the iteration process to save the computational cost. The applicative conditions of Equation (3.31) are summarised in Table 3.7 (Martin and Goswami 2000).

$$\varepsilon_h = 1 - 3.77\left(\frac{L}{G}\right)^{\left(0.289\frac{\gamma_L}{\gamma_c}-1.12\right)}\left(\frac{h_{ai}}{h_{Li}}\right)^{-0.528}(a_t.z)^{\left(-0.0044\frac{\gamma_L}{\gamma_c}-0.365\right)} \quad (3.31)$$

Table 3.7 Applicative conditions of Equation (3.31).

Parameter	Range
L/G	3.5-15.4
h_{ai}/h_{Li}	0.4-1.9
a_t.Z	84-262
γ_L/γ_c	0.8-3.2

The air and solution outlet enthalpies from the absorber and regenerator are calculated by using Equations (3.32) and (3.33), respectively.

$$h_{ao} = (1 - \varepsilon_h) \cdot h_{ai} + \varepsilon_h \cdot h_{eq} \quad (3.32)$$

$$h_{so} = \frac{G}{L_o} \cdot h_{ai} + \frac{L_i}{L_o} \cdot h_{si} - \frac{G}{L_o} \cdot h_{ao} \quad (3.33)$$

The c-source code of the Simulink models of the absorber and regenerator can be found in Appendix (A) and Appendix (B).

3.3.3 Modelling of the evaporative cooler

In order to predict the outlet air temperature of the evaporative cooler, the actual air vapour pressure (e_a) and the air saturation vapour pressure (e_{sa}) are calculated by using Equations (3.34) and (3.35), respectively (ASHRAE 2009; Martinez 1994).

$$e_a = (w \times 101.325)/(0.621945 + w) \quad (3.34)$$

$$e_{sa} = at_a^3 + bt_a^2 + ct_a + d \quad (3.35)$$

where, *a*, *b*, *c*, and *d* are constants with values of 6.6×10^{-4}, 4.6×10^{-3}, 4.58×10^{-1} and 6.63, respectively. For pressure units conversion, Equation (3.35) must be multiplied by 0.1. The relative humidity of the air is given by Equation (3.36). The wet-bulb

temperature can be determined by using Equation (3.37), in which the air vapour pressure at the wet-bulb temperature can be determined by Equation (3.35) (Martinez 1994).

$$\mathrm{RH}(\%) = \frac{\mathrm{e_a}}{\mathrm{e_{sa}}} \times 100 \tag{3.36}$$

$$t_{wb} = t - \frac{(e_{sw} - (RH/100)e_s)}{k \cdot p_{atm}} \tag{3.37}$$

where, k is a constant (6.53×10^{-4}), p is the atmospheric pressure, and e_{sw} is the air vapour pressure at the wet-bulb temperature. An iteration subroutine must be used to solve these equations.

The temperature of the air leaving the evaporative cooler is given by Equation (3.38).

$$t_{ao} = t_{ai} - \varepsilon(t_{ai} - t_{wb,i}) \tag{3.38}$$

where, t_{ao} is the outlet air temperature, t_{ai} is inlet air temperature, $t_{wb,i}$ is the inlet air wet-bulb temperature, and ε is the effectiveness of the evaporative cooler.

3.3.4 Modelling of the heat exchangers

Counter-current flow heat exchangers are used in the proposed solar-assisted liquid desiccant dehumidification air-conditioning system, and the classical ε-NTU method is used to model these heat exchangers (Incropera and DeWitt 1990). The effectiveness of the heat exchanger is defined as:

$$\varepsilon = q/q_{\max} \tag{3.39}$$

where, q and q_{max} are the actual and maximum heat that can be transferred across the heat exchanger, which can be calculated by using Equations (3.40) and (3.41), respectively.

$$q = \varepsilon \cdot C_{min}(t_{hi} - t_{ci}) \tag{3.40}$$

$$q_{max} = C_{min}(t_{hi} - t_{ci}) \tag{3.41}$$

where, t_{hi} is the inlet temperature of the hot stream, t_{ci} is the inlet temperatures of the cold stream, and C_{min} is the minimum heat capacity rate. Equations (3.42) and (3.43) are used to calculate the minimum heat capacity rate and the maximum heat capacity rate, respectively.

$$C_{min} = \min(C_h, C_c) \tag{3.42}$$

$$C_{max} = \max(C_h, C_c) \tag{3.43}$$

where, C_C is the cold stream heat capacity rate, and C_h is the hot stream heat capacity rate.

The effectiveness of the heat exchanger can be calculated by Equation (3.44).

$$\varepsilon = \frac{1-\exp[-NTU(1-C_r)]}{1-C_r \cdot \exp[-NTU(1-C_r)]} \tag{3.44}$$

where, C_r is heat capacity rate ratio, and NTU is number of transfer units, which can be calculated by Equations (3.45) and (3.46), respectively.

$$C_r = C_{min}/C_{max} \tag{3.45}$$

$$NTU = UA/C_{min} \tag{3.46}$$

The effectiveness of the heat exchanger is calculated by Equation (4.47) if the value of C_r is equal to zero.

$$\varepsilon = 1 - exp(-NTU) \tag{3.47}$$

The heat transfer coefficient (UA) value needs to be calculated to obtain the number of transfer units (NTU). Therefore, the logarithmic mean temperature difference method is used to predict the *UA* value at the design condition as follows.

$$LMTD = \frac{(t_{hi} - t_{co}) - (t_{ho} - t_{ci})}{\ln\left(\frac{t_{hi} - t_{co}}{t_{ho} - t_{ci}}\right)} \quad (3.48)$$

$$Q = UA\ (LMTD) \quad (3.49)$$

Or,

$$UA = \frac{\dot{m} \cdot c_p \cdot \Delta t}{LMTD} \quad (3.50)$$

where, t_{hi} and t_{ho} are the inlet and outlet temperatures of the hot stream, t_{ci} and t_{co} are the inlet and outlet temperatures of the cold stream, and c_p is the specific heat capacity.

3.3.5 Modelling of the cooling tower

The model of the cooling tower used was developed by Lebrun *et al.* (2004). In this model, the cooling tower is treated as a classical heat exchanger and modelled using the effectiveness-NTU method.

The air side energy balance is given by Equation (3.51):

$$Q = M_a \cdot \left(h_{a,ex} - h_{a,su}\right) = C_{af} \cdot (t_{wb,ex} - t_{wb,su}) \quad (3.51)$$

where, $t_{wb,ex}$ and $t_{wb,su}$ are the exit and supply wet-bulb temperatures of the air across the cooling tower, $h_{a,ex}$ and $h_{a,su}$ are the exit and supply enthalpies of the air across the cooling tower, and C_{af} is the air fictitious heat capacity rate which can be calculated by Equation (3.52).

$$C_{af} = M_a \cdot C_{p,af} \quad (3.52)$$

where, $C_{p,af}$ is the fictitious specific heat of air, and can be obtained by the following equation:

$$c_{p,af} = \frac{(h_{a,ex} - h_{a,su})}{(t_{wb,ex} - t_{wb,su})} \quad (3.53)$$

The refrigerant (the refrigerant in this particular case is water) side heat balance is represented by Equation (3.54).

$$Q = C_r \cdot (t_{r,su} - t_{r,ex}) \tag{3.54}$$

where, $t_{r,su}$ and $t_{r,ex}$ are the supply and exit temperatures of the refrigerant, and C_r is the refrigerant heat capacity rate.

The global heat transfer coefficient is calculated by Equation (3.55).

$$UA_{fic} = UA_{fic,dry,n} \cdot \left[\frac{M_w}{M_{w,n}}\right]^m \cdot \left[\frac{M_a}{M_{a,n}}\right]^n \cdot \frac{C_{p,af}}{c_{p,a}} \tag{3.55}$$

where, $M_{w,n}$ and $M_{a,n}$ are the mass flow rates of the water and air at the design conditions. m, n and $AU_{fic,dry,n}$ are coefficents. The effectiveness and the number of transfer units of the cooling tower can be calculated by Equations (3.56) and (3.57), respectively.

$$\varepsilon_{fic} = \frac{1-e^{-NTU_{fic}(1-\omega)}}{1-\omega \cdot e^{-NTU_{fic}(1-\omega)}} \tag{3.56}$$

$$NTU_{fic} = \frac{AU_{fic}}{C_{min}} \tag{3.57}$$

where, ω is the heat capacity rate ratio which is calculated by Equation (3.58). The minimum or maximimum heat capacity rate ($C_{min,max}$) can be calculcuated by Equation (3.59).

$$\omega = C_{min}/C_{max} \tag{3.58}$$

$$C_{min,max} = min, max(C_r; C_{af}) \tag{3.59}$$

3.3.6 Modelling of the solar water heating system

The model of the solar water heating system used was developed based on the fundamental equations presented in a number of references (Al-Rawahi 2011; Ben

Bacha *et al.* 2007; NSW Public Works Dept. 1993; Stine and Geyer 2001). The properties and parameters that are related to the solar collector are summarised in Table 3.8.

Table 3.8 Properties and orientation of the solar collector.

Parameters	**Value/ type/ location**
Solar collector type	Flat plate collector
Location	Sydney
Latitude angle ($\varphi°$)	33.87°S
Surface tilt angle ($\beta°$)	15º
Surface azimuth angle ($\gamma°$)	15º

Equation (3.60) is used for the correction of the earth's rotational perturbations.

$$SDT = ST + 4(L_{st} - L_{loc}) + E \tag{3.60}$$

where, L_{st} and L_{loc} are the local standard and local longitudes, *ST* is the standard time, and *E* is the equation of time which can be determined by Equation (3.61).

$$E = 229.2(7.5 \times 10^{-5} + 0.00186\ cosB - 0.03207\ sinB - 0.014625\ cos2B - 0.04089\ sin2B) \tag{3.61}$$

where, *B* is calculated as $(360\frac{n-1}{365})$ in which *n* is the day of the year.

In order to determine the useful solar energy from a solar collector, the following angles must be known.

The hour angle (w) and the declination angle (δ) can be calculated by Equations (3.62) and (3.63), respectively.

$$w = (360/24) \cdot \left(\frac{STD}{60} - 12\right) \tag{3.62}$$

$$\delta = 23.45 \sin(360 \frac{284+n}{365}) \quad (3.63)$$

The declination angle is the angular position of the sun at noon with respect to the plane of the equator. The incidence angle of the beam irradiance is calculated by Equation (3.64) (Stine and Geyer 2001).

$$\theta = \cos^{-1}(\sin\delta \sin\varphi \cos\beta + \sin\delta \cos\phi \sin\beta \cos\gamma + \cdots) \quad (3.64)$$

where, θ represents the angle of the beam radiation incidence to a surface.

Equation (3.65) is used to calculate the incident beam radiation on an inclined surface.

$$G_{inc} = I_b \cdot \cos\theta + \frac{I_d}{2}(1 + \cos\beta) + 0.2\frac{I_b+I_d}{2}(1 - \cos\beta) \quad (3.65)$$

where, I_d is the diffuse beam irradiance, and I_b is the direct beam irradiance on a horizontal surface.

Based on the Australian Solar Data (2006), the direct beam and the diffuse irradiance for the 15th and 16th of January, as an example, are shown in Fig. 3.4. By applying the above equations, the incident irradiance on the solar collector can be calculated. Fig. 3.5 shows that up to 700 W/m^2 incident irradiance could be obtained with the above-mentioned orientation.

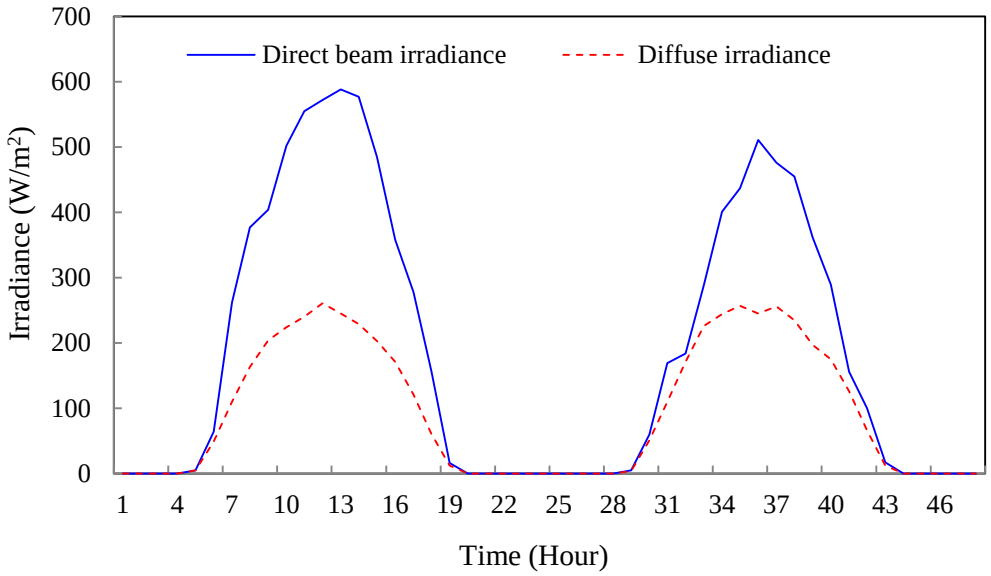

Fig. 3.4 Direct beam and diffuse irradiances for two summer days in Sydney.

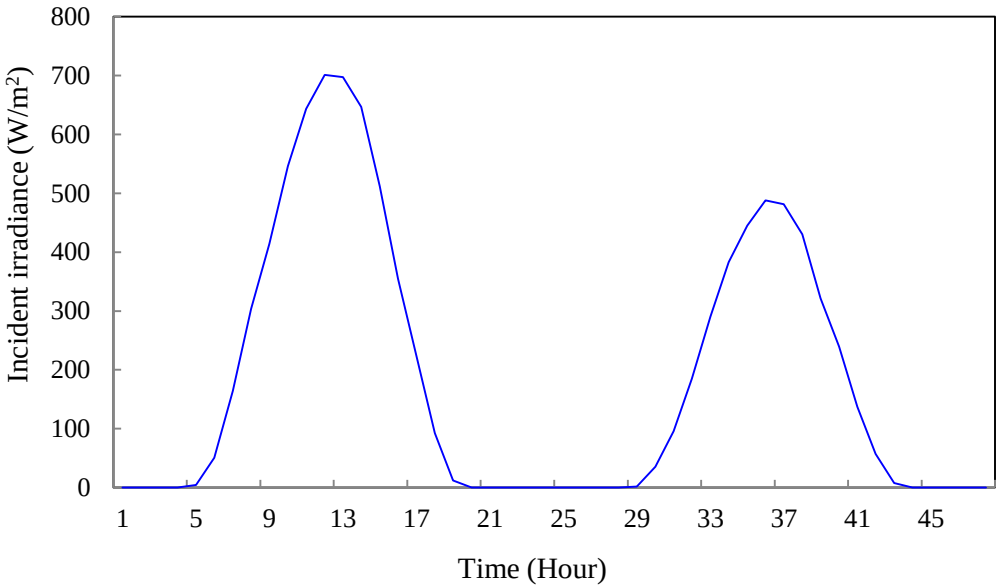

Fig. 3.5 Incident irradiance versus time.

Theoretically, the normal beam radiation through clear atmosphere can be calculated by using the method developed by Hottel (1976) as follows.

$$G_{bn} = G_{on}\left(a_o + a_1\, exp\left(-\frac{K}{cos\theta_z}\right)\right) \tag{3.66}$$

where, G_{on} is the normal extraterrestrial radiation, which can be calculated by Equation (3.67).

$$G_{on} = G_{sc}\left(1 + 0.033\, cos\frac{360n}{365}\right) \tag{3.67}$$

where, G_{sc} is the solar constant with a value of 1367 W/m^2.

Equations (3.68) to (3.70) can be used to calculate the correlation factors used in Equation (3.66).

$$a_o = \left[0.4237 - 0.00821\left(6 - A_e\right)^2\right].r_o \tag{3.68}$$

$$a_1 = \left[0.5055 + 0.00595\left(6.5 - A_e\right)^2\right].r_1 \tag{3.69}$$

$$K = \left[0.2711 + 0.01858\left(2.5 - A_e\right)^2\right].r_k \tag{3.70}$$

where, A_e is the elevation (in km) of the observer, and the correlation factors r_o, r_1, and r_k for different climates (at sea level) are given in Table 3.9.

Table 3.9 Correlations factors in Equations (3.68) to (3.70).

Climate Type	r_o	r_1	r_k
Tropical	0.95	0.98	1.02
Mid-latitude summer	0.97	0.99	1.02
Sub-arctic summer	0.99	0.99	1.01
Mid-latitude winter	1.03	1.01	1.00

By the implementation of this method for Sydney location, and choosing a mid-latitude summer climate, the normal beam radiation can be predicted, and the results are shown in Fig. 3.6.

It can be seen that up to around 700 W/m^2 of beam radiation can be obtained, reflecting that high solar energy can be utilised in the proposed system. In this study, the data of diffuse beam irradiance and direct beam irradiance is used in the modelling of the solar heating system.

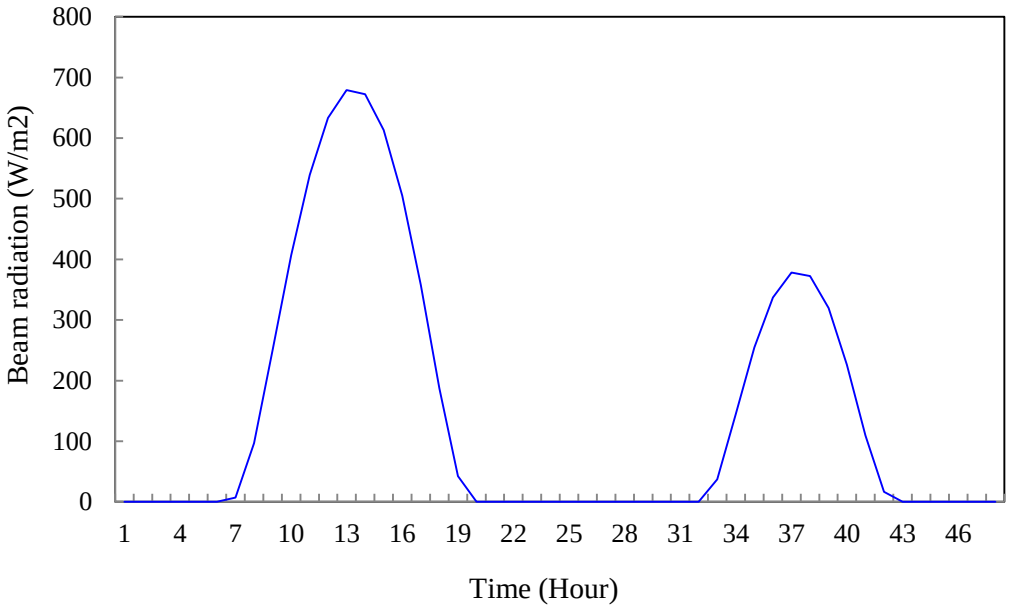

Fig. 3.6 Predicted beam radiation for clear days versus time.

The water temperature in the thermal storage tank is predicted by using Equation (3.71).

$$M\ c_{p,w}\ \frac{dt_{tank}}{dt} = \dot{m}_{w,c}\ C_{p,w}\ (t_{co} - t_{ci}) - \dot{m}_{w,ex}\ c_{p,w}\ (t_2 - t_1) + Q_{aux,h} \qquad (3.71)$$

where, $c_{p,w}$ is the specific heat capacity of the water, $m_{w,c}$ is the water flow rate across the collector, and $\dot{m}_{w,ex}$ is the water flow rate of the required heat load, t_{co} and t_{ci} are the temperatures across the collector, t_2 and t_1 are the temperatures of the heat load. In this equation, the term $\left[\dot{m}_{w,ex}\ c_{p,w}\ (t_2 - t_1)\right]$ represents the heat needed for the regeneration process.

3.3.7 Modelling of the pumps and air fans

The pumps and air fans are simply modelled based on the principle equations presented by Rishel (2001) and ASHRAE (2008). The pump and air fans were simulated by using Matlab Simulink as the shaft torque and the power consumption can be easily calculated by using the different sub-libraries in Simscape within Simulink. The pump efficiency is assumed as 80% in this study. The torque applied

to the shaft of the fan motor is a quadratic function of the speed as in Equation (3.72).

$$T = k' \cdot \omega^2 \tag{3.72}$$

where, ω is the motor speed, and k' is a coefficient that can be calculated based on the design power and speed of the motor by using Equations (3.72) and (3.73).

$$P_n = T_n \cdot \omega_n \tag{3.73}$$

where, P_n and ω_n are the design power and speed which are usually provided by the manufacturer. The fan used is assumed to be a centrifugal and backward-curved blade fan with an efficiency of 75%.

All above components models as well as system controllers are interconnected and integrated together to serve as a simulation platform in this study to evaluate the performance of the proposed solar-assisted liquid desiccant dehumidification air-conditioning system. The integration of the components models and system controllers are presented in Chapter 6.

3.4 Model validation

The performance of the key component models such as the absorber and regenerator was validated based on the experimental data obtained from Fumo and Goswami (2002). In the experimental setup, Fumo and Goswami (2002) used an absorber constructed from 25.4 cm diameter and 60 cm height acrylic tube that randomly filled by 2.54 cm polypropylene Rauschart Hiflow rings. Heating and cooling coils were used to provide the required test conditions. Fig. 3.7 shows a comparison between the results from the model simulation and experimental data in terms of the outlet air moisture-content, outlet desiccant concentration, outlet air temperature, outlet solution temperature and moisture condensation rate across the absorber.

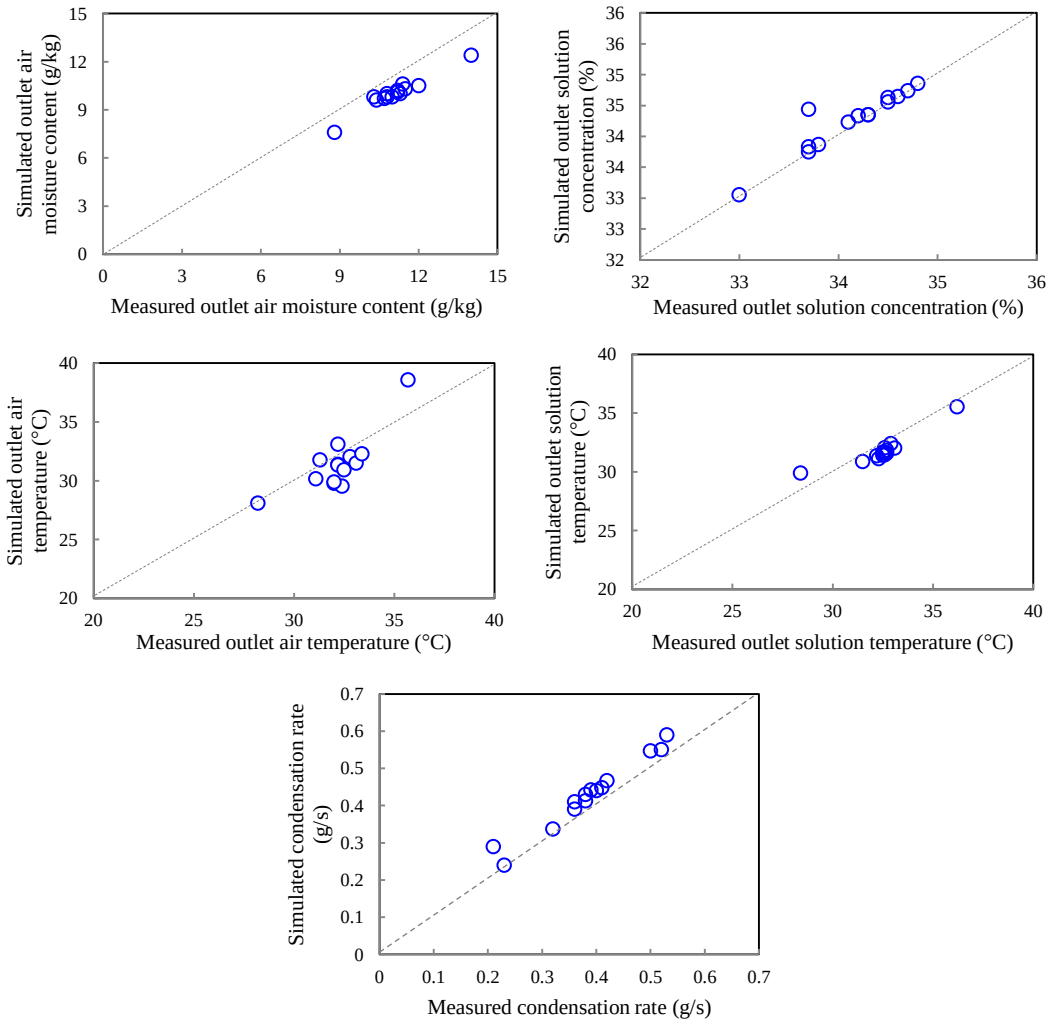

Fig. 3.7 Comparison between the results from model simulation and experimental tests – Absorber.

From Fig. 3.7, it can be seen that the model simulation results agreed well with the experimental data, demonstrating good performance prediction of the model used. The model validation results for the regenerator are presented in Fig. 3.8. A good agreement between the model simulation results and experimental data can also be observed.

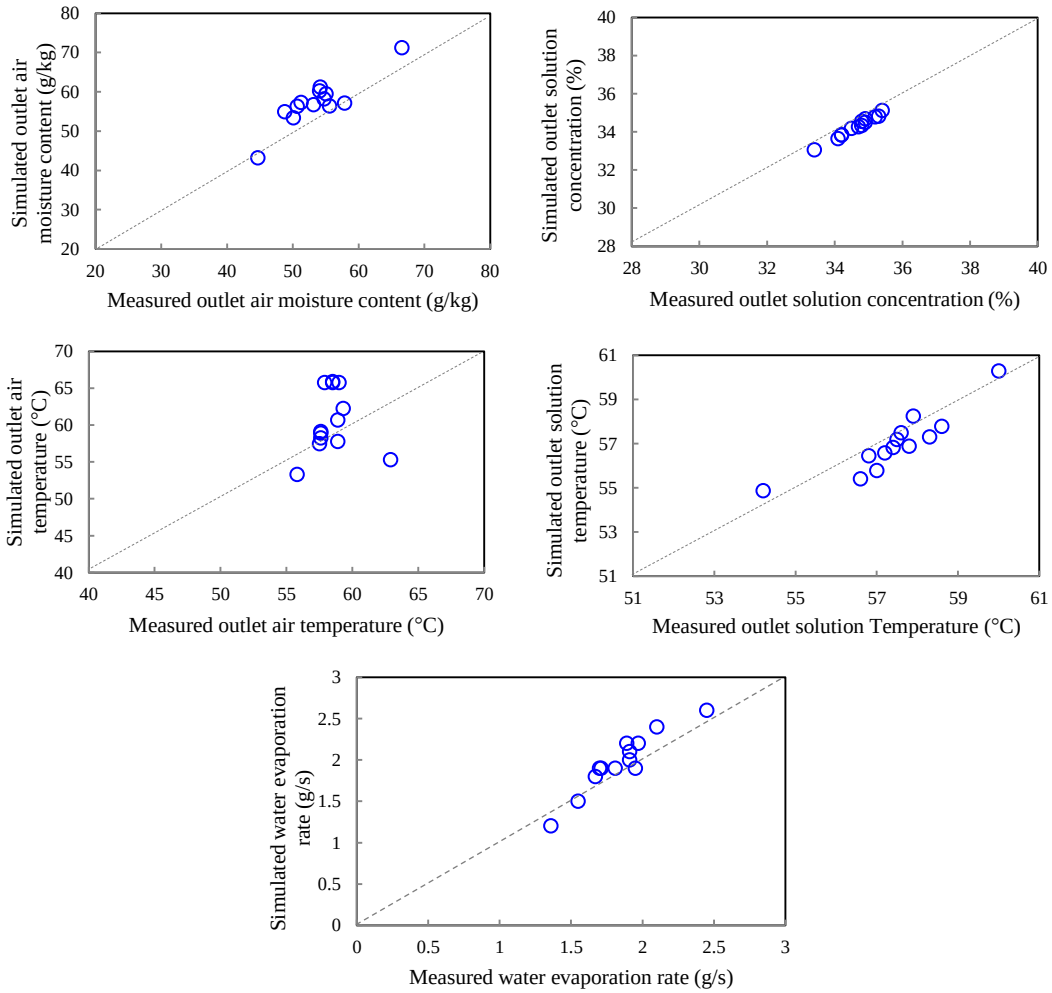

Fig. 3.8 Comparison between the results from model simulation and experimental tests – Regenerator.

3.5 Conclusion

The proposed solar-assisted liquid desiccant dehumidification air-conditioning system has been described. The models from different components including absorber, regenerator, evaporative cooler, solar heating system, cooling tower, heat exchangers, fluid pumps and air fans have been developed and selected, which will be used to develop a full-scale simulation platform for the proposed system to facilitate the system performance analysis and optimisation. The validation of major components (i.e. absorber and regenerator) indicated that these models can provide reliable estimates under ever-changing working conditions.

4 Design of the absorber and regenerator

4.1 Introduction

Based on the literature, the effects of the design parameters such as the height and diameter of the absorber and regenerator have not been extensively considered in the design of the liquid desiccant dehumidification air-conditioning systems. Some of the design parameters were chosen randomly and might not be suitable for a particular application. In this chapter, a simplified approach is presented to predict the design variables of the absorber and regenerator, including the column height, the cross-sectional area, the pressure drop across both dry (i.e. no liquid flow) and wetted (i.e. with liquid flow) columns, the weight of the column, and the quantity of the required packings. Developing an appropriate model is quite useful to estimate the maximum design parameters required in the proposed solar-assisted liquid desiccant air-conditioning system.

4.2 Appropriate sizing of the absorber and regenerator

The proposed approach has been built based on the key parameters stated in Table 4.1.

Table 4.1 Main parameters used in the design approach.

Parameters	Description
L	liquid specific flow rate (kg/m^2.s)
G	gas specific flow rate (kg/m^2.s)
Q_v	volumetric flow rate (m^3/s)
ρ_G, ρ_L	gas and liquid densities (Kg/m^3)
μ_L, μ_G	liquid and gas viscosities (Pa.s)
D_f	gas diffusion coefficient (m/s)
F_p	packing factor (m^{-1})
F_{pd}	dry packing factor (m^{-1})
d_p	particle diameter (m)
ε	void fraction (%)
D_h	hydraulic diameter (m)
a	surface area of packings (m^2/m^3)
F_f	flooding factor (%)

The hydraulic diameter of the particles (D_h) can be calculated by using the following equation (Rautenbach 2009).

$$D_h = 4\,\varepsilon/a_t \tag{4.1}$$

Fig. 4.1 shows the developed approach of sizing the absorber and regenerator, to predict the height, diameter, and pressure drop. It can be seen the different steps that are required to size the absorber and regenerator in terms of inputs, correlations, etc.

4.2.1 Determination of the absorber and regenerator diameter

The determination of the diameter of the column is related to other parameters such as the packing type, packing properties, liquid flow rate, gas flow rate, and flooding rate. The column diameter can be simply calculated by using Equation (4.2).

$$D = 1.13A^{0.5} \tag{4.2}$$

where, A is the cross-sectional area, which can be calculated by Equation (4.3) (Richards 2000).

$$\mathrm{A} = m_G \left(\frac{\mathrm{kg}}{s}\right) / \mathrm{G_{opt}} \left(\frac{\mathrm{Kg}}{\mathrm{m^2}.s}\right) \tag{4.3}$$

where, m_G is the gas mass flow rate, and G_{opt} is the gas operation specific flow rate, which can be calculated by Equation (4.4) (Richards 2000).

$$G_{opt} = F_f \,.\, G_f \tag{4.4}$$

where, F_f is the flooding factor which usually ranges from 50 to 75%, and G_f is the gas specific flow rate at flooding. The flooding factor (F_f) has a significant impact on calculating the packed bed diameter as it has a direct impact on determining the operation specific flow rate (G_{opt}). Fig. 4.2 presents the relation between the gas operation specific flow rate and the flooding factor at a gas specific flow rate at flooding (G_f) of 1.0 kg/m^2.s. It can be seen that the operation flow rate changed significantly (i.e. the difference is 0.25 kg/m^2.s) when the flooding factor is increased from 0.5 to 0.75.

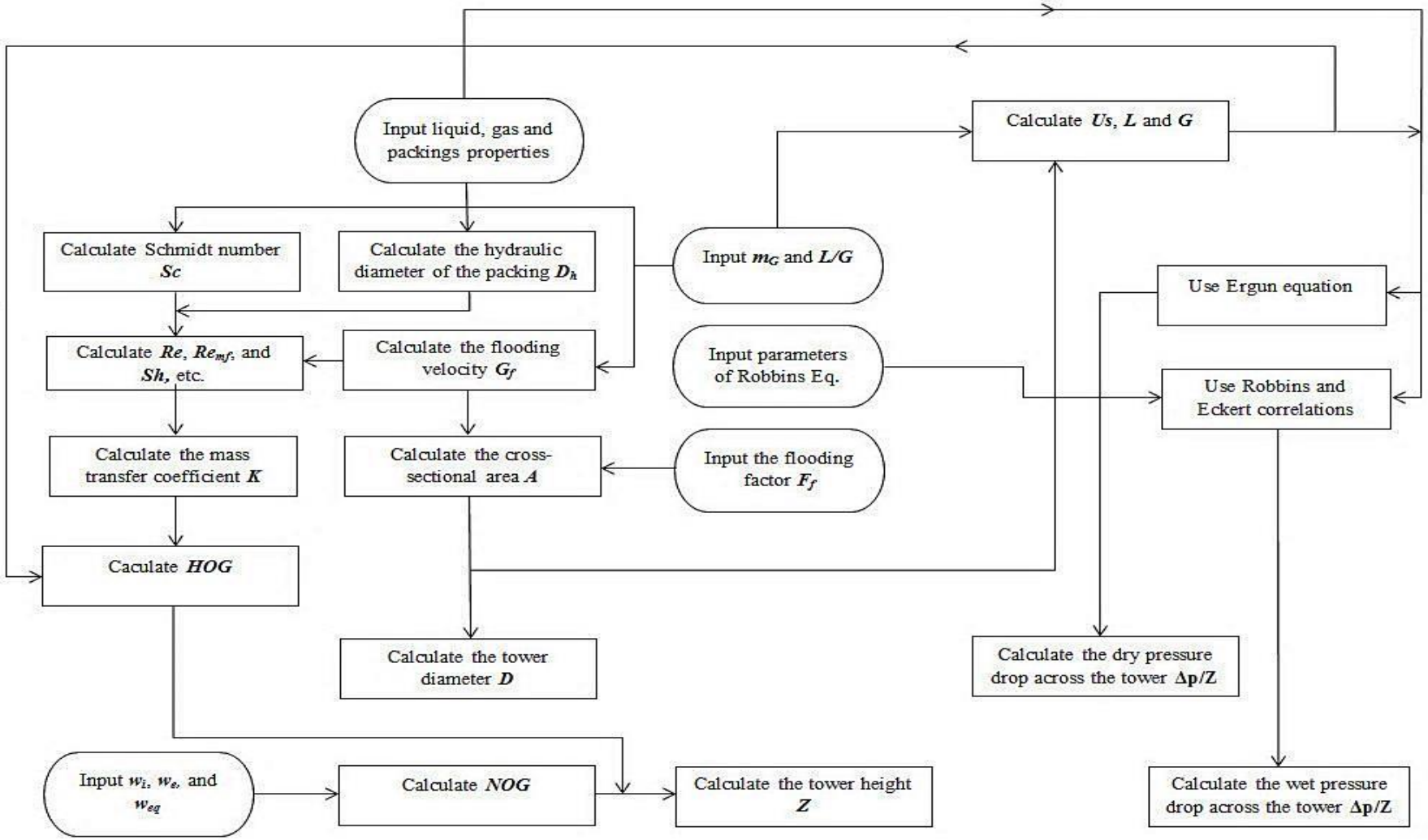

Fig. 4.1 Flow diagram of sizing the absorber and the regenerator.

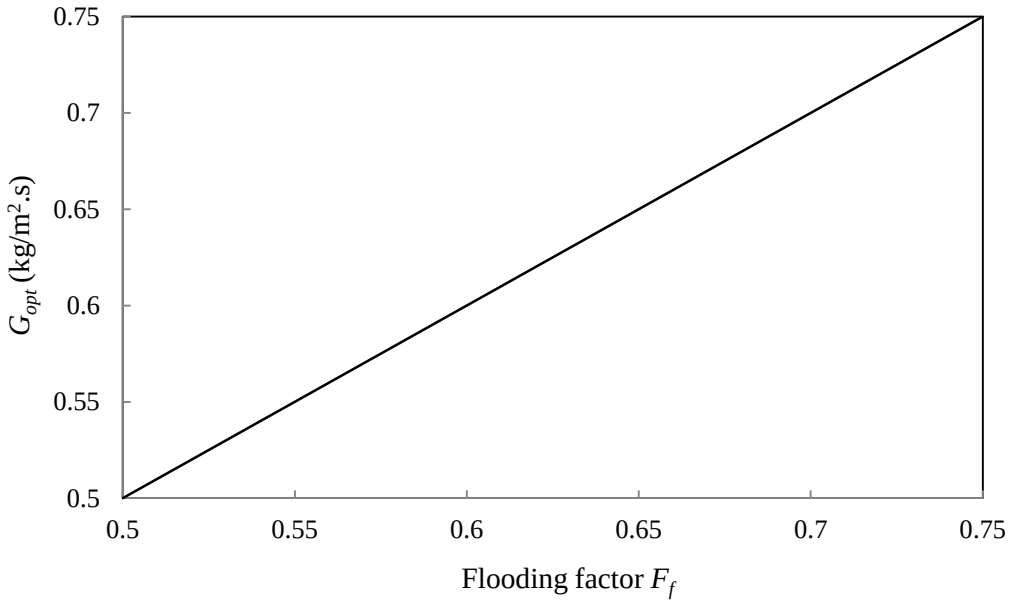

Fig. 4.2 Effects of the flooding factor on the operation flow rate.

In Fig. 4.2, it is worthwhile to mention that the gas operation specific flow rate coincidentally equals to the flooding factor as the gas specific flow rate at flooding is 1 kg/m^2.s. In order to calculate the flooding specific flow rate (G_f), a correlation, as expressed in Equation (4.5), developed by Eckert (1961 cited in Piche *et al.* 2001) is used.

$$\log(y) = -0.289\log^2(x) - 1.081\log(x) - 1.682 \tag{4.5}$$

where, the variables x and y can be calculated by using Equations (4.6) and (4.7), respectively.

$$x = \left(\frac{U_L}{U_{Gf}}\right)\left(\frac{\rho_G}{\rho_L}\right)^{0.5} \tag{4.6}$$

$$y = \frac{U_{Gf}^2}{g}\left(\frac{\rho_G}{\rho_L}\right)\left(\frac{\rho_w}{\rho_L}\right)\mu_L^{0.2}\,F_p \tag{4.7}$$

where, g is the acceleration of gravity (9.81 m/s^2), U_{Gf} is the gas superficial velocity at flooding (m/s), ρ_w is the water density, and U_L is the liquid superficial velocity (m/s).

The pressure drop at the flooding can be calculated by using Equation (4.8) (Kister *et al.* 2008).

$$\Delta p_f = 0.12 F_p^{0.7} \tag{4.8}$$

where, F_p is the packing factor.

The normal packing factor (F_p), dry packing factor (F_{pd}) which will be used later in the Robbins correlation, and useful properties of various packings can be found in (Kister *et al.* 2008).

Fig. 4.3 illustrates the flooding velocity and pressure drop of two types of packings. It can be found that the plastic Pall Rings packings produce higher flooding velocity when compared with the ceramic Pall Rings packings. When designing the packing bed using these types of packings, the flooding velocity can be taken directly from Fig. 4.3.

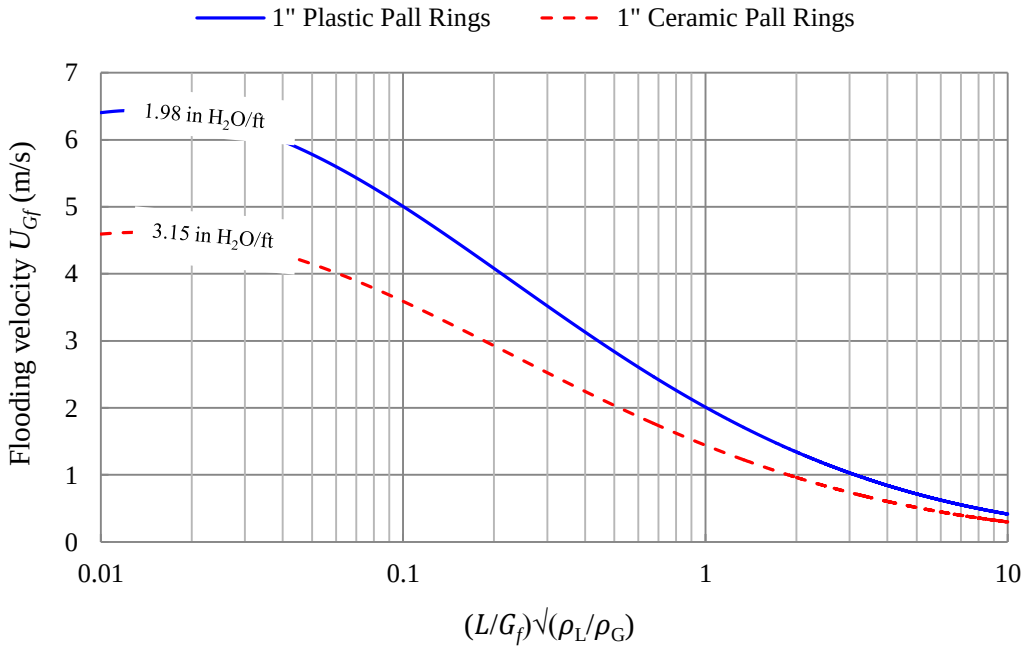

Fig. 4.3 Velocity and pressure drop at flooding in a packed bed using two types of packings.

Once the flooding velocity (U_{G_f}) is calculated, the specific flooding velocity (G_f) can be obtained by applying the following equation.

$$G_f = U_{G_f}\,\rho_G \tag{4.9}$$

Hence, the cross-sectional area and the diameter of the column can be obtained. Fig. 4.4 presents the effect of the packing factor (F_p) on the flooding pressure drop (Δp_f). It can be seen that choosing packings with high packing factor leads to a high flooding pressure drop.

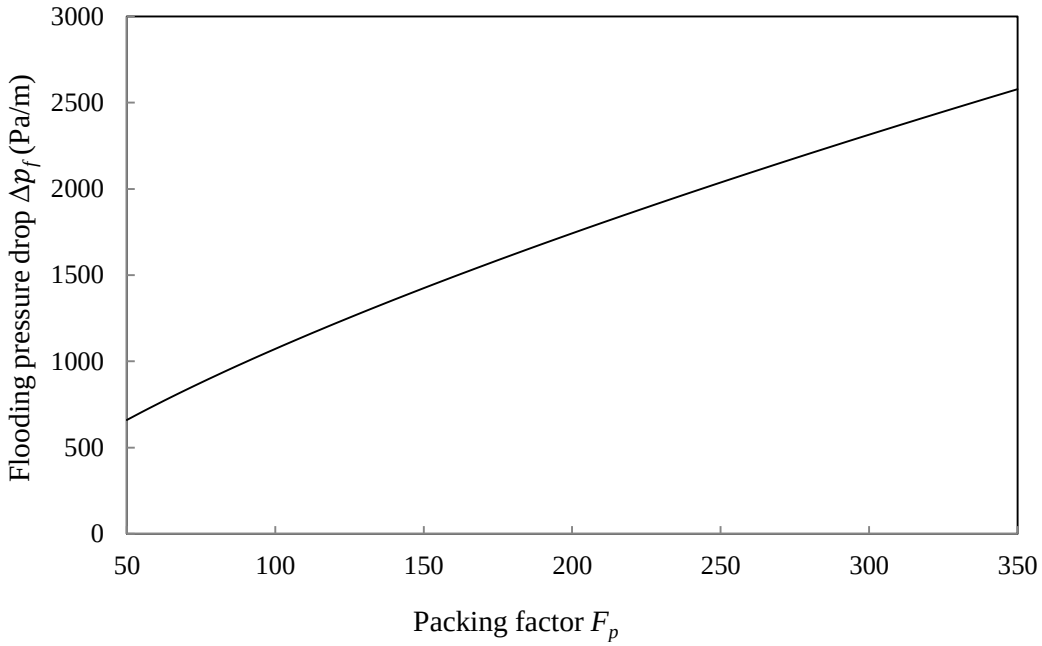

Fig. 4.4 Flooding pressure drop versus packing factor.

4.2.2 Determination of the absorber and regenerator height

The packed bed height can be calculated by using the following equation (Billet 1995 cited in Liang *et al.* 2011).

$$Z(m) = \frac{G}{K_{OG}ap}\int_{y_1}^{y_2}\frac{dy}{(1-y)^2\,(y-y_{eq})} = HOG\cdot NOG \tag{4.10}$$

where, Z is the column height, K_{OG} is the gas-phase overall mass transfer coefficient ($\frac{g.mol}{hr.m^2.Pa}$), p is the pressure of the system, a is the specific surface contact area, y_1, y_2

and y_{eq} are the inlet, outlet and equilibrium molar concentration, respectively. Equation (4.10) can be re-written as Equation (4.11) in order to be more suitable for desiccant dehumidification applications.

$$Z(m) = \frac{G}{K_{OG}a.\rho_G} \int_{w_i}^{w_o} \frac{dw}{(1-w)^2\,(w-w_{eq})} = HOG \cdot NOG \tag{4.11}$$

where, *NOG* is the number of transfer units and represents the integral term in Equations (4.10) and (4.11), and *HOG* is the height of transfer units and represents the fractional term in Equations (4.10) and (4.11). The mass transfer coefficient (K_{OG}) can be calculated by using Equation (4.12).

$$Sh = k_{OG}.\frac{l}{D_f} \tag{4.12}$$

where, *l* is the characteristic length of the packing, and *Sh* is the Sherwood number which can be calculated by using Equations (4.13)-(4.17) (Gnielinski 1980 cited in Groenewold and Tsotsas 1999).

$$Sh = \left(1 + 1.5\left(1 - \varepsilon_{mf}\right)\right) Sh_{sp} \tag{4.13}$$

$$Sh_{sp} = 2 + (sh_{lam}^2 + sh_{turb}^2)^{0.5} \tag{4.14}$$

$$sh_{lam} = 0.664\,\sqrt{Re_{mf}}\,Sc^{\frac{1}{3}} \tag{4.15}$$

$$sh_{turb} = \frac{0.037\,(\mathrm{Re})^{0.8}\,\mathrm{Sc}}{1+2.443\,(\mathrm{Re})^{-0.1}(\mathrm{Sc}^{\frac{2}{3}}-1)} \tag{4.16}$$

$$Re = \frac{Re_{mf}}{\varepsilon_{mf}} \tag{4.17}$$

where, *Re* is the Reynolds number, *Sc* is the Schmidt number, and the subscripts *mf*, *lam* and *turb* stand for minimum fluidisation, laminar flow and turbulent flow, respectively. The Reynolds number and the Schmidt number can be calculated by Equations (4.18) and (4.19), respectively.

$$Re = \rho\, U \frac{D_h}{\mu} \tag{4.18}$$

$$Sc = \frac{\mu_G}{d_p.\rho_G} \tag{4.19}$$

4.2.3 The pressure drop across the absorber and regenerator

In this section, three correlations are used to estimate the pressure drop across the column for two different cases, i.e. there is no liquid flow across the column by using Ergun equation, and there is a liquid flow in the column by using the Robbins and Eckert correlations. The Robbins correlation is suitable for low liquid flow rates (Kister 1992). Thus, it might be useful to use a general correlation to predict the pressure drop such as Eckert correlation.

Dry bed pressure drop

Ergun equation (cited in Nauman 2008) can be used to evaluate the pressure drop of the dry packed bed column as shown in Equation (4.20).

$$\frac{\Delta p}{Z} = \frac{150\ \mu\ (1-\varepsilon)^2\ U_s}{\varepsilon^3\ d_p^2} + \frac{1.75\ (1-\varepsilon)\rho\ U_s^2}{\varepsilon^3 d_p} \tag{4.20}$$

where, U_s is the superficial velocity of the gas entering the column, ρ is the density, d_p is the particle diameter, and ε is the void fraction.

Fig. 4.5 shows the pressure drop of the column when it is dry (i.e. no liquid flow) by implementing the Ergun equation and using 2.5 cm plastic Pall Ring packings. It is shown that a higher pressure drop will be developed in the column if a higher air velocity is used. The proposed solar-assisted liquid desiccant dehumidification air-conditioning system was designed to operate at a relatively low flow rate. Running the system at low flow rates can assist in eliminating the desiccant carryover problems that may result at high air flow rates.

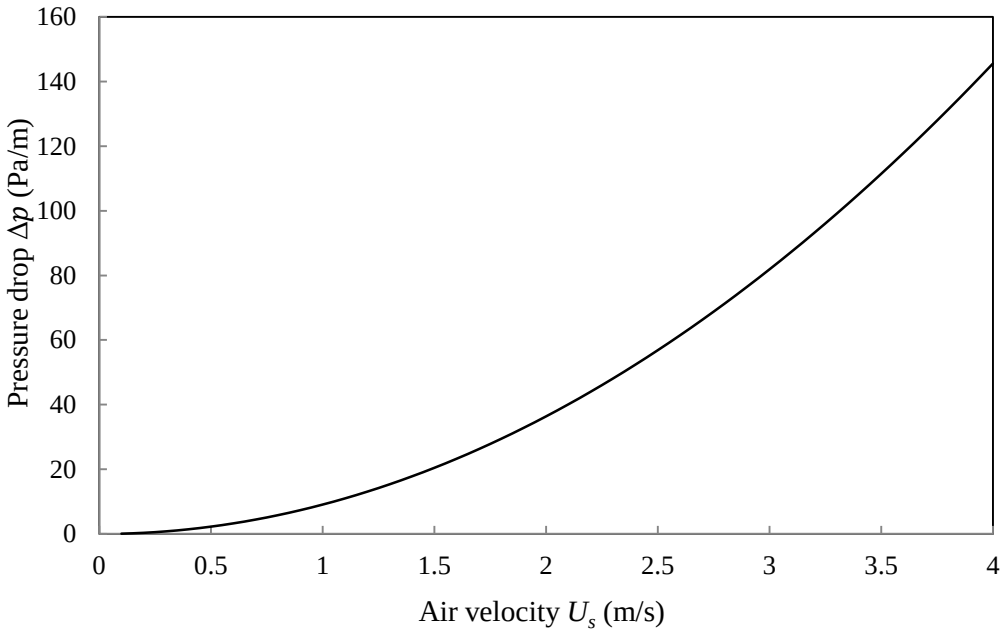

Fig. 4.5 Pressure drop across a dry packed bed randomly filled with plastic Pall Rings.

Fig. 4.6 shows the pressure drop versus the column height at an air velocity of 1.0 m/s. It can be found that, at a particular gas velocity, the relation between the pressure drop and column height seems to be linear. For example, the pressure drop is 13.6 Pa when the height is 1.5 m while it is 4.52 Pa when the height is 0.5 m.

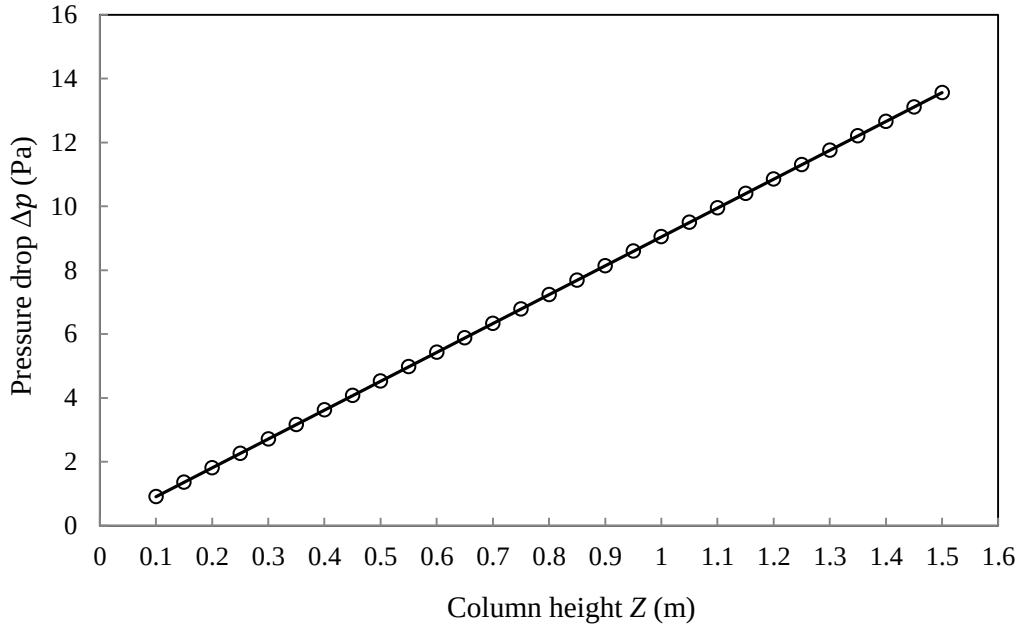

Fig. 4.6 Pressure drop versus column height of a dry packed bed.

Wet bed pressure drop

The Robbins correlation can be applied to estimate the pressure drop across the wet column. Attention must be paid to the dimensions used when implementing this equation because the units are in British measurement (Kister 1992).

$$\Delta p = C_3\, G_f^2\, 10^{C_4\, L_f} + 0.4 \left(\frac{L_f}{20000}\right)^{0.1} \left(C_3\, G_f^2\, 10^{C_4\, L_f}\right)^4 \qquad (4.21)$$

where, G_f and L_f are the gas and liquid loading factors which can be calculated by using Equations (4.22)-(4.25), and C_3 and C_4 are constants with values of 7.4×10^{-8} and 2.7×10^{-5}, respectively.

$$G_f = 986 \cdot G \left(\frac{\rho_g^{-0.5}}{3600}\right) \left(\frac{F_{pd}}{20}\right)^{0.5} \qquad (4.22)$$

$$L_f = L \left(\frac{62.4}{\rho_L}\right) \left(\frac{F_{pd}}{20}\right)^{0.5} \mu_L^{0.2} \quad \text{for } F_{pd} > 200 \qquad (4.23)$$

$$L_f = L \left(\frac{62.4}{\rho_L}\right) \left(\frac{F_{pd}}{20}\right)^{0.5} \mu_L^{0.1} \quad \text{for } F_{pd} > 15 \qquad (4.24)$$

$$L_f = L \left(\frac{62.4}{\rho_L}\right) \left(\frac{20}{F_{pd}}\right)^{0.5} \mu_L^{0.1} \quad \text{for } F_{pd} < 15 \qquad (4.25)$$

Fig. 4.7 shows the pressure drop of a packed bed filled with 2.5 cm plastic Pall Rings packings when using the above equations at an air specific flow rate of 1.0 kg/m^2.s and using different liquid flow rates. It can be seen that there is an increase in the pressure drop across the packed bed when increasing the fluid flow rate. Nevertheless, increasing the air flow rate will result in a higher pressure drop across the packed bed column.

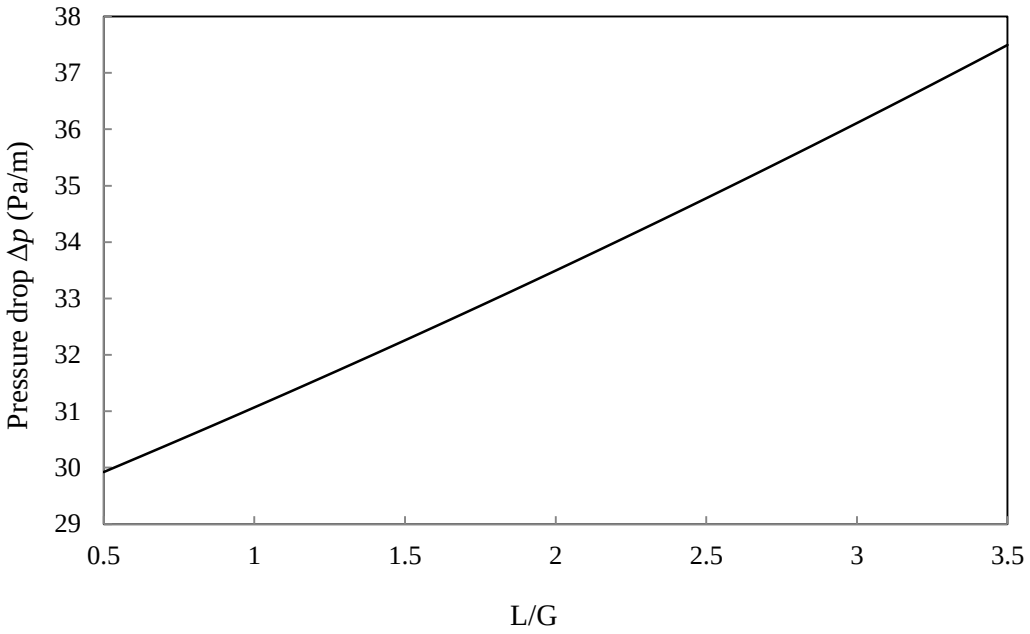

Fig. 4.7 Pressure drop across a wetted packed bed randomly filled with plastic Pall Rings.

Another correlation that can be used in predicting the pressure drop is the Eckert generalised pressure drop correlation (GPDC) (Kister 1992), and it is commonly used in this field. This correlation depends on two parameters, i.e. capacity and flow, which can be calculated by using Equations (4.26) and (4.27), respectively.

$$Capacity\ Parameter = CP = U_s \left(\frac{\rho_G}{(\rho_L - \rho_G)}\right)^{0.5} F_p^{0.5}\, \nu^{0.05} \qquad (4.26)$$

$$Flow\ Parameter = F_{LG} = \frac{L}{G}\left(\frac{\rho_G}{\rho_L}\right)^{0.5} \qquad (4.27)$$

The pressure drop is the intersection between the capacity and flow parameters with respect to the pressure drop lines in the correlation chart shown in Fig. 4.8.

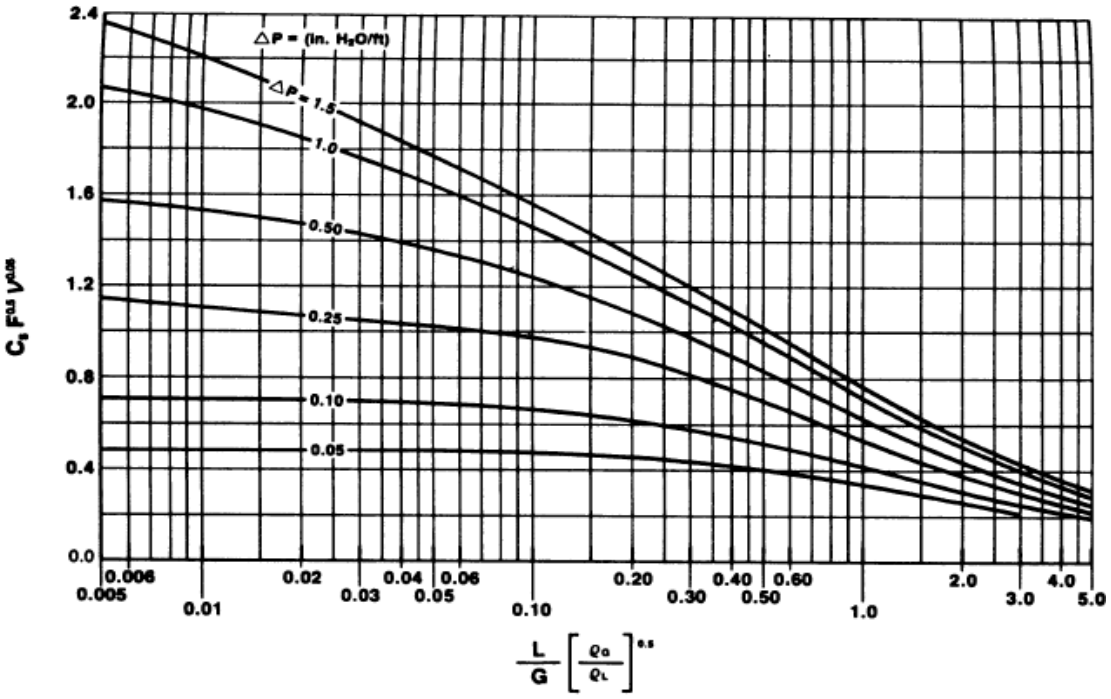

Fig. 4.8 Eckert generalised pressure drop correlation GPDC (Kister 1992).

The regenerator simply releases the absorbed moisture-content due to the absorption process, from the liquid desiccant to a scavenging air stream. Therefore, by assuming the maximum moisture evaporation rate to re-concentrate the liquid desiccant in the regenerator equals to the maximum moisture condensation rate in the absorber, at the same flow rate, the configuration design parameters (diameter and height) of the regenerator would be the same as that of the absorber.

4.3 The main results and discussion

The design parameters were modelled by using Excel. The packed bed used in this study is randomly filled with 1" random plastic Pall Rings packings. Table 4.2 summarises the main parameters used in the model, and the results are summarised in Table 4.3.

The air flow rate has been chosen based on the maximum cooling load required for a solar decathlon house which will be described in detail in Chapter 6.

Table 4.2 Main parameters of the absorber and regenerator used.

Parameter	Value
Bed density	71 kg/m^3
Water Density	1000 kg/m^3
Gas density	1.17 kg/m^3
Liquid density	1210 kg/m^3
Gas viscosity	1.5×10^{-5} Pa.s
Liquid viscosity	0.0053 Pa.s
Packing factor (F_p)	180 m^{-1}
Dry packing factor (F_{pd})	180 m^{-1}
gravitational constant	9.81 m/s^2
Gas diffusion coefficient	1.40×10^{-5} m/s
Particle diameter	0.0256 m
Hydraulic diameter	0.039 m
Void fraction	90%
Flooding factor	50%
L/G	3.5
Air flow rate	0.315 kg/s

Table 4.3 Main results of the modelled design parameters.

Parameter	Value
Tower diameter	≅0.4 m
Tower height	≅0.6 m
Pressure drop (no liquid flow)	41.4 Pa/m: (Ergun equation)
Pressure drop (with liquid flow)	606 Pa/m: (Robbins correlation)

Fig. 4.9 shows the pressure drop measured by using the Eckert correlation. The pressure drop across the column is about 0.76 inch H_2O/ft (621 Pa/m). This is the design pressure drop, and it is expected to be lower when the system is in operation. For example, the pressure drop across the packed bed would be 33.6 Pa/m if the air specific flow rate is 0.8 kg/m^2.s.

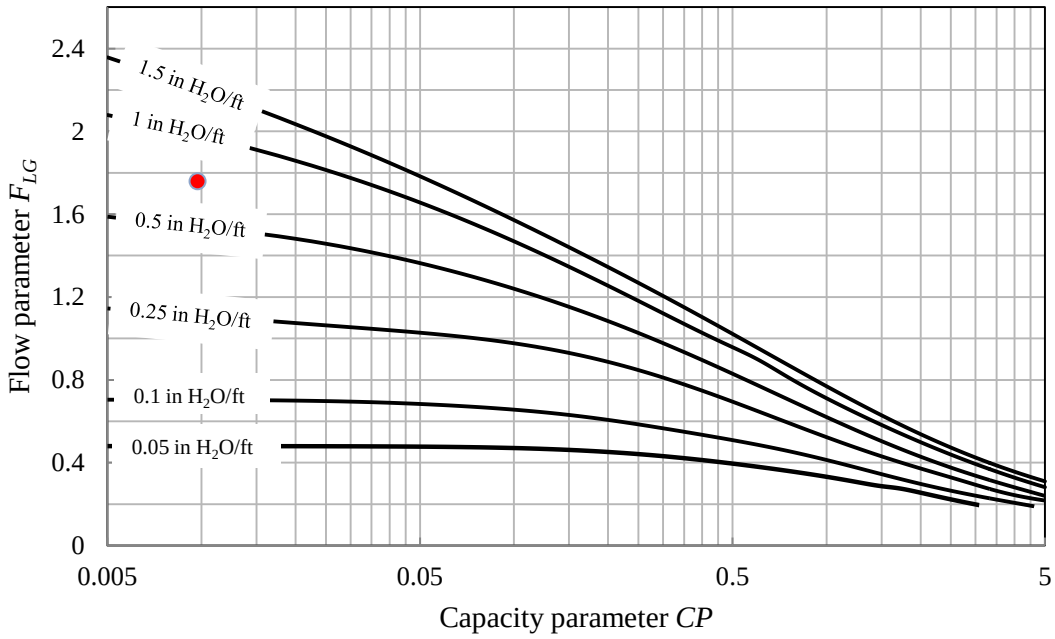

Fig. 4.9 Design pressure drop across the packed bed by using Eckert correlation.

The results indicate that a good agreement between the pressure drops of the column measured by the Robbins and Eckert correlations could be achieved. Measuring the pressure drop is quite important in designing the packed bed as it affects the air flow across the absorber and regenerator, and hence the selection of appropriate air fans.

It might be useful to estimate the weight of the column when designing the absorber and regenerator in terms of measuring the flexibility of transporting these components. The weight can be simply calculated by using Equation (4.28).

$$w_t = V \cdot \rho_p \tag{4.28}$$

where, w_t is the weight of the dry column, V is the volume of the absorber or the

regenerator, and ρ_p is the packing density.

The total number of packings required to fill the absorber or the regenerator is calculated by Equation (4.29).

$$Np = Q_p \left(\frac{1}{m^3}\right) \cdot V \tag{4.29}$$

where, N_p is the number of packings, and Q_p is the quantity of packings per cubic meter (i.e. usually provided by the manufacturer).

By applying the above equations, the results indicate that the weight of the packed bed is about 5.35 kg. This is the weight of dry packed bed, and it is expected to be higher when there is liquid flow. The total number of packings required is about 3830 pieces.

The previously constructed approach facilitates the estimation of the required size of the absorber and regenerator at the design stage. However, the absorption and regeneration processes in the absorber and regenerator are affected by other operational parameters including the solution temperature, the air temperature, the humidity of the air, and the solution concentration so that lower or higher design parameters may be used if these parameters are optimised. Accordingly, a parametric study will be carried out in Chapter 5.

4.4 Conclusion

In this chapter, a simplified approach was developed to predict the key design parameters including the height, diameter, and pressure drops of the absorber and regenerator within the proposed air-conditioning system. The main results showed that the maximum height and the maximum diameter could be 0.6 m and 0.4 m, respectively, which were found sufficient to specify the required absorbing or

regeneration processes for the proposed solar-assisted liquid desiccant dehumidification air-conditioning system. The study showed that 2.56 cm plastic Pall Rings packings offer low pressure drops. Three correlations were used to estimate the pressure drop across the packed bed. Ergun equation was used to calculate the pressure drop when the packed bed is dry (i.e. no liquid flow). Robbins and Eckert correlations were used to calculate the pressure drop when the packed bed is wetted (i.e. with liquid flow). The results showed that there is a good agreement between the pressure drops calculated by using the Robbins and Eckert correlations.

5 Parametric study

5.1 Introduction

The performance of the proposed solar-assisted liquid desiccant dehumidification air-conditioning system mainly depends on the performance of the regenerator and absorber used. In order to understand the effects of different design and operational parameters on the performance of the absorber and regenerator, a parametric study is presented in this chapter. The operational parameters include the liquid to air specific mass flow rate ratio (L/G), the inlet solution temperature (T_{si}), the inlet solution concentration (X_{si}), the inlet air temperature (T_{ai}), and the inlet air moisture-content (w_i). The design parameters considered include the dry specific surface area of packings (a_t), the absorber and regenerator height (Z), and the absorber and regenerator diameter (D).

5.2 Parametric study for the absorber

In this study, the parametric study was performed based on changing one variable only each time while keeping other variables constant. The parametric study was conducted by using the models of the absorber and regenerator validated in Chapter 3. Table 5.1 summarises the major tests performed in the absorber parametric study and the test conditions used.

Table 5.1 Ranges of the variables used in the absorber parametric study.

Parameter		Value range	L/G	T_{ai} (°C)	T_{si} (°C)	X_{si} (%)	w_i (kg/kg)	a_t (m^{-1})	Z (m)	D (m)
Operational parameters	L/G	1-4	V*	25	25	35	0.018	210	1	0.5
	T_{ai}	25-35 (°C)	3.5	V	25	35	0.018	210	1	0.5
	T_{si}	25-35 (°C)	3.5	25	V	35	0.018	210	1	0.5
	X_{si}	30-40 (%)	3.5	25	25	V	0.018	210	1	0.5
	w_i	0.01-0.025 (kg/kg)	3.5	25	25	35	V	210	1	0.5
Design parameters	a_t	50-250 (m^{-1})	3.5	25	25	35	0.018	V	1	0.5
	Z	0.5-1.5 (m)	3.5	25	25	35	0.018	210	V	0.5
	D	0.5-1.5 (m)	3.5	25	25	35	0.018	210	1	V

* V stands for variable

These test values were chosen by taking into account the expected high ambient temperatures, the required regeneration energy, as well as the difficulty of cooling the solution during the hot summer days. Fig. 5.1 shows the variations of the outlet variables from the absorber with changing the ratio of the desiccant specific flow rate to air specific flow rate (L/G) while keeping the inlet air temperature (T_{ai}), the inlet solution temperature (T_{si}), the inlet desiccant concentration (X_{si}) and the inlet air moisture-content (w_i) at 25ºC, 25ºC, 35% and 0.018 kg/kg, respectively. It can be observed that the ratio of the liquid to air specific flow rate (L/G) has great impacts on the absorber performance, but increasing this ratio beyond 3.5 is meaningless as the change is not significant in the moisture condensation rate ($\dot{m}_{cond}$) and the absorber dehumidification effectiveness (ε_d). The pumping cost must be considered and balanced if further increasing the ratio of the specific liquid to air flow rate. The outlet solution temperature (T_{so}) slightly reduced when increasing L/G, which means that a higher regeneration temperature is required to heat the solution before entering

the regenerator. It is shown that the variation of the temperature is around 5°C when increasing L/G from 1.0 to 2.0, while the change after that (i.e. L/G increased from 2 to 3.85) is only 2.7°C. It is also shown that a higher L/G leads to less change in the concentration of the outlet liquid desiccant. For example, the outlet desiccant concentration is 34.68 % at L/G of 1.0, while it is 34.89 % at L/G of 3.5.

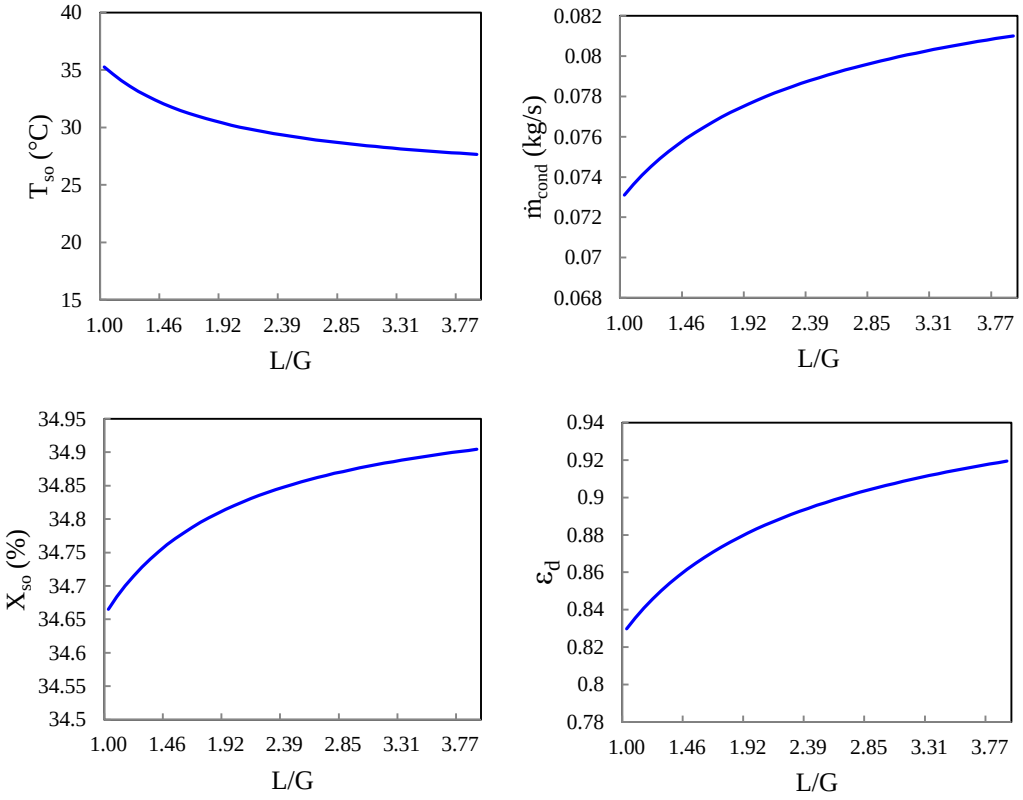

Fig. 5.1 Variation of outlet variables across the absorber with increasing solution to gas specific flow rate ratio.

The effects of changing the inlet solution temperature on the absorber behaviour are presented in Fig. 5.2. It is shown that a significant reduction in the dehumidification performance of the absorber resulted when increasing the inlet solution temperature (T_{si}). For example, the outlet air moisture-content (w_o) is about 7.4×10^{-3} kg/kg if the inlet solution temperature is 25°C, while it is around 0.012 kg/kg when the inlet solution temperature increased to 35°C. Therefore, the inlet solution temperature must be low enough to ensure the good dehumidification performance of the

absorber during the operational period of the liquid desiccant dehumidification air-conditioning system. From Fig. 5.2, it can also be found that the relation between the absorber inlet solution temperature and outlet solution temperature (T_{so}) is almost linear. This might be useful in decreasing the regeneration temperature required to re-concentrate the liquid desiccant. The increase of the inlet solution temperature also leads to better wettability (a_w) of the absorber. For instance, the wet surface area of packing was increased from 139 to 145.37 m^2/m^3, when the inlet solution temperature is increased from 25°C to 35°C.

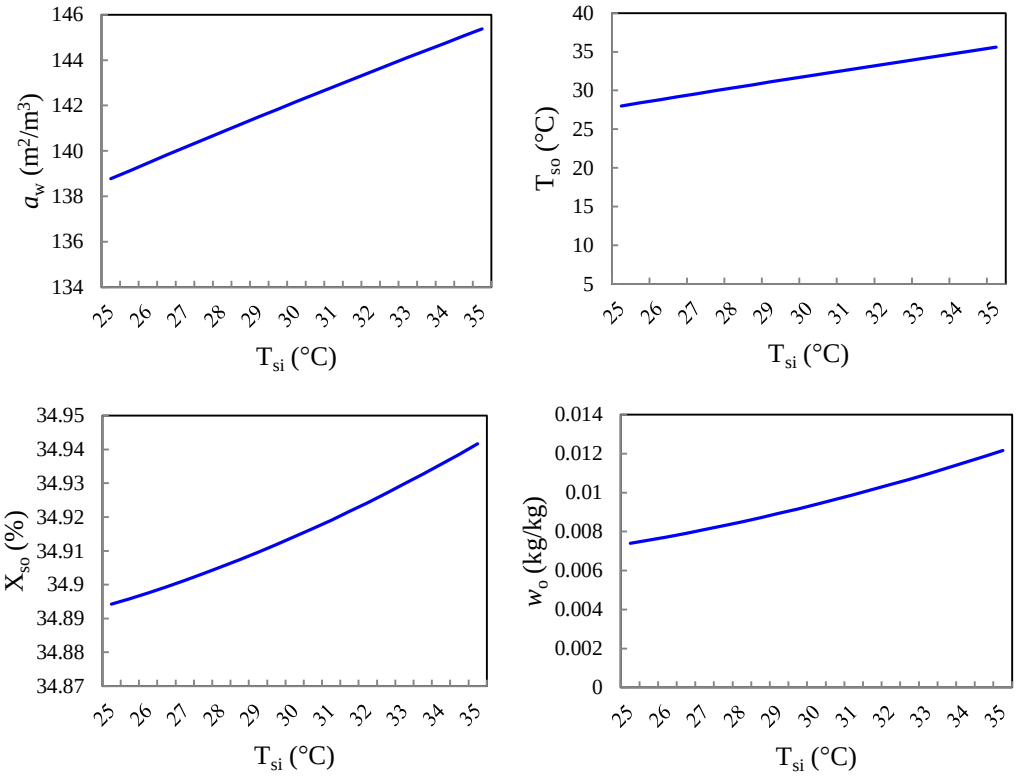

Fig. 5.2 Variation of outlet variables across the absorber with increasing the inlet solution temperature.

In general, increasing the inlet desiccant concentration can enhance the dehumidification performance of the absorber (i.e. the maximum concentration of LiCl solution should not be higher than 45% to avoid crystallisation problems), but this means that extra energy will be required to re-concentrate the liquid desiccant. Fig. 5.3 shows that, at the same inlet conditions, the condensation rate is about 0.062

kg/s, when the inlet solution concentration (X_{si}) is 30%, while it increases to about 0.095 kg/s when the inlet solution concentration increases to 40%. Nevertheless, the good dehumidification behaviour is still achievable when the inlet solution concentration is 35%. Therefore, the concentration of 35% of lithium chloride solution can be considered as a typical set-point in the proposed solar-assisted liquid desiccant dehumidification air-conditioning system. It is shown that the outlet solution temperature (T_{so}) increased due to the increase of the absorption rate when increasing the inlet desiccant concentration. From Fig. 5.3, it also can be seen that a less wettability is developed when a higher inlet desiccant concentration is employed, which means that the liquid desiccant flow rate may not be high enough in this case.

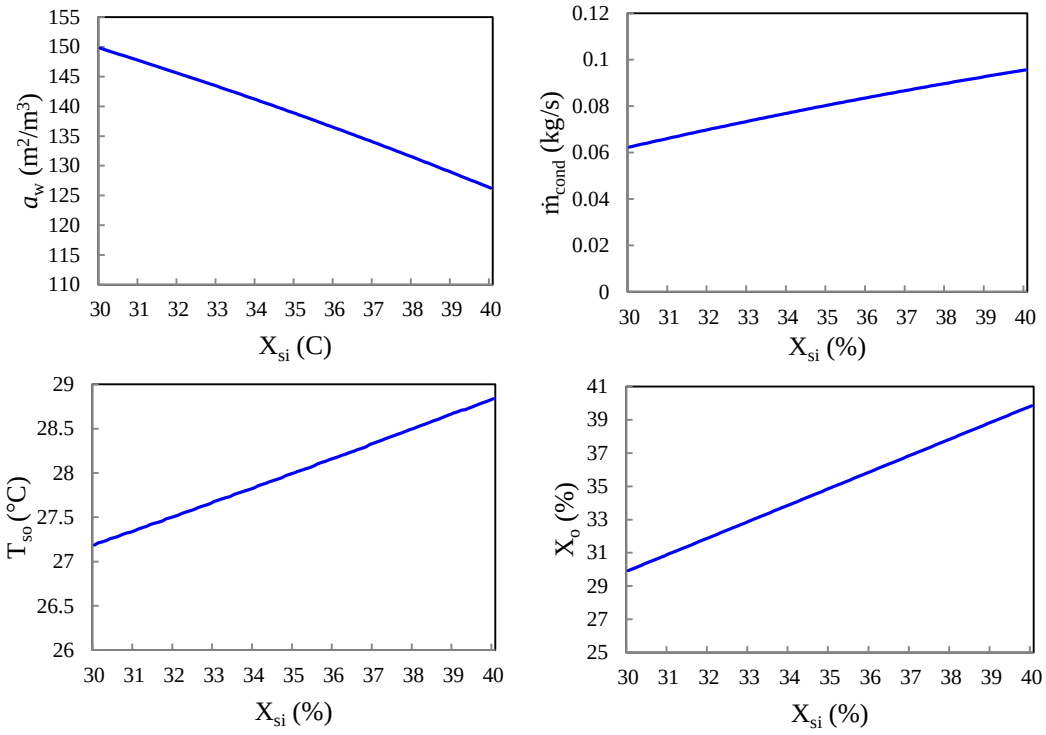

Fig. 5.3 Variation of outlet variables across the absorber with increasing the inlet solution concentration.

Fig. 5.4 illustrates the behaviour of the absorber when changing the height of the absorber. It is shown that a low dehumidification performance will result when

increasing the height of the absorber (Z) under the same inlet working conditions. This is because, increasing the absorber height requires a higher solution flow rate to provide an acceptable level of wettability, which means a higher pumping cost requirement. However, from Fig. 5.4, it can be found that excellent dehumidification performance can be achieved when the absorber height is in the range of 0.5-0.7 m. For instance, the condensation rate ($\dot{m}_{cond}$) is 0.0716 kg/s at the height of 0.6 m while it is about 0.0684 kg/s at the height of 1.5 m. It is worthwhile to notice that the difference in the concentration is not significant when increasing the absorber height. For example, the desiccant concentration difference is only 0.01% when the absorber height increases from 0.5 to 1.5 m.

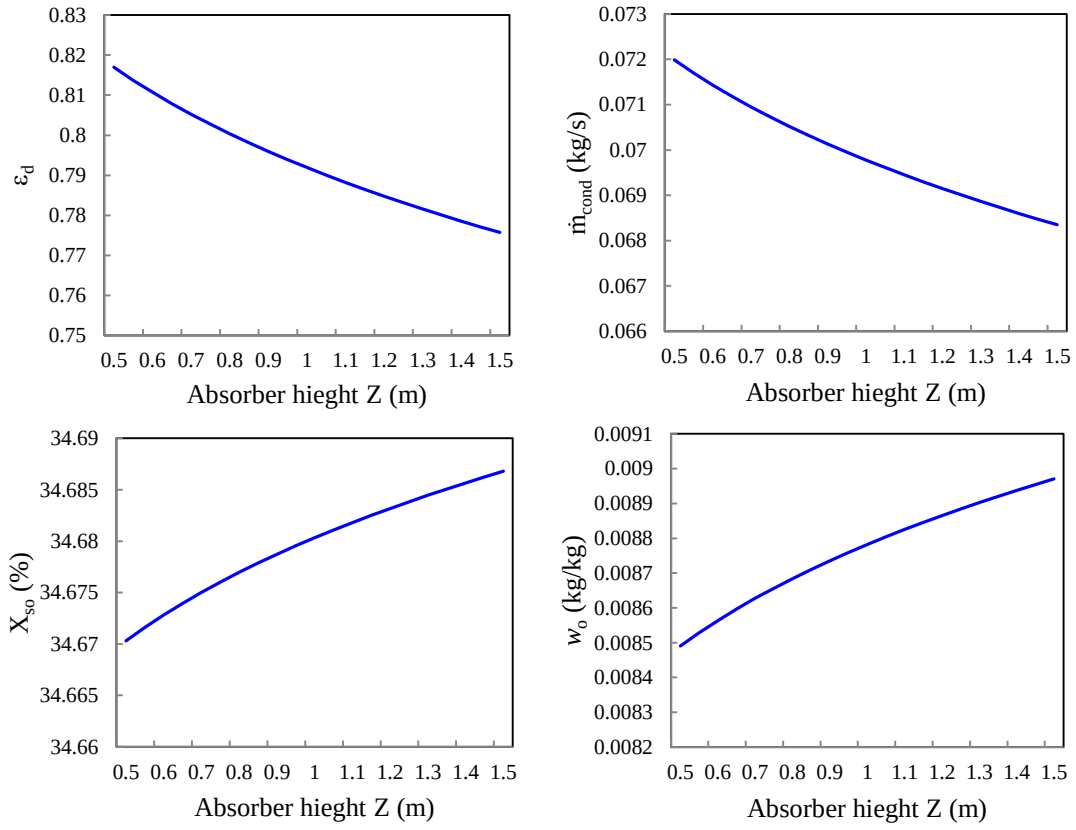

Fig. 5.4 Variation of outlet variables across the absorber with increasing the absorber height.

The effects of changing the absorber diameter are examined in Fig. 5.5. It can be found that the absorber effectiveness and water condensation rate increased slightly

when increasing the column diameter (D). In contrast, a smaller wetted surface area of packing (i.e. the reduction is about 64.88 m^2/m^3 when increasing the diameter from 0.05 to 1.5 m), and a weaker outlet solution concentration (X_{so}) will be resulted when increasing the absorber diameter under the same inlet solution flow rate. The change in the outlet solution concentration (X_{so}) is only about 7.6×10^{-4} % when increasing the absorber diameter.

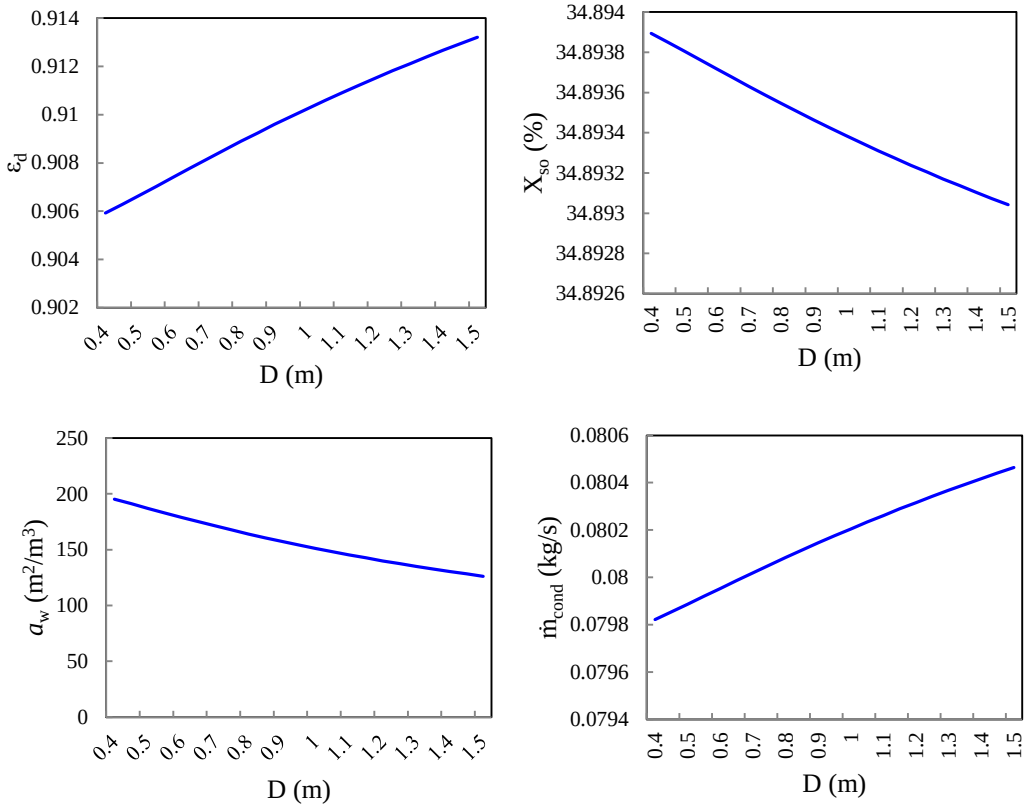

Fig. 5.5 Variation of outlet variables across the absorber with increasing the absorber diameter.

The effects of changing the inlet air moisture-content on the absorber performance are examined in Fig. 5.6. It is shown that, under the specified inlet conditions, the absorber can well dehumidify the processed air. For example, at the inlet air moisture-content of 0.025 kg/kg, the outlet air moisture-content is about 0.008 kg/kg. This reveals the high dehumidification ability of the absorber and implies that an evaporative cooler can efficiently provide the required cooling if it is utilised in

cooling the processed air after leaving the absorber due to the ability of controlling the humidity.

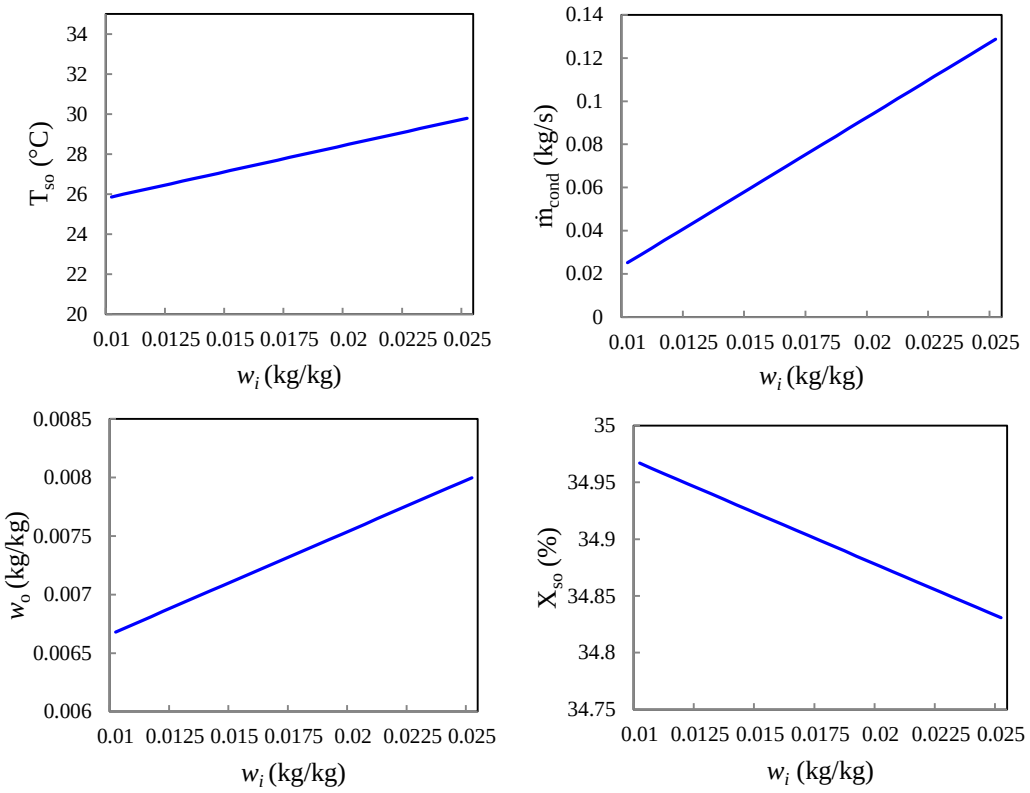

Fig. 5.6 Variation of outlet variables across the absorber with increasing the inlet air moisture-content.

Based on the above analysis, it can be concluded that using a diameter of 0.4 m and a height of 0.6 m as the design diameter and height of the absorber is sufficient to provide the required level of humidity reduction for the proposed solar-assisted liquid desiccant dehumidification air-conditioning system.

Table 5.2 summarises the variation of the absorber performance with the changes of each operational or design parameter. All parameters were found to have a direct impact on increasing or decreasing the humidity reduction. The inlet air moisture-content and the inlet desiccant concentration were found to have less impact on the dehumidification effectiveness. The design variables which are the dry specific surface area of packing (a_t), the absorber height (Z), and the absorber diameter (D)

do not have significant effects on the outlet solution temperature. The results show that changing the dry specific surface area of packing has a minimal effect on the absorber outlet solution temperature and outlet air temperature as well as the moisture condensation rate.

Table 5.2 Summary of the key findings from the absorber parametric study.

Variable	**Tested parameters**						
	T_{ao}	T_{so}	a_w	$\dot{m}_{cond}$	w_o	X_o	ε_d
↥ L/G	⇌	↧	↥	↥	↧	↥	↥
↥ T_{ai}	⇌	↥	⇌	↧	↥	↥	↥
↥ T_{si}	↥	↥	↥	⇌	↥	↥	↥
↥ X_{si}	⇌	↥	↧	↥	↧	↥	⇌
↥ a_t	⇌	⇌	↥	⇌	↧	↥	↧
↥ Z	↧	⇌	⇌	↧	↥	↥	↧
↥ D	↥	⇌	↧	↥	↧	↧	↥
↥ w_i	⇌	↥	⇌	↥	↥	↧	⇌

↥ Increase; ↧ decrease; ⇌ no or less impact

5.3 Parametric study for the regenerator

A similar parametric study was also performed for the regenerator. The ranges of the variables used in examining the regenerator performance are summarised in Table 5.3.

Table 5.3 Ranges of the variables used in the regenerator parametric study.

Parameter		Value range	L/G	T_{ai} (°C)	T_{si} (°C)	X_{si} (%)	w_i (kg/kg)	a_t (m^{-1})	Z (m)	D (m)
Operational parameters	L/G	1-3.5	V*	25	56	35	0.018	210	1	0.4
	T_{ai}	25-35 (°C)	3.5	V	56	35	0.018	210	1	0.4
	T_{si}	45-65 (°C)	3.5	25	V	35	0.018	210	1	0.4
	X_{si}	30-45 (%)	3.5	25	56	V	0.018	210	1	0.4
	w_i	0.015-0.03 (kg/kg)	3.5	25	25	35	V	210	1	0.4
Design parameters	a_t	50-250 (m^{-1})	3.5	25	56	35	0.018	V	1	0.4
	Z	0.3-1.5 (m)	3.5	25	56	35	0.018	210	V	0.4
	D	0.5-1.5 (m)	3.5	25	56	35	0.018	210	1	V

* V stands for variable

Fig. 5.7 shows the variations of the outlet variables from the regenerator with the change of the ratio of the liquid desiccant flow rate to air flow rate (L/G) while holding the inlet air temperature, inlet solution temperature, the inlet desiccant concentration and inlet air moisture-content constant at 25ºC, 56ºC, 35% and 0.018 kg/kg, respectively. It is shown that a significant reduction (i.e. about 0.31%) of the outlet solution concentration (X_{so}) is resulted when increasing the liquid to gas flow rate ratio (L/G) from 1.0 to 3.5. This is because the regeneration temperature is taken as constant, whereas it must be high enough to provide the regeneration required when increasing the flow rate of the solution. In other words, if the same regeneration temperature is used, the required regeneration time is higher, and this is not acceptable in the air-conditioning system as it affects the whole system performance due to the fact that the desiccant regeneration must be instantaneous. From Fig. 5.7, it can also be seen that increasing L/G leads to an increase in the water evaporation rate ($\dot{m}_{evap}$) and the packing wettability (a_w). The increase of the

evaporation rate and wet surface area of packing is 8.9×10^{-4} kg/s and 37.34 m^2/m^3, respectively, when L/G increases from 1.0 to 3.5.

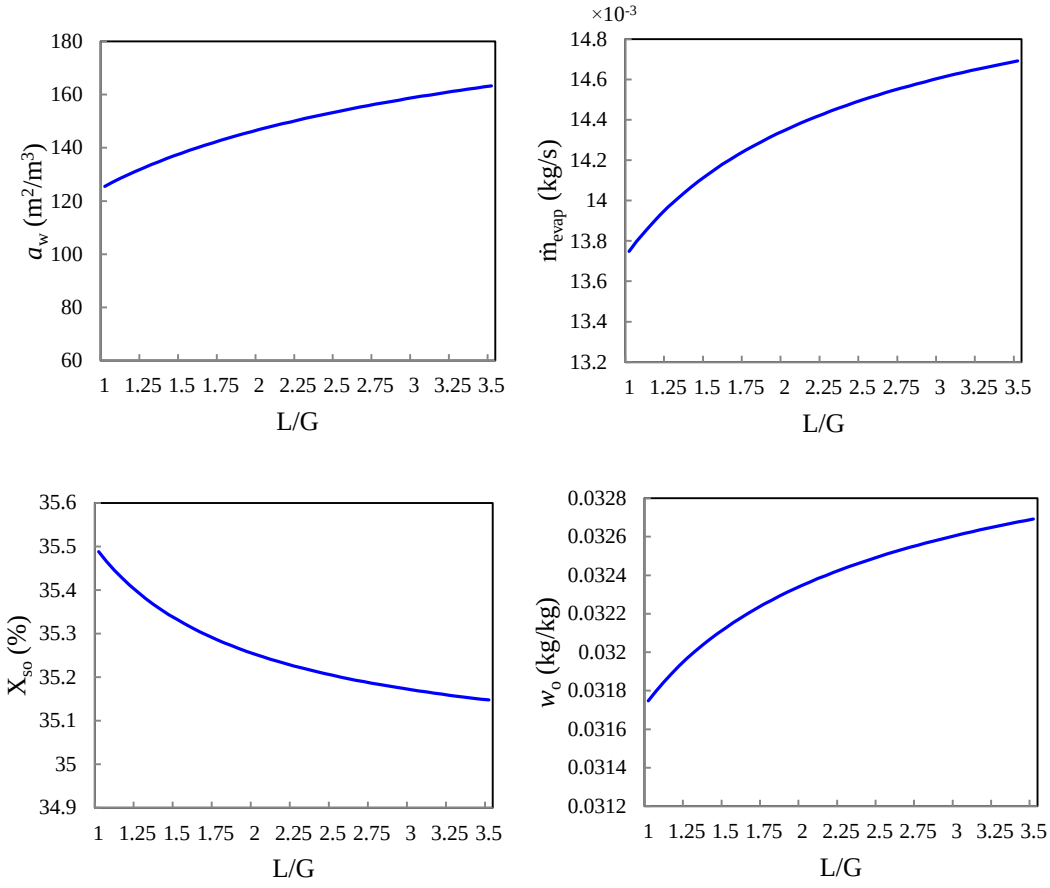

Fig. 5.7 Variation of outlet variables across the regenerator with increasing solution to gas specific flow rate ratio.

The effects of changing the inlet solution temperature on the regenerator performance are presented in Fig. 5.8. It can be observed that increasing the inlet solution temperature results in excellent regeneration performance. For instance, under the same inlet conditions, the variation of the re-concentration change is about 0.35% if the inlet solution temperature (T_{si}) is 65ºC, while if the inlet solution temperature is 45ºC, the re-concentration change is about 0.058%. It is worthwhile to mention that higher regeneration temperature means higher regeneration cost even with the use of the solar heating system. This is because using a large solar heating system requires high initial and maintenance costs. From Fig. 5.8, it can also be seen

that there is almost no water evaporation or re-concentration of the liquid desiccant at 45°C, and thus this temperature can be taken as the critical point between the absorption phase and the regeneration phase for this particular case. Fig. 5.8 also shows that increasing the inlet solution temperature can result in a slight increment in the outlet solution temperature (i.e. by about 7°C).

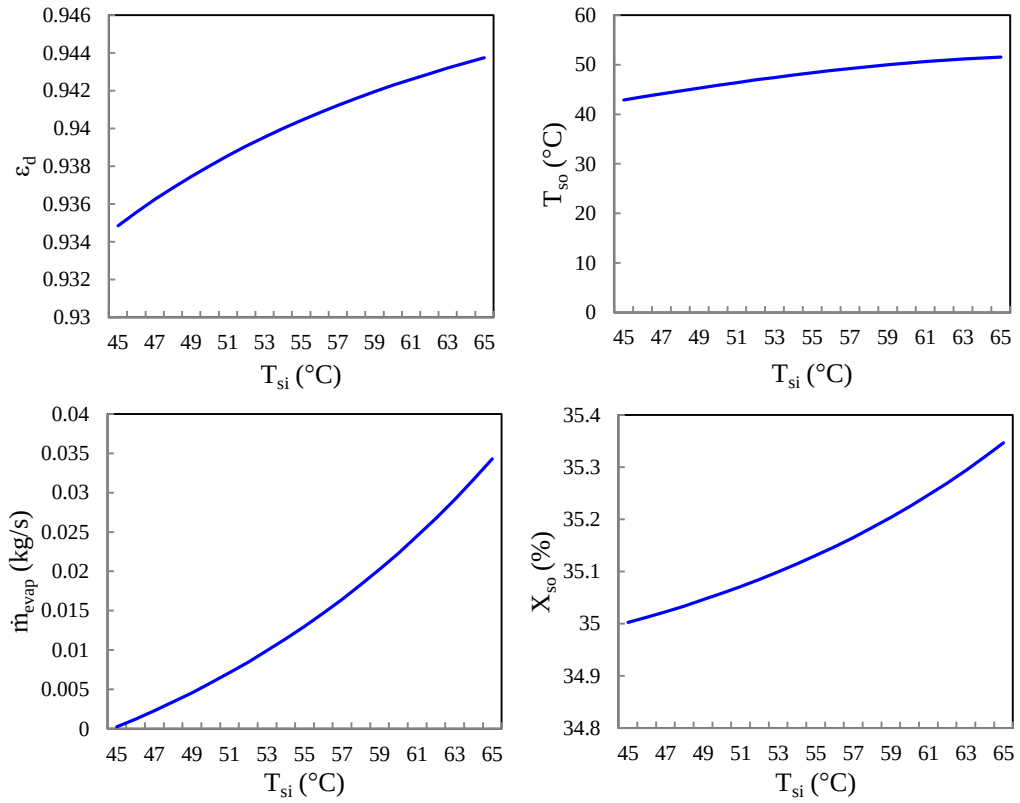

Fig. 5.8 Variation of outlet variables across the regenerator with increasing the inlet solution temperature.

Fig. 5.9 shows that the outlet solution temperature (T_{so}) increases when the inlet desiccant concentration (X_{si}) increases. This is because of the extra heat launched due to the further liquid desiccant regeneration. It is shown that increasing the inlet desiccant concentration needs a higher regeneration temperature than 56°C. For instance, the outlet desiccant concentration (X_{so}) is 44.97% if the inlet desiccant concentration is 45%, while the outlet solution concentration is 35.15% when the inlet desiccant concentration is 35%. This means that if the regeneration temperature

is not high enough, the process may turn into absorbing the humidity from the scavenging air instead of releasing the water vapour from the weak solution as it can be seen from the change in the water evaporation rate ($\dot{m}_{evap}$). It is shown that the regenerator effectiveness is increased about 0.02 when increasing the inlet desiccant concentration from 30% to 45%.

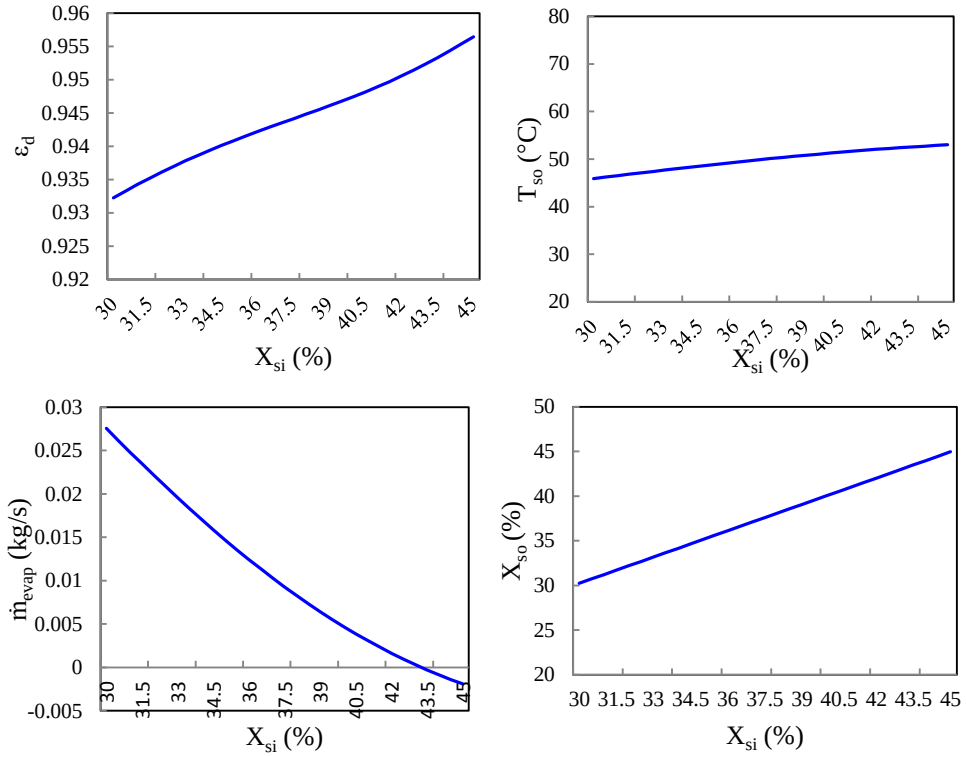

Fig. 5.9 Variation of outlet variables across the regenerator with increasing the inlet solution concentration.

Fig. 5.10 illustrates the impact of changing the regenerator diameter on the performance of the regenerator. It can be seen that the water vapour evaporation rate is slightly increased when the regenerator diameter increases. For instance, the change of the evaporation rate is 9×10^{-5} kg/s when the diameter is increased from 0.5 to 1.5 m. It is shown that increasing the regenerator diameter leads to a slight increase in the regenerator effectiveness (i.e. by about 6×10^{-3}), and no significant change in the outlet liquid desiccant concentration (X_{so}).

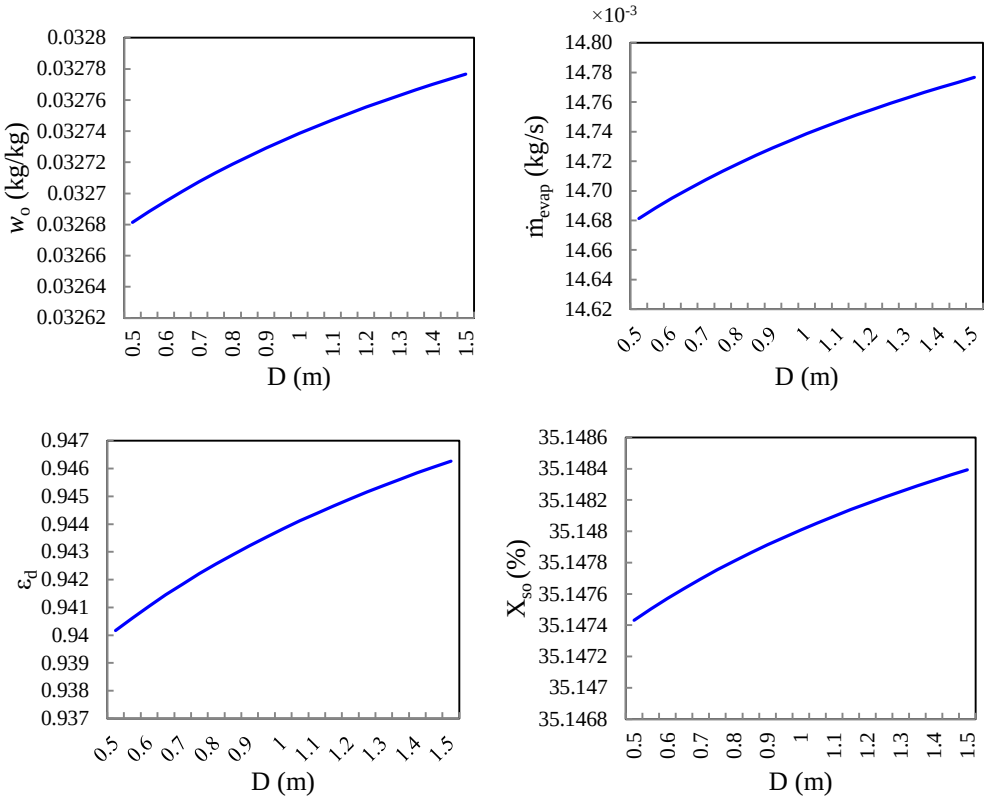

Fig. 5.10 Variation of outlet variables across the regenerator with increasing the regenerator diameter.

Fig. 5.11 shows that increasing the regenerator height leads to a reduction in the regeneration performance which is similar to the case of the absorber. It is shown that increasing the regenerator height leads to a reduction in the evaporation rate ($\dot{m}_{evap}$) under the same inlet conditions. It can be seen that the reduction change in the outlet solution concentration is negligible and the water evaporation rate is reduced by 0.3×10^{-3} kg/s when increasing the regenerator height from 0.3 to 1.5 m.

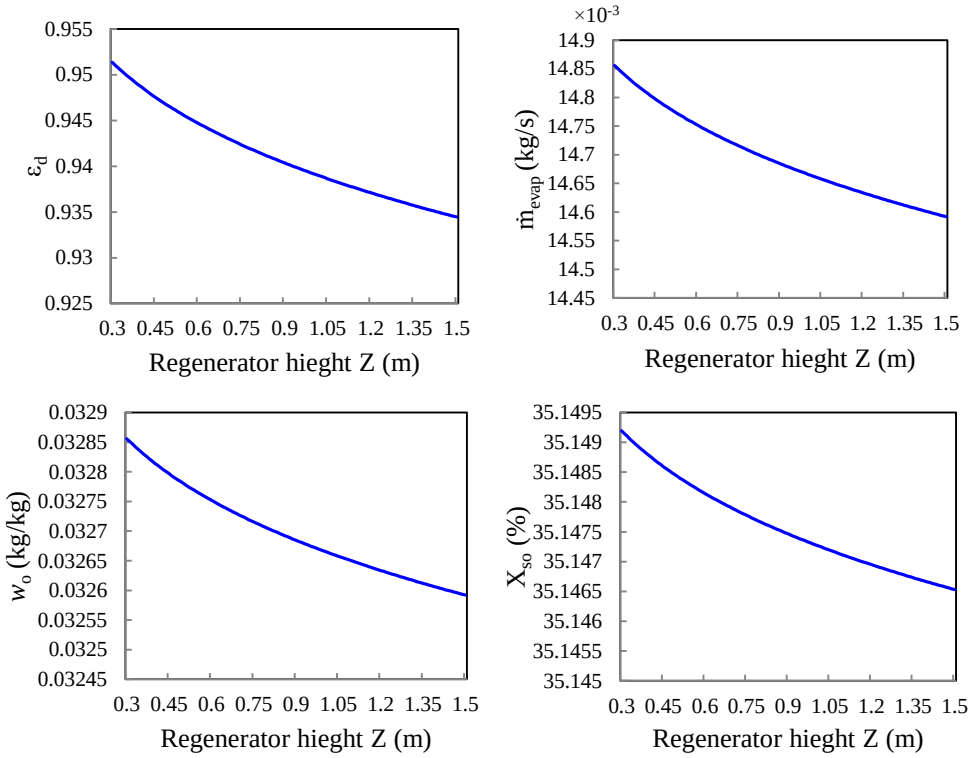

Fig. 5.11 Variation of outlet variables across the regenerator with increasing the regenerator height.

In general, the regeneration process across the regenerator is strongly affected by the moisture-content of the scavenging air. Fig. 5.12 examines the impact of increasing the inlet air moisture-content on the regenerator performance. It is shown that a significant reduction in the water evaporation rate is resulted when increasing the inlet air moisture-content (w_i). For instance, the reduction is about 14.4×10^{-3} kg/s when increasing the inlet air moisture-content from 0.015 to 0.03 kg/kg. It can be observed that low evaporation rate ($\dot{m}_{evap}$) leads to low re-concentration behaviour of the regenerator. It is also shown that the reduction is about 0.136% in the outlet solution concentration, when increasing the inlet air moisture-content from 0.015 to 0.03 kg/kg.

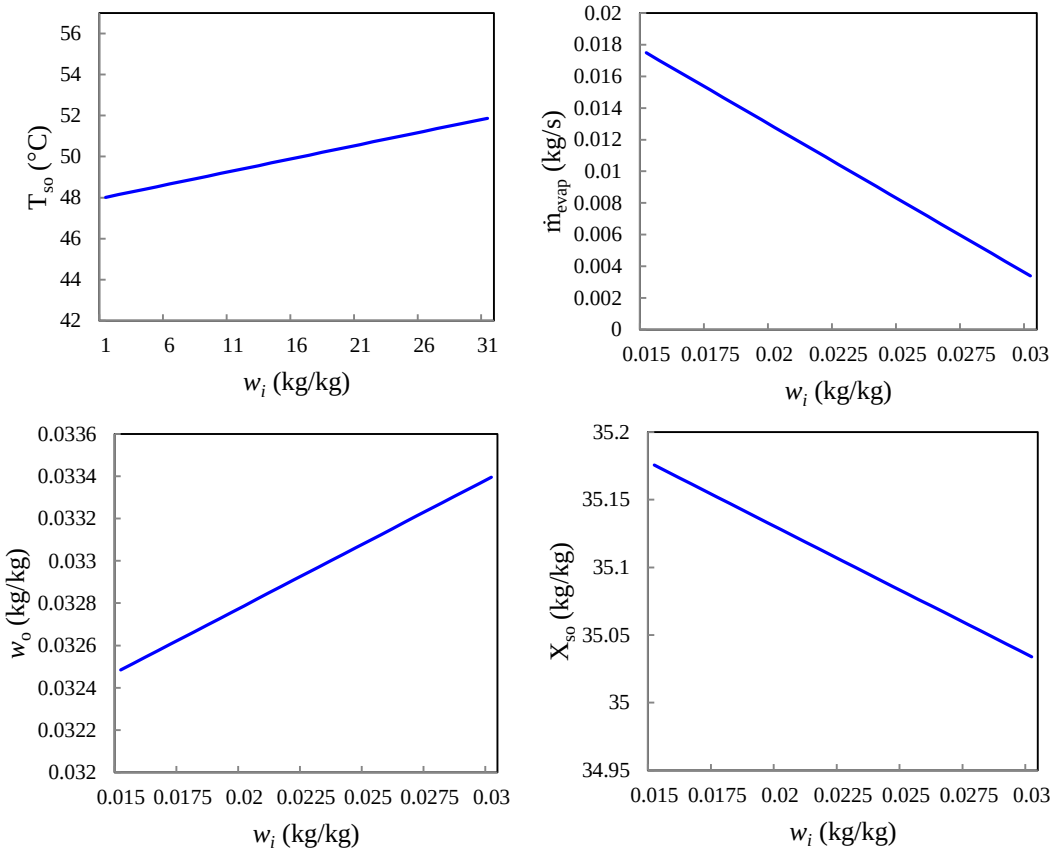

Fig.5.12 Variation of outlet variables across the regenerator with increasing the inlet air moisture-content.

Table 5.4 summarises the variations of the regenerator performance with the changes of each design or operational parameter. The main results showed that the design variables which are the dry specific surface area of packings (a_t), the regenerator height (Z), and the regenerator diameter (D) have almost no or minimal effects on the solution outlet temperature (T_{so}) . The liquid to air flow rate ratio (L/G) and the inlet air moisture-content (w_i) have almost no impact on the regeneration effectiveness. The water vapour evaporation rate ($\dot{m}_{evap}$) increases when increasing the inlet solution temperature (T_{si}), L/G, and D, while increasing the inlet air temperature (T_{ai}), the inlet solution concentration (X_{si}) and Z leads to a decrease in the evaporation rate.

All the variables were found to have a direct impact on the desiccant concentration. However, the re-concentration level of the outlet desiccant solution (X_{so}) decreased with the increase of L/G, T_{ai}, a_t, and Z.

Table 5.4 Summary of the key findings from the regenerator parametric study.

Changed variable	**Tested parameters**						
	T_{ao}	T_{so}	a_w	$\dot{m}_{evap}$	w_o	X_{so}	ε_d
↥ L/G	↧	↥	↥	↥	↥	↧	⇌
↥ T_{ai}	↥	↥	⇌	↧	↧	↧	↧
↥ T_{si}	↥	↥	↥	↥	↥	↥	↥
↥ X_{si}	↧	↥	↧	↧	↧	↥	↥
↥ a_t	↥	⇌	↥	↧	↧	↧	↧
↥ Z	↥	⇌	⇌	↧	↧	↧	↧
↥ D	⇌	⇌	↧	↥	↥	↥	↥
↥ w_i	↧	↥	⇌	↧	↥	↧	⇌

↥ Increase; ↧ decrease; ⇌ no or less impact

Based on the above parametric study and the design model of the absorber and regenerator, the configuration design parameters are chosen to be implemented in the simulation system. The findings indicated that, using the design variables Z and D, which were estimated by the model developed in Chapter 4, at the design stage can provide excellent dehumidification and regeneration performance, and gives acceptable reliability to the developed model.

5.4 Conclusion

Performing a parametric study is of importance to explore the effects of the different design parameters on the performance of the absorber and regenerator used in the proposed solar-assisted liquid desiccant dehumidification air-conditioning systems. It can also provide a clear picture of the operational behaviour of these components

with the changes of design and operational parameters. The results from the parametric study showed that using an absorber and regenerator of 0.6 m height and 0.4 m diameter is enough to provide excellent absorption and regeneration behaviour for the case study. Increasing the ratio of liquid to air flow rate has great impacts on the absorber performance, but increasing this ratio above 3.5 is not useful as the change is not significant, and the pumping cost should be considered and balanced when further increasing this ratio. In contrast, increasing the ratio of liquid to air flow rate has negative impacts on re-concentrating the liquid desiccant such that high liquid to air flow rate ratio requires high regeneration temperature. The results show that excellent dehumidification can be achieved, and at the same time relatively low regeneration temperature is required if a solution concentration of 35% is used. The operational parameters have been found to have a high impact on the performance of the absorber and regenerator. Appropriate control of these parameters can assist in maximising the overall performance of the proposed solar-assisted liquid desiccant dehumidification air-conditioning system as it will be demonstrated in Chapter 6.

6 Performance test and evaluation of the solar-assisted liquid desiccant dehumidification air-conditioning system

6.1 Introduction

Energy modelling and simulation have been extensively used to analyse and evaluate the performance of buildings and building services systems, alternative design configurations and operational strategies (Ma and Wang 2011; Zhai and McNeill 2014). As liquid desiccant systems are highly nonlinear and interactive, whole system simulation is essential to test the system performance and understand the system-level and subsystem-level interactions and characteristics. In this chapter, a full-scale simulation system for the proposed solar-assisted liquid desiccant dehumidification air-conditioning system is first developed and then used to facilitate the system performance evaluation and analysis.

6.2 Brief description of the simulation system

Fig. 6.1 illustrates the schematic of the simulation system developed for the proposed solar-assisted liquid desiccant dehumidification air-conditioning system, which was developed by using Matlab Simulink. Matlab Simulink offers multi-purpose simulation and design-based model environment to support various levels of programming, including system-level design, simulation and system code generation (Matlab 2013). It has different blocks and libraries that can be used to simulate several types of systems, including mechanical, electrical and hydraulic, and even to combine more than one system in a single simulation environment.

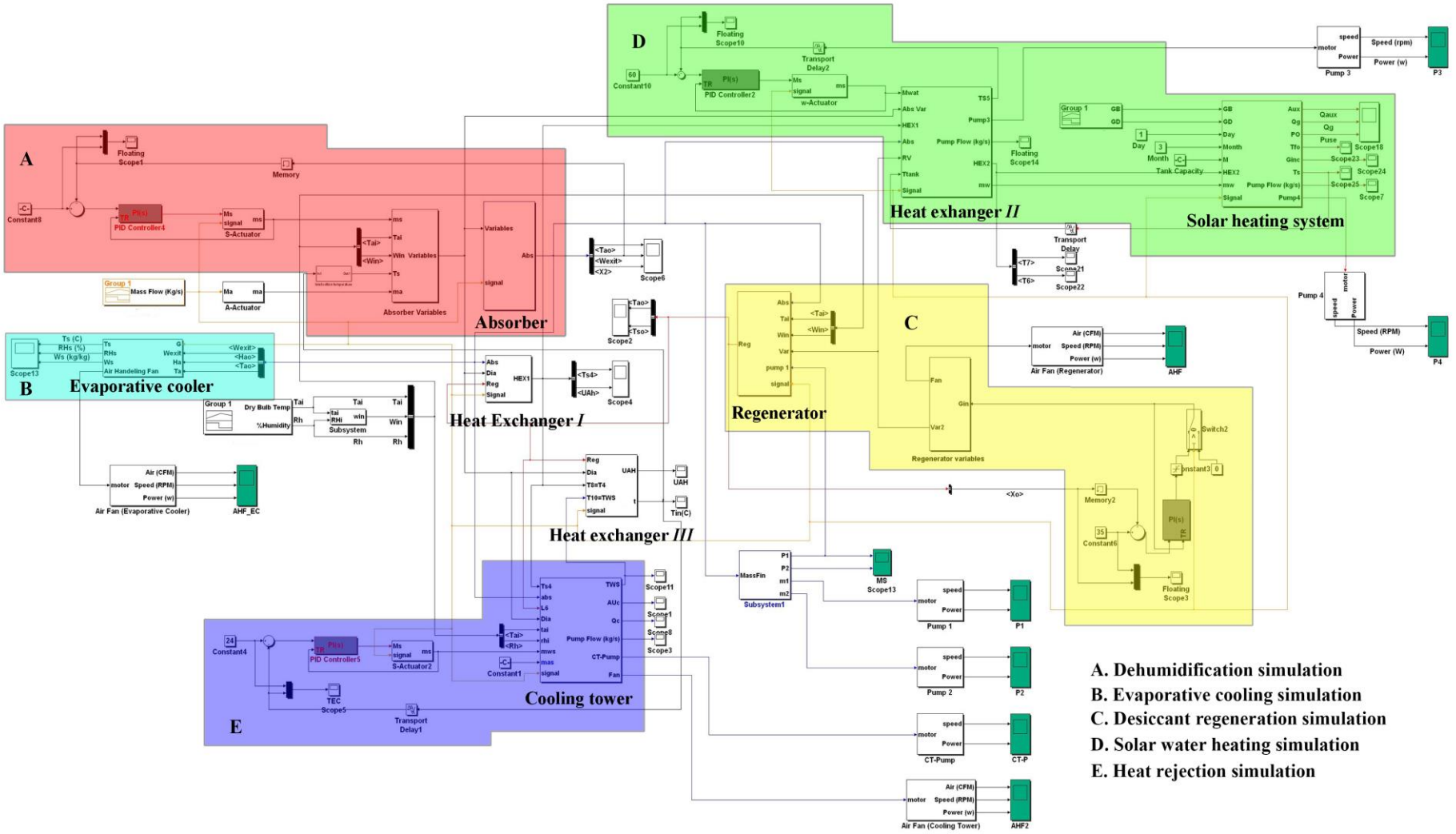

Fig. 6.1 Full-scale simulation system developed for the proposed air-conditioning system.

As illustrated in Fig. 6.1, the full-scale simulation system mainly includes the solar water heating system simulation, desiccant regeneration simulation, dehumidification simulation, evaporative cooling simulation and the cooling tower heat rejection simulation. These subsystems are interconnected and interact with each other to allow an investigation of the system-level and subsystem-level interactions and characteristics. In the simulation system, PID controllers were used to control the operation of the fluid pumps and air ventilation fans. The proposed liquid desiccant dehumidification air-conditioning system was tested against the Sydney weather condition. As shown in Fig. 6.2, the relative humidity in Sydney is quite high and in a range of 50%-95% during the most time periods. Therefore, utilising the proposed liquid desiccant dehumidification air-conditioning system in this type of weather condition is essential to provide acceptable indoor thermal comfort with minimised energy consumption.

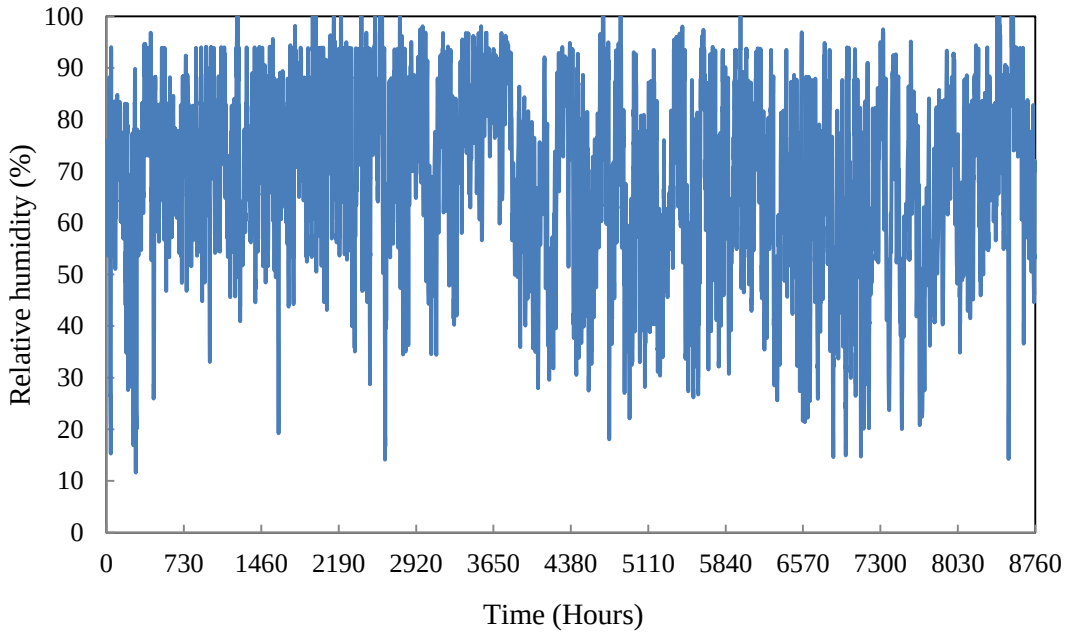

Fig. 6.2 Relative humidity versus time in Sydney (IWEC).

6.3 Performance test and evaluation

6.3.1 Setup of the test

The performance of the proposed system was simulated and evaluated based on a Solar Decathlon (SD) house, which was built for the Solar Decathlon China 2013 competition (See Fig. 6.3). This SD house is the retrofit of a typical Australian timber-framed fibro house incorporating effective architectural retrofit, house envelope retrofit, air-conditioning system retrofit and the use of solar photovoltaic (PV) panels, solar photovoltaic thermal (PVT) systems and solar hot water systems. The total floor area of the house under study is 80.4 m^2, and the conditioned space is 71.7 m^2. In this study, the building simulation software DesignBuilder (DesignBuilder 2013) was used to simulate the cooling demand of the SD house. In the simulation, the International Weather for Energy Calculations (IWEC) data of Sydney was used as the test conditions. The weather conditions will have a direct impact on the system performance. In order to achieve the desired supply air temperature and moisture-content, more regeneration energy will be required during the peak hours with high ambient air temperature and moisture-content as it will be illustrated later. The simulated cooling load profile was then used as an input to the Matlab Simulink platform serving as the working condition of the proposed solar-assisted liquid desiccant dehumidification air-conditioning system.

Fig. 6.3 Solar Decathlon house used as the test case.

Fig. 6.4 shows the temperature and relative humidity in Sydney for three typical consecutive summer days, which were used as the working conditions of the proposed solar-assisted liquid desiccant dehumidification air-conditioning system in this study. Fig. 6.5 presents the simulated cooling load demands of the solar decathlon house under these three typical summer days.

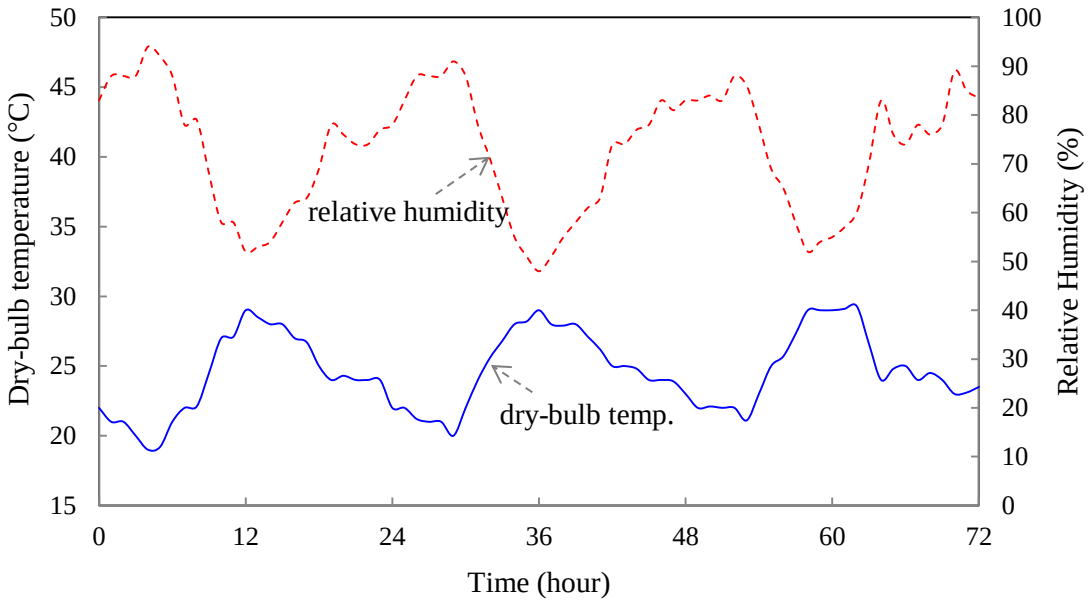

Fig. 6.4 Weather conditions of Sydney in three typical summer days.

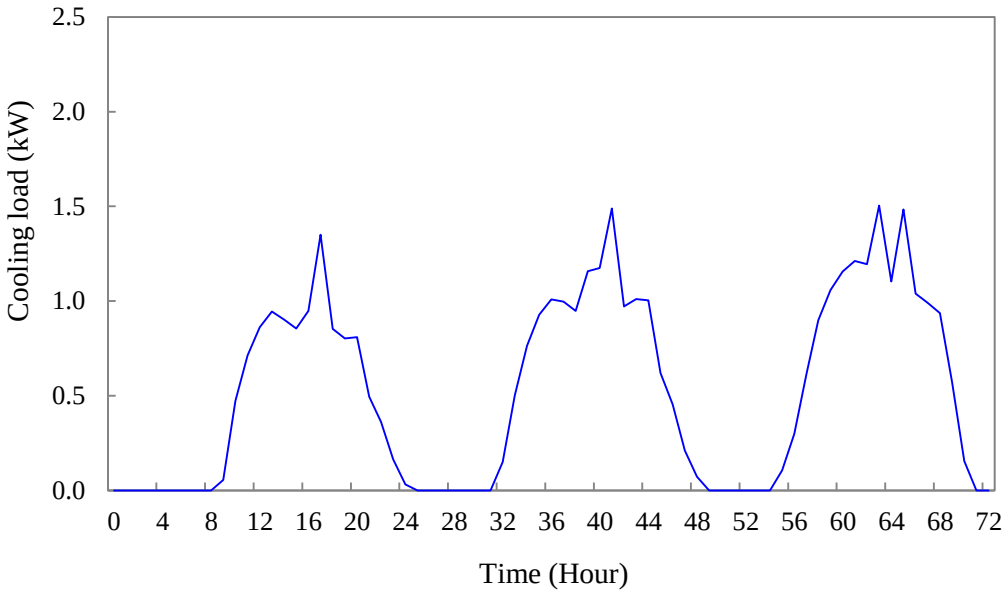

Fig. 6.5 Cooling load profiles of the SD house for three consecutive summer days.

In order to maximise the system performance, a PID controller was used to control the operating speed of the variable speed pump in the cooling tower circuit (i.e. CT-pump) so that the inlet desiccant temperature of the absorber can be controlled at the desired condition (i.e. a set-point of 24°C was used in this study). It is worthwhile to mention that this set-point temperature was determined based on trial and error tests by taking into account the performance of the cooling tower and outdoor weather conditions. The PID controllers for the fluid pumps 1 and 2 were used to adjust the desiccant flow rate to control the humidity of the outlet air from the absorber (i.e. the set-point of the air moisture-content is set to be 6.5×10^{-3} kg/kg). The regeneration temperature was controlled by changing the operating speed of the fluid pump 3 to adjust the water flow rate between the tank and the heat exchanger *II*. The solution regeneration temperature was set to be 60°C. The outlet solution concentration from the regenerator was controlled by changing the air flow rate flowing through the regenerator. The regenerator outlet solution concentration was set to be 35%. The fluid pump 4 is considered as a constant speed. The system was run only when there is a cooling demand.

Table 6.1 summarises the main parameters of the different components used in the simulation platform. These parameters were determined based on the manufacturing data, the design approach and the parametric study (to obtain the optimal values). The efficiency of the flat plate is nonlinear, and it is calculated by Equation (6.1) (SDH 2013).

$$\eta_c = 0.8 - 3.0\,\frac{T_m - T_a}{G_{inc}} - 0.008\,\frac{(T_m - T_a)^2}{G_{inc}} \tag{6.1}$$

where, T_a is the ambient air temperature, T_m is the mean temperature of the fluid across the solar collector, and G_{inc} is the total incident irradiance on the solar collector.

The water circulation pump was programmed to be off when the tank temperature exceeds 120°C. The auxiliary electric heater was used only when the water temperature in the thermal storage tank is less than the required temperature of 60°C, or there is no sufficient solar irradiance.

Table 6.1 Main parameters of the different components used in the simulated system.

Component	Key parameters	Values
Absorber	Tower diameter	0.4 m
	Tower height	0.6 m
	Packing diameter	2.56 cm
	Specific surface area of packings	210 m^2/m^3
Regenerator	Tower diameter	0.4 m
	Tower height	0.6 m
	Packing diameter	2.56 cm
	Specific surface area of packings	210 m^2/m^3
	Regeneration temperature	60°C
Cooling Tower	Model	T-25/CST
	Design heat rejection capacity	21.98 kW
Heat Exchanger	AU_I	40 kW/K
	AU_{II}	10 kW/K
	AU_{III}	20 kW/K
Evaporative Cooler	Efficiency	85%
Solar water heating system	Collector area	8 m^2
	Tank capacity	0.32 m^3
	Location	Sydney
	Collector inclination angle	15º

In this study, the chosen cooling tower (T-25 CTS) which is manufactured by Cooling Tower Systems Inc., was used to size the capacity of the cooling tower and determine the major parameters (ONS 2013). The cooling tower was modelled and sized according to the design load required to cool down the desiccant solution, and

the manufacturer data including the water flow rate, the air flow rate, the design cooling load, the inlet water temperature, the outlet air temperature, and the inlet air wet-bulb temperature. Based on the provided data, the estimated $AU_{fic,dry,n}$ is equal to 3.447 kW/k. The designated model requires another two variables, which are *n* and *m*, and can be taken averagely according to values calculated experimentally by previous researchers that cited in (Lebrun and Silva 2002) to be 0.65 and 0.43, respectively.

6.3.2 Results from the performance tests and discussion

Fig. 6.6 shows the dry-bulb temperature and relative humidity of the air leaving from the absorber. It can be seen that the relative humidity (RH) of the processed air can be handled to 21.6-33.7% while the air temperature was slightly increased due to the absorption process. It is also shown that the lowest RH and the highest air temperature occurred during the peak load periods, due to the fact that the outdoor air has a low relative humidity during the peak load periods as illustrated in Fig. 6.4. The dehumidification ability of the absorber is usually described by the moisture condensation rate across the absorber. Fig. 6.6(c) shows the condensation rate of the air moisture during the operation time. It is shown that the maximum condensation rate was achieved at the peak load periods.

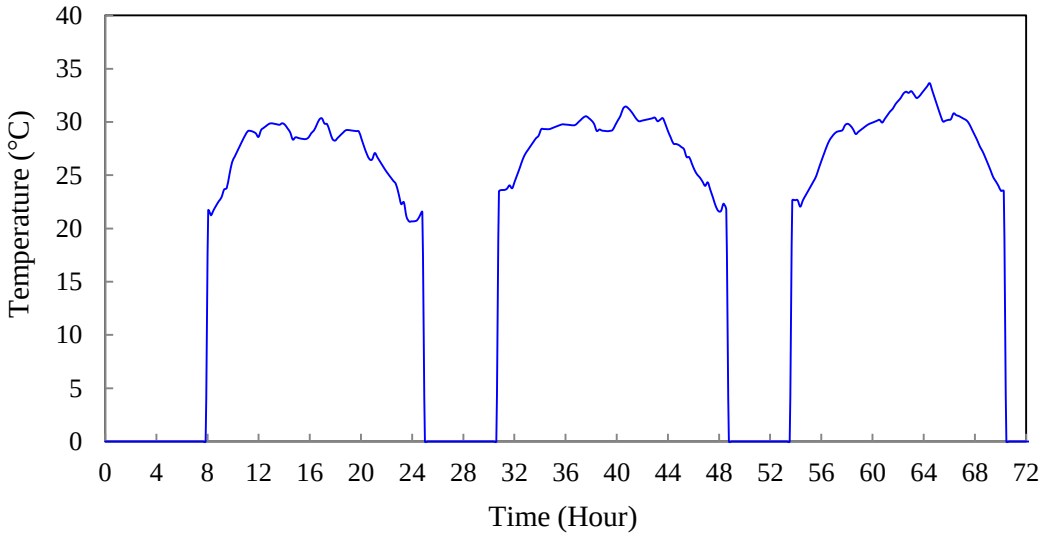

(a) Outlet air temperature

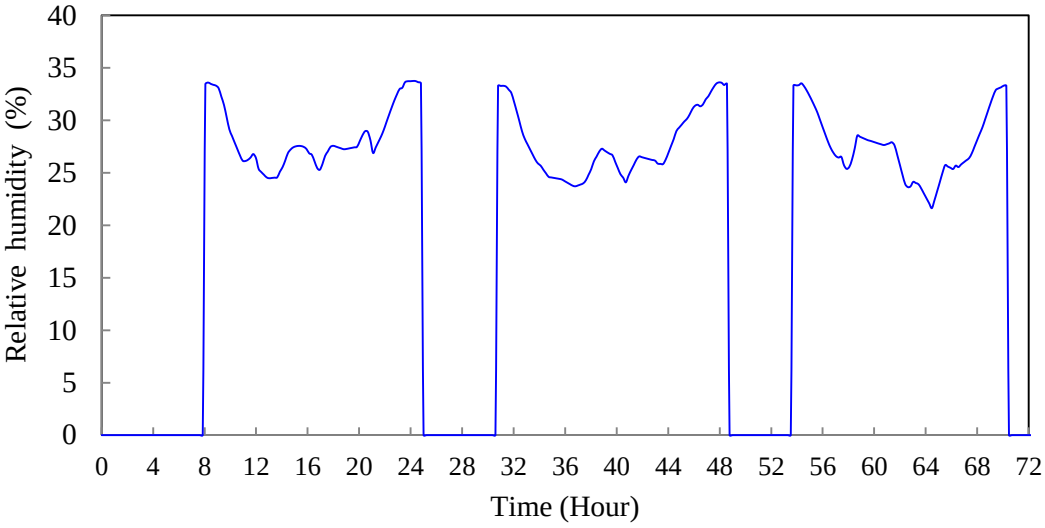

(b) Outlet air relative humidity

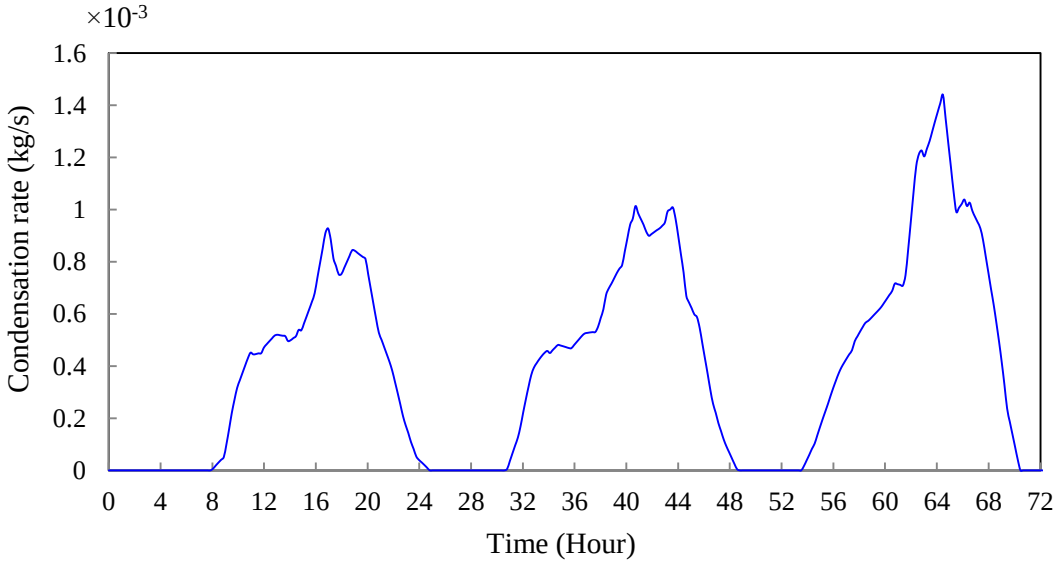

(c) Moisture condensation rate

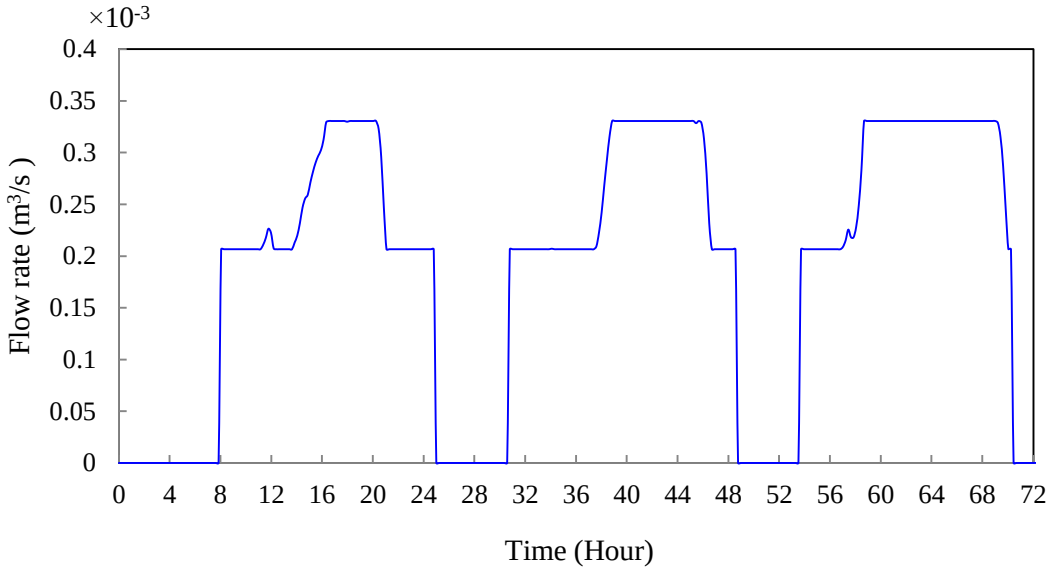

(d) Solution flow rate

Fig. 6.6 Air status leaving from the absorber.

Fig. 6.6(d) shows the variation of the solution flow rate across the absorber which is required to maintain the relative humidity at the desired set-point. It is shown that the minimal solution flow rate was about 0.2×10^{-3} m^3/s, whereas the maximum flow rate was about 0.34×10^{-3} m^3/s. It is also shown that a high flow rate is needed during the afternoon period due to the high cooling demand. Pump 2 was controlled to provide exactly the same flow rate as that of Pump 1.

Fig. 6.7 shows the relative humidity and dry-bulb temperature of the ventilation air leaving from the evaporative cooler. The air temperature can be well controlled to below 21.15°C at the peak load periods while the relative humidity ranged between 78% and 90%. A lower temperature can be achieved by increasing the absorber inlet solution flow rate. However, this will increase the required regeneration energy. Better evaporation cooling performance can be achieved by using variable speed water pumps, although constant speed pumps are often used in practice.

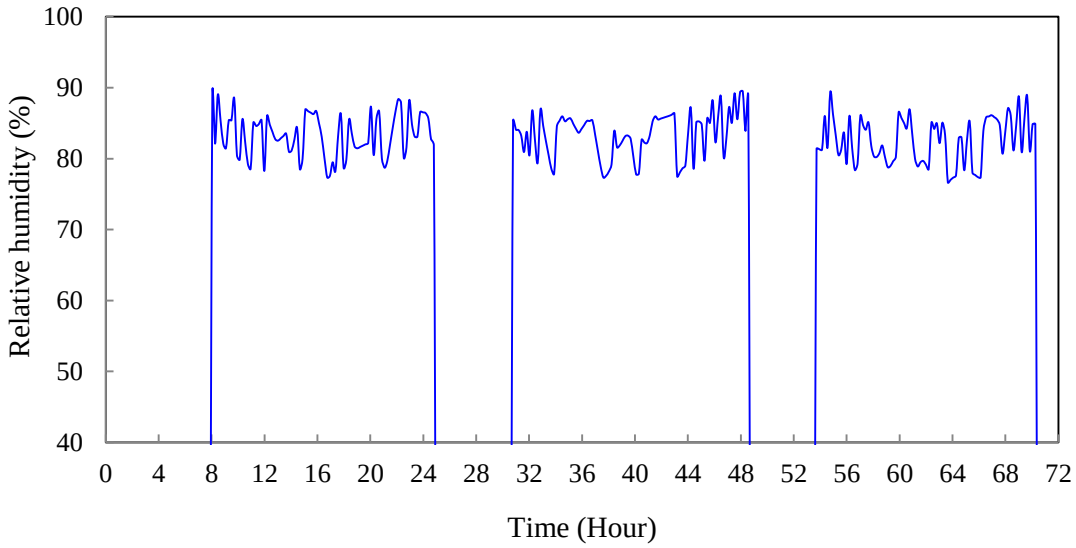

(a) Air relative humidity

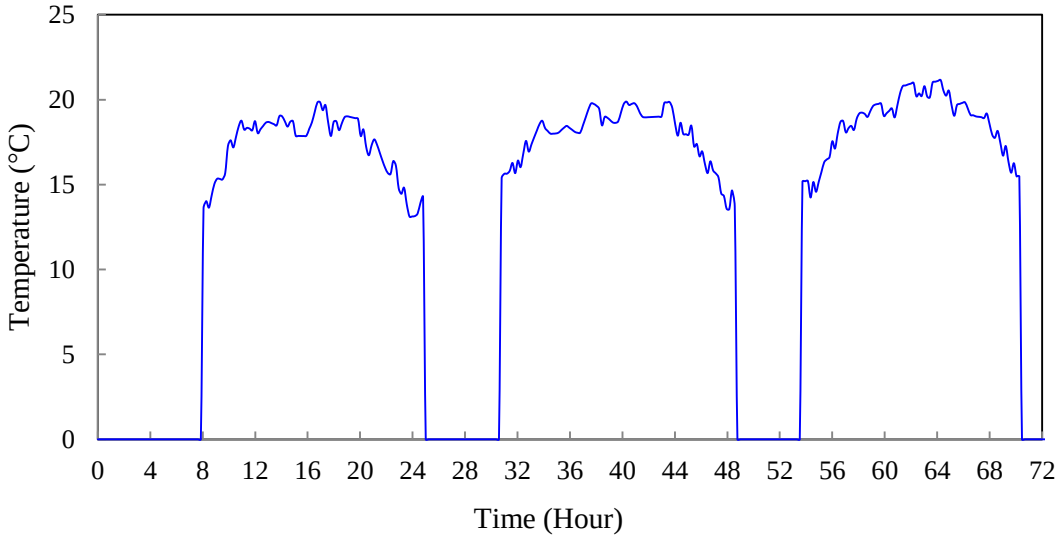

(b) Air dry-bulb temperature

Fig. 6.7 Air status leaving from the evaporative cooler.

Fig. 6.8 shows the performance of the regenerator for re-concentration of the liquid desiccant solution. As shown in Fig. 6.8(a), the outlet solution temperature from the regenerator was around 60ºC during most time periods, which is close to the regeneration temperature. This high temperature solution was utilised for preheating the diluted solution from the absorber. The concentration of the liquid desiccant solution leaving from the regenerator can be well controlled near the set-point of 35% as shown in Fig. 6.8(b).

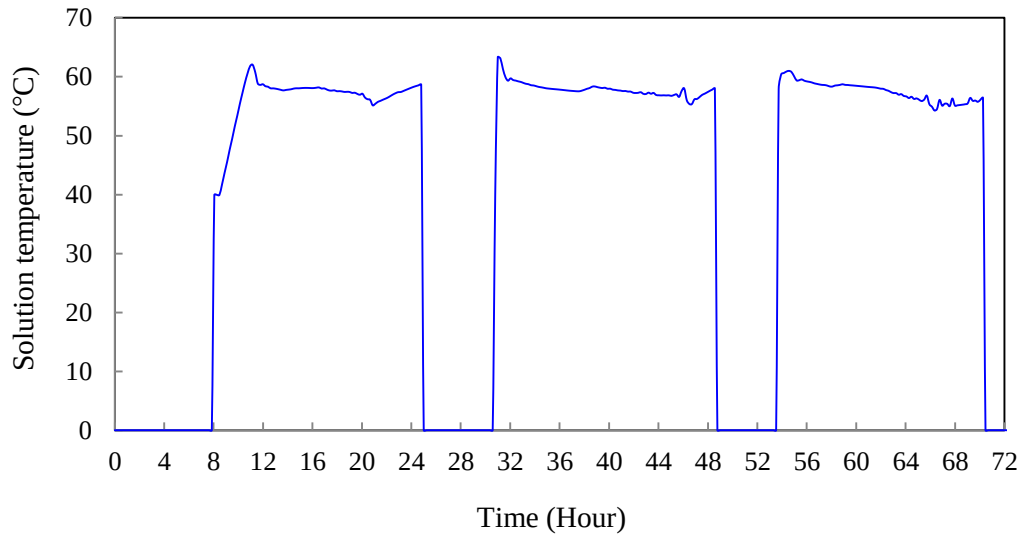

(a) Outlet solution temperature

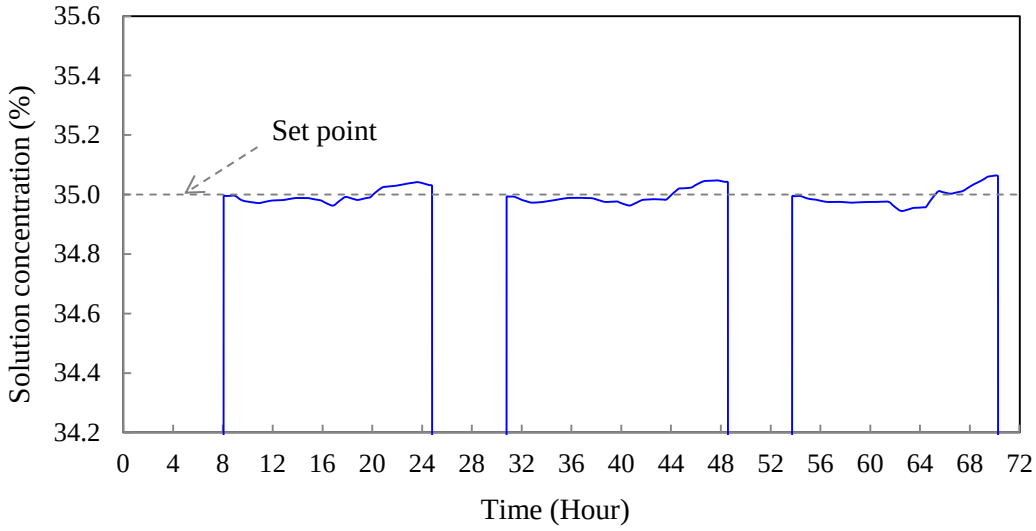

(b) Outlet solution concentration

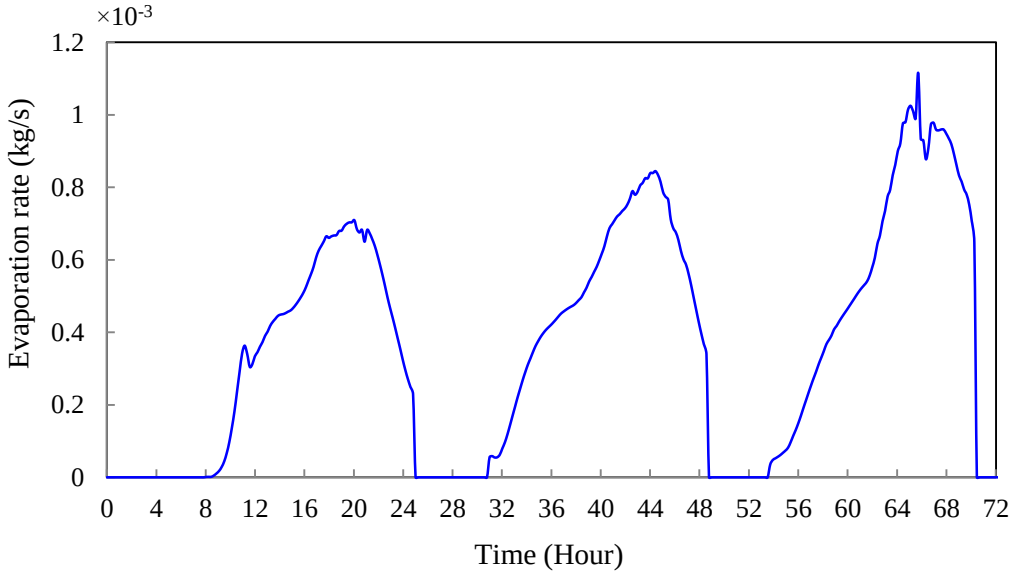

(c) Water vapour evaporation rate

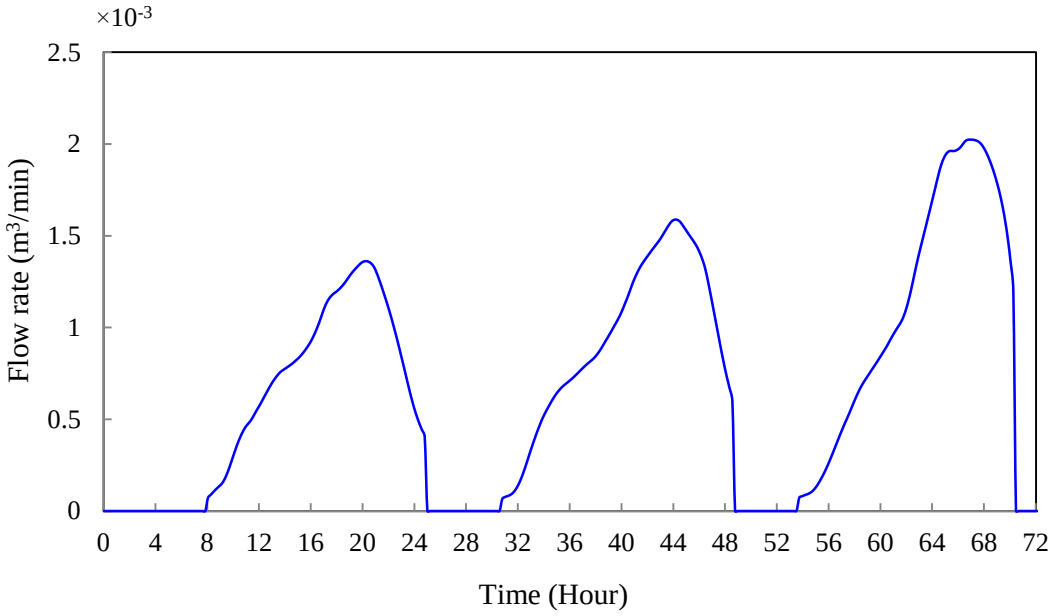

(d) Air flow rate

Fig. 6.8 The performance of the regenerator.

Fig. 6.8(c) shows the liquid desiccant regeneration ability of the regenerator represented by the water vapour evaporation rate during the operation time. Compared with the absorber condensation rate, the evaporation rate is slightly lower at the peak time, resulting that the re-concentrated solution is slightly lower than the set-point of 35% at the peak load periods. Fig. 6.8(d) shows the required air flow rate across the regenerator to control the re-concentration process of the liquid desiccant.

In order to ensure good performance of the absorber, the inlet desiccant solution temperature needs to be low enough to avoid decreasing the system dehumidification performance, which will have a negative impact on the overall performance of the evaporative cooler. Fig. 6.9 shows the variations of the absorber inlet solution temperature, which was controlled by changing the operating speed of the CT−pump in the cooling tower circuit. It can be easily seen that the absorber inlet solution temperature was acceptably controlled near a set-point of 24°C during the whole operation period ensuring good performance of the absorber.

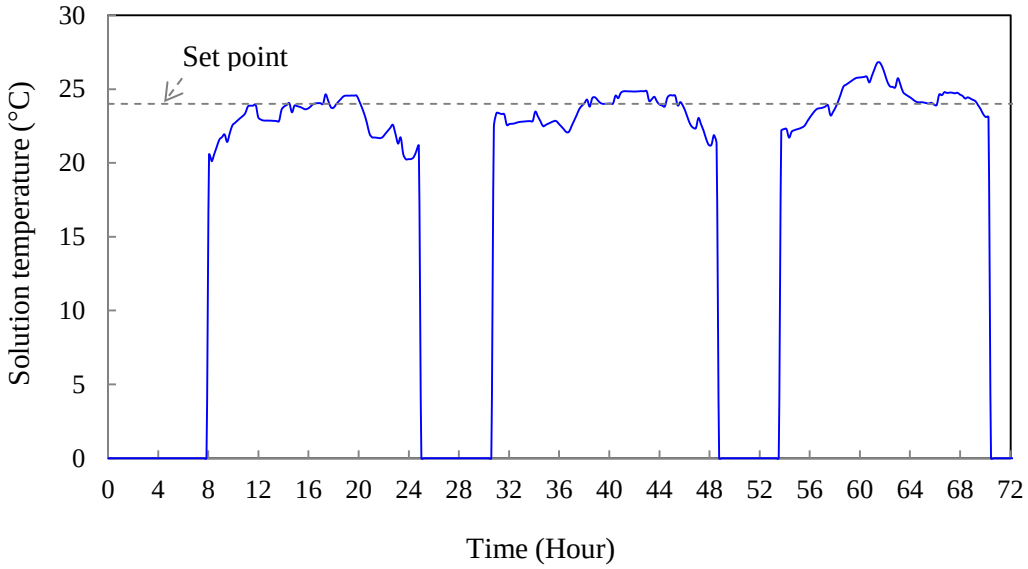

Fig. 6.9 The absorber inlet solution temperature.

The proposed system intends to utilise the solar energy as far as possible to re-concentrate the liquid desiccant and reduce the electric power demand. Fig. 6.10(a) shows the required heating energy for regeneration of the liquid desiccant (Q_{reg}) and the electric heating power required ($Q_{aux,h}$), as well as the useful energy obtained from the solar water heating system (Q_{sol}). It can be observed that the solar water heating system represents an efficient source of energy supply such that up to around 5 kW could be obtained during the peak demand periods. It is able to provide the amount of energy needed to re-concentrate the liquid desiccant during the daytime periods of the three test days while the auxiliary electric heater will be required during the night time if there is no sufficient heat in the thermal storage tank. It is worthwhile to note that solar energy collected in the first day was higher than that used for regeneration while the auxiliary electric heater was still used. This is because part of the solar energy gained was used to preheat the water in the thermal storage tank as its initial temperature was only 25°C as illustrated in Fig. 6.10(b). For the test days, about 73.4% of regeneration energy was provided by the solar water heating system while the auxiliary electric heater provided the rest. From Fig.

6.10(b), it can also be seen that the highest water temperature stored in the storage tank was around 120°C. Fig. 6.10(c) illustrates the regeneration temperature, which was well controlled at the desired set-point during most of the test periods.

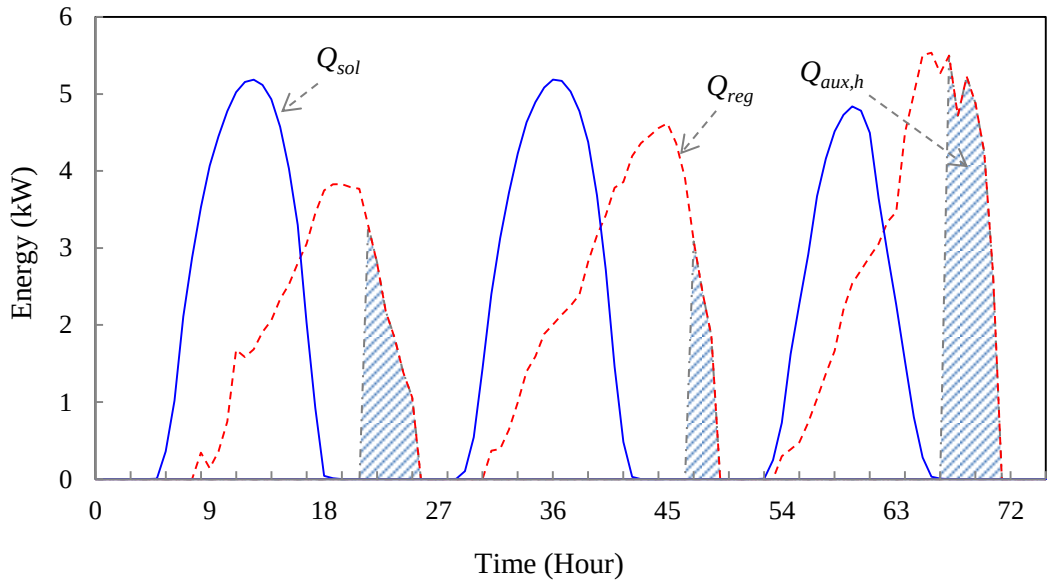

(a) Solar heat gained, regeneration energy, and auxiliary heater energy

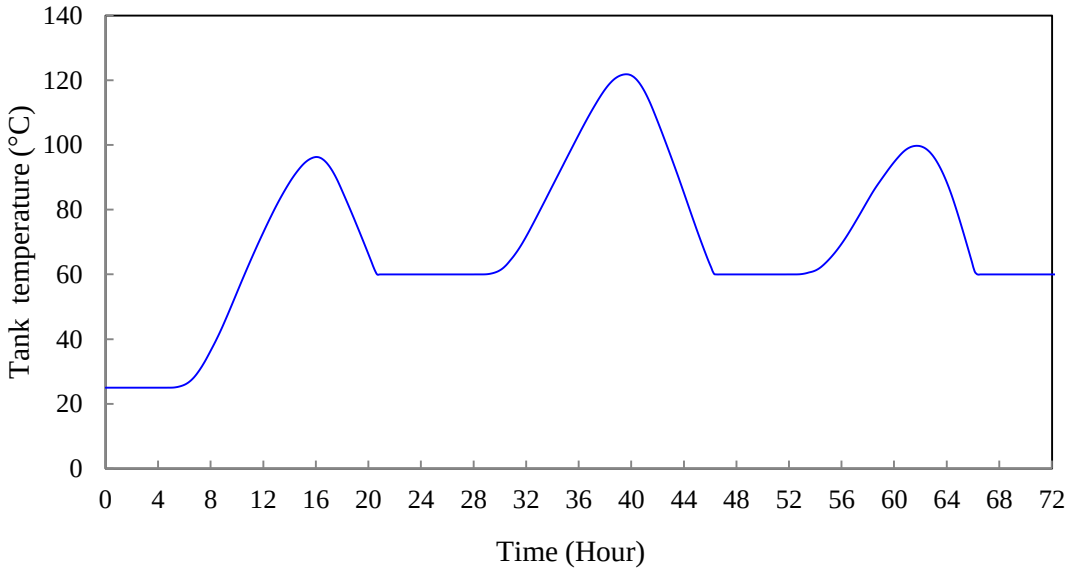

(b) The water tank temperature

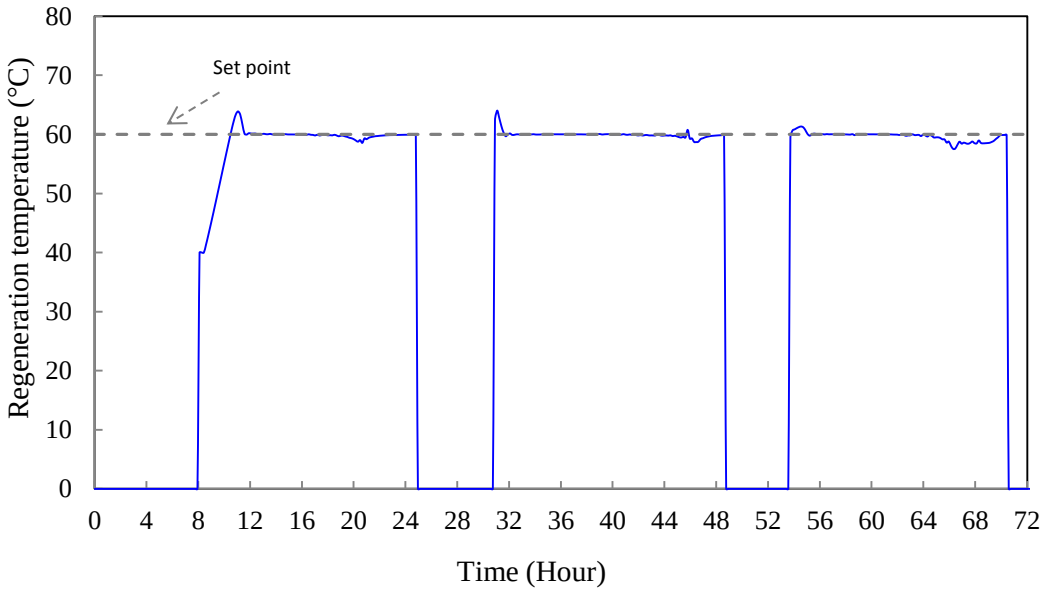

(c) Solution regeneration temperature

Figure 6.10 Performance of the solar water heating system.

Fig. 6.11 shows the total heat rejected by the cooling tower to cool the liquid desiccant down to the set-point before entering the absorber. The variation in the load is due to the change in the solution temperature which leaves the heat exchanger *I* and the controlled water flow in the cooling tower circuit.

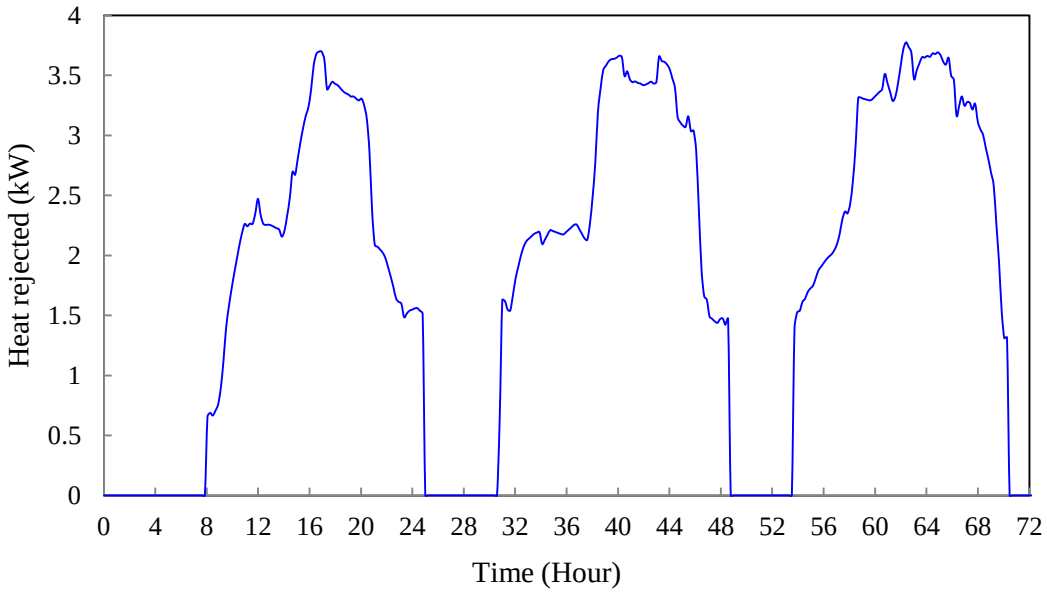

Fig. 6.11 Heat rejected by the cooling tower.

Fig. 6.12 shows the power consumed by the two air fans. The air handling fan consumes 10-186 W depending on the cooling load required by the building. Less

energy was consumed by the regenerator air fan because low flow of the scavenging air was required across the regenerator.

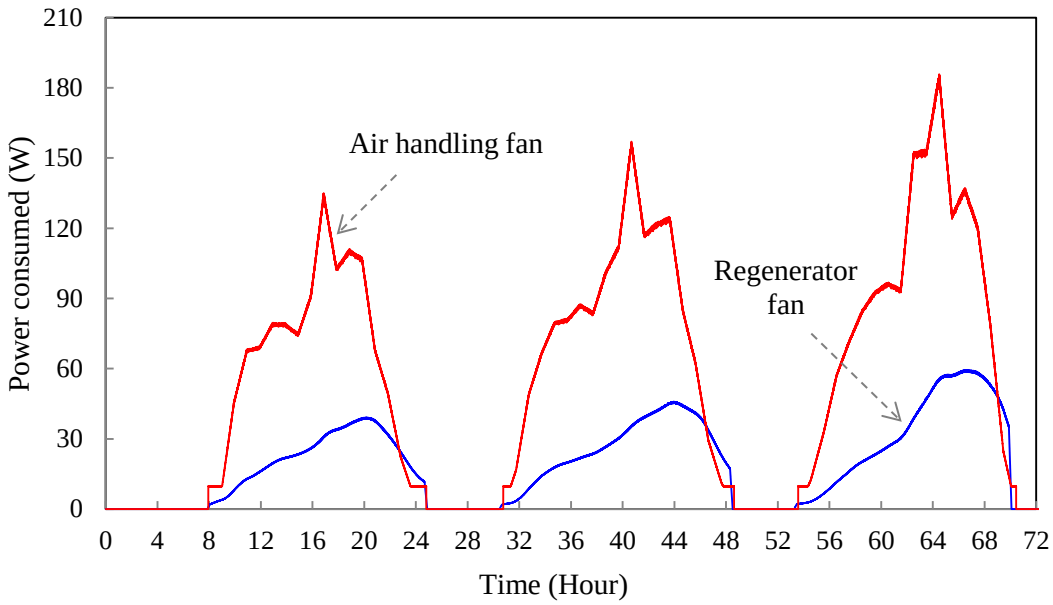

Fig. 6.12 Power consumed by the air fans.

Fig. 6.13 presents the power required to pump the water and solution across the absorber, regenerator, cooling tower and pump 3. The variation in the pump power consumption is due to the PID controllers that are used to control the operating speeds of variable speed pumps. The CT−pump has the highest power consumption among all the variable speed pumps due to the high flow rate needed to circulate the water in the cooling tower circuit. It can also be found that the electricity consumed by pump 3 is relatively low, especially during the peak periods. This is because, pump 3 circulates the water between the tank and the heat exchanger *II*, and during the peak periods, there is a low water flow requirement due to the high water temperature in the storage tank.

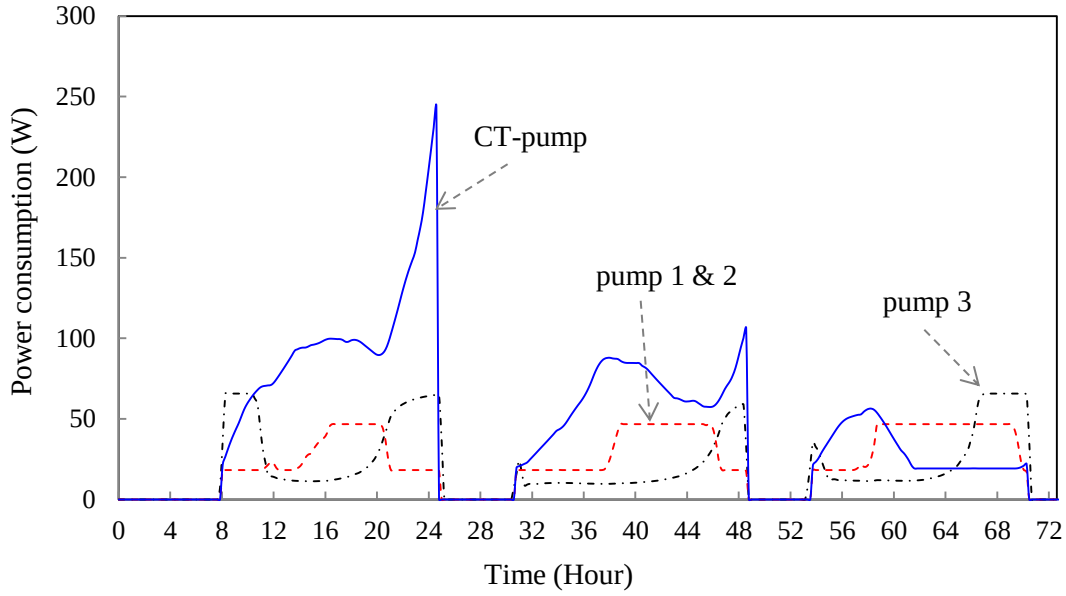

Fig. 6.13 Power consumed by the pumps.

In order to demonstrate the effectiveness of the proposed system, the thermal coefficient of performance (COP_{th}) as expressed in the following equation was used as a performance indicator in this study.

$$COP_{th} = \frac{Cooling\ Capacity}{Regeneration\ energy\ consumed} \tag{6.2}$$

Fig. 6.14 shows the variation of the thermal coefficient of performance of the system with the changes of the working conditions. The maximum COP_{th} was achieved during 8.00am-12.00pm due to the relatively low cooling demand of the building. The daily average COP_{th} was in the range of 0.5-0.55 during the three test days, demonstrating good performance of the system proposed.

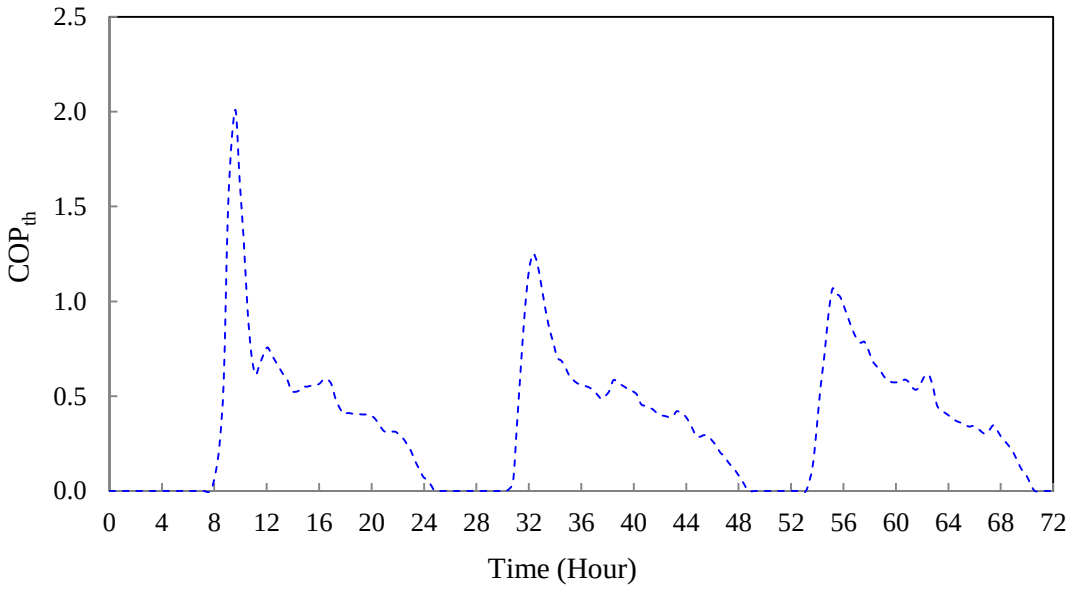

Fig. 6.14 System thermal coefficient of performance.

Fig. 6.15 shows the total power consumed by the air-conditioning system during the three test days including power consumptions of all pumps, air fans and the auxiliary heater. It is shown that, during the night time, the system consumes the highest power rate as the auxiliary heater is in operation.

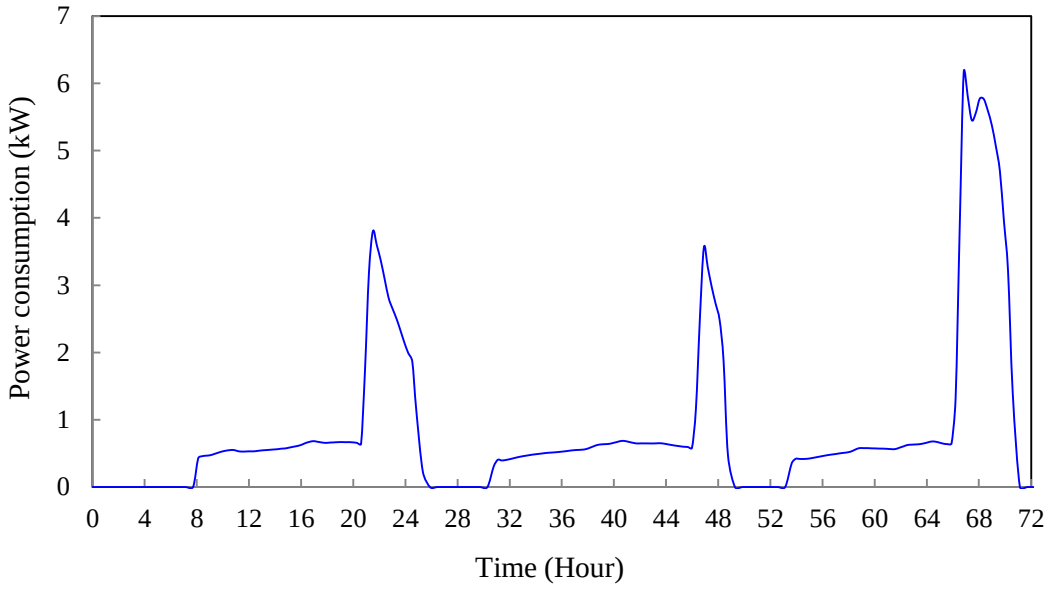

Fig. 6.15 Total electricity consumed by the system during the three test days.

6.4 Conclusion

The performance of the solar-assisted liquid desiccant dehumidification air-conditioning system by using whole system simulation was evaluated on the basis of Matlab Simulink platform developed, by taking into account the system-level and subsystem-level characteristics and interactions, and using the PID controllers to control the system to operate at the desired conditions. The evaporative cooler worked effectively in cooling the processed air such that the air could be delivered to the conditioned space with a temperature below 21.15°C, and the relative humidity of the processed air leaving from the absorber can be handled in the range of 21.6-33.7%. The inlet regenerator solution temperature and the outlet regenerator solution concentration were well controlled at around 60°C and 35%, respectively. A high share of the regeneration energy (i.e. about 73.4%) was provided by the solar water heating system. The cooling tower could reject the extra heat from the solution before entering the absorber with a set-point of 24°C. An average daily thermal coefficient of performance for the three typical consecutive sunny summer days of 0.5-0.55 could be achieved, revealing the good performance of the proposed solar-assisted liquid desiccant dehumidification air-conditioning system.

7 Conclusions and recommendations

Energy efficiency and conservation as well as decarbonising our energy sources are essential to create a sustainable energy future. Development of advanced liquid desiccant dehumidification air-conditioning systems may offer an alternative solution to reduce building energy consumption and provide good indoor thermal comfort. The current thesis has addressed these needs in some aspects. This chapter concludes the progress course of this study to examine the achievements towards this goal. This chapter then provides some suggested recommendations, which might be useful for further research in this area.

7.1 Summary of major findings

7.1.1 Development of an advanced solar-assisted liquid desiccant dehumidification air-conditioning system

The system was designed based on key findings and gaps were presented in the literature review chapter. Counter-flow random packed-bed absorber was employed in the proposed air-conditioning system as it provides high dehumidification effectiveness. The liquid desiccant used was lithium chloride solution due to its excellent dehumidification performance. A counter-current heat exchanger was used to preheat the weak solution that leaves the absorber by utilising the high temperature of the strong solution that leaves the regenerator to reduce the required regeneration heat. The system was integrated with a solar water heating system to provide the required heat for regeneration by using an array of flat plate solar collectors. The evaporative cooling technique was used to cool the processed air after leaving the absorber, and to provide the required thermal comfort for the conditioned space. A cooling tower was used to cool the liquid desiccant before entering the absorber.

7.1.2 Development of mathematical models of the system components

The models of the different components, including the absorber, regenerator, solar water heating system, air fans, fluid pumps, heat exchangers, and the evaporative cooler were developed on the basis of thermodynamics fundamentals and key correlations presented by other researchers. The model of the cooling tower was selected from the references. The validation of the models of the absorber and regenerator showed acceptable agreement between the experimental (i.e. sourced from the literature) and simulated results.

7.1.3 Development of a design approach to size the absorber and regenerator

In order to optimise the system performance, it was important to size the key components in the proposed solar-assisted liquid desiccant dehumidification air-conditioning system. Therefore, a simplified approach was developed to predict the height, diameter, weight, quantity of packings, and pressure drop of the absorber and regenerator. The pressure drop was calculated for both conditions, i.e. there is no liquid flow across the column by using Ergun equation, and there is a liquid flow in the column by using the Robbins and Eckert correlations. The pressure drop across the absorber was about 41.4 Pa/m for the dry column. Robbins and Eckert correlations in the calculation of the pressure drop when the column is wet showed good agreement. The results showed that 606 and 621 Pa/m could be achieved at the design stage by using Robbins and Eckert correlations, respectively. The study showed that 2.5 cm plastic Pall Rings packing offer low pressure drop, with flooding pressure drop of about 1.98 in H_2O/ft. The main results indicated that using an absorber and a regenerator with 0.6 m height and 0.4 m diameter is enough to provide the required mass transfer for the case studied in terms of the air dehumidification and desiccant regeneration for the proposed air-conditioning

system. The results also showed that 3830 piece of packings were required to fill the absorber and regenerator.

7.1.4 Whole system simulation

The different models were then integrated and internally linked in a detailed simulation platform by using Simulink Matlab. The simulation was run for three consecutive sunny summer days to explore and evaluate the various components' response and the whole system performance. It was found that the different components are highly interactive. The presence of the PID controllers played an important role in controlling the operating speed of the pumps and air fans, and hence providing the required thermal conditions in terms of air temperature and relative humidity, as well as controlling the regeneration temperature. The absorber could handle the processed air with humidity ratio ranging between 21.6-33.7%. Due to the ability of controlling the humidity ratio of the air across the absorber, the evaporative cooler could excellently handle the processed air with temperature below 21.15°C, and humidity ratio ranging between 78-90%. In order to ensure the continual high dehumidification performance of the absorber, the solution temperature must be low enough, and therefore, a cooling tower was used to reject the extra heat that gained by the solution due to the regeneration process, before entering the absorber.

The presence of the heat exchanger between the absorber and the regenerator assisted in reducing the heat of the strong solution and preheating the weak solution. The regeneration temperature was well controlled at around 60°C. The solar heating system provided 73.4% of the total heat energy needed, while an electric heater provided the rest. It is worthwhile to mention that, at the mid sunny days, the system

is expected to consume less energy by the auxiliary heater when less cooling is required, and high solar energy is stored. Thermally, the system achieved a good level of thermal performance such that average daily thermal coefficient of performance of about 0.5-0.55 could be achieved.

7.2 Recommendations

Due to the time constraints, no experimental tests were carried out in this study. The experimental investigations are important to estimate the system performance by taking into account the interactions among the different components. This issue thus will be addressed in a future study.

It is also important to optimise the solar water heating system which is utilised to provide the regeneration energy to re-concentrate the liquid desiccant. The optimisation can be established based on the local climate conditions, the economic aspects, and the building load demands.

Further research is also needed to explore the benefits of utilising the wasted heat from the regenerator such that higher thermal performance can be achieved if the hot air leaving the regenerator is utilised in preheating the weak solution before entering the regenerator.

References

Abdalla SA and Abdalla KN (2006), 'A radiant air-conditioning system using solar-driven liquid desiccant evaporative water cooler', *Journal of Engineering Science and Technology*, 1: 139 – 157.

Abdul-Wahab SA, Zurigat YH and Abu-Arabi MK (2004), 'Predictions of moisture removal rate and dehumidification effectiveness for structured liquid desiccant air dehumidifier', *Energy*, 29:19 – 34.

AGDA, Australian government department of industry (2008), 'Energy use in the Australian residential sector 1986 – 2020', accessed on 4 March 2014, available at http://ee.ret.gov.au/sites/default/files/documents/04_2013/energy-use-australian-residential-sector-1986-2020-part1.pdf.

Agrarwal RS (2001), *Emerging Technologies in Air-conditioning and Refrigeration*, Allied Publishers, New Delhi.

Al-Rawahi NZ, Zurigat YH and Al-Azri NA (2011), 'Prediction of hourly solar radiation on horizontal and inclined surfaces for muscat/oman', The journal of engineering research, 8: 19 – 31.

Arundel AV, Sterling EM, Sterling TD and Biggin JH (1986), 'Indirect Health Effects of Relative Humidity in Indoor Environments', *Environmental Health Perspectives*, 65: 351 – 361.

ASD (2006), *Australian solar radiation data handbook*, 4th edition, Australian and New Zealand Solar Energy Society, Sydney.

ASHRAE (2008), *ASHRAE Handbook - Heating, Ventilating, and Air-Conditioning Systems and Equipment*, Atlanta: American Society of Heating, Refrigerating and Air-Conditioning Engineers, Inc.

ASHRAE (2009), *ASHRAE handbook: fundamentals*, Atlanta: American Society of Heating, Refrigerating and Air-Conditioning Engineers, Inc.

Audah N, Ghaddar N and Ghali K (2011), 'Optimized solar-powered liquid desiccant system to supply building fresh water and cooling needs', *Applied Energy*, 88: 3726 – 3736.

Babakhani D and Soleymani M (2010), 'Simplified analysis of heat and mass transfer model in liquid desiccant regeneration process', *Journal of the Taiwan Institute of Chemical Engineers*, 41: 259 – 267.

Baughman AV and Arens EA (1996), 'Indoor humidity and human health - Part I: Literature review of health effects of humidity-influenced indoor pollutants', *ASHRAE Transactions*, 102: 193 – 211.

Ben Bacha H, Dammak T, Ben Abdalah AA and Maalej AY (2007), 'Desalination unit coupled with solar collectors and a storage tank: modelling and simulation', *Desalination*, 206: 341 – 352.

Chau CK and Worek WM (2009), 'Cosorption processes of triethylene glycol in a packed-bed liquid desiccant dehumidifier', *HVAC & R Research*, 15: 189 – 210.

Chaudhari SK and Patil KR (2002), 'Thermodynamic Properties of Aqueous Solutions of Lithium Chloride', *Physics and Chemistry of Liquids*, 40: 317 – 325.

Cheng Q and Zhang XS (2013), 'Review of solar regeneration methods for liquid desiccant air-conditioning system', *Energy and Buildings*, 67: 426 – 433.

Chung TW and Luo CM (1999), 'Vapour pressure of aqueous desiccant', *Journal Of Chemical And Engineering Data*, 44: 1024 – 1027.

Conde-Petit MR (2009), 'Aqueous solutions of lithium and calcium chlorides: property formulations for use in air-conditioning equipment design', *M.Conde Engineering*, 1 – 27.

Crabtree A and Siman-Tov M (1993), Report on 'Thermodynamic Properties of saturated light and heavy water for advanced neutron source applications', Oak Ridge Natlonal Moratory, USA.

Daou K, Wang RZ and Xia ZZ (2006), 'Desiccant cooling air conditioning: a review', *Renewable and Sustainable Energy Reviews*, 10: 55 – 77.

Das RS, Saha PK and Jain S (2012), 'Investigations on solar energy driven liquid desiccant cooling systems for tropical climates', Australian solar energy society the 5th annual conference 2012, Malburn, accessed 15June 2012, available at http://www.solar.org.au.

Davanagere BS, Sherif SA and Goswami DY (1999), 'A feasibility study of a solar desiccant air-conditioning system—Part I: psychrometrics and analysis of the conditioned zone', *International Journal of Energy Research*, 23: 7 – 21.

DesignBuilder (2013), http://www.designbuilder.com.au.

Elsarrag E (2006), 'Dehumidification of Air by Chemical Liquid Desiccant in a Packed Column and Its Heat and Mass Transfer Effectiveness' *HVAC&R Research*, 12: 3 – 16.

Fumo N and Goswami DY (2002), 'Study of an aqueous lithium chloride desiccant system: air dehumidification and desiccant regeneration', *Solar Energy*, 72: 351 – 361.

Gandhidasan P (1994), 'Performance analysis of an open-cycle liquid desiccant cooling system using solar energy for regeneration', *International Journal of Refrigeration*, 17: 475 – 480.

Gommed K and Grossman G (2007), 'Experimental investigation of a liquid desiccant system for solar cooling and dehumidification', *Solar Energy*, 81: 131 – 138.

Gommed K and Grossman G (2007), 'Experimental investigation of a liquid desiccant system for solar cooling and dehumidification', *Solar Energy*, 81: 131 – 138.

Groenewold H and Tsotsas E (1999), 'Predicting apparent Sherwood numbers for fluidized bed', *Drying Technology*, 17: 1557 – 1570.

Harriman LG (ed.) (2002), *The Dehumidification Handbook*, 2nd edition, Munters Corporation, Amesbury, USA.

Hottel HC (1976), 'A simple model for estimating the transmittance of direct solar radiation through clear atmospheres', *Solar Energy*, 18:129 – 134.

Huang SM and Zhang LZ (2013), 'Researches and trends in membrane-based liquid desiccant air dehumidification', *Renewable and Sustainable Energy Reviews*, 28: 425 – 440.

Incropera FP and DeWitt DP (1990), *Introduction to heat transfer*, Wiley and Sons, New York.

Jain S and Bansal PK (2007), 'Performance analysis of liquid desiccant dehumidification systems', *International Journal of Refrigeration*, 30: 861 – 872.

Jain S, Dhar PL and Kaushik SC (2000), 'Optimal design of liquid desiccant cooling systems', *ASHRAE Transactions*, 106: 79 – 86.

Kessling W, Laevemann E and Kapfhammer C (1998), 'Energy storage for desiccant cooling systems component development', *Solar Energy*, 64: 209 – 221.

Kister HZ (1992), *Distillation design*, McGraw-Hill, New York, accessed 8 Jan 2014, available at www.library.edu.au.

Kister HZ, Mathias PM, Steinmeyer DE, Penney WR, Crocker BB and Fair JR (2008), 'Equipment for distillation, gas absorption, phase dispersion, and phase separation' in Perry RH and Green DW, *Perry's chemical engineers' handbook*, McGraw-Hill, New York.

Koch-Glitsch, LP (2013), 'Structured Packings', accessed 2 February 2013, available at http://www.koch-glitsch.com.

Lazzarin RM and D'Ascanio A (2006), 'Investigation of an open cycle liquid desiccant system for the air-conditioning of an university building', *International Journal of Energy Research*, 31: 376 – 389.

Lazzarin RM, Gasparella A and Longo GA (1999), 'Chemical dehumidification by liquid desiccants: theory and experiment', *International Journal of Refrigeration*, 22: 334 – 347.

Lebrun J, Silva AC (2002), 'Cooling tower-model and experimental validation', *ASHRAE Transactions*, 108: 751 – 759.

Lebrun J, Silva CA, Trebilcock F, Winandy E (2004), 'Simplified models for direct and indirect contact cooling towers and evaporative condensers', *Building Services Engineering Research & Technology*, 25: 25 – 31.

Li X, Zhang, X and Quan S (2011), 'Single-stage and double-stage photovoltaic driven regeneration for liquid desiccant cooling system', *Applied Energy*, 88: 4908 – 4917.

Li YT and Yang HX (2008), 'Investigation on solar desiccant dehumidification process for energy conservation of central air-conditioning systems', *Applied Thermal Engineering*, 28: 1118 – 1126.

Liang Z, Jianhua L, Haijiang Z, Qilin G, Liwei Z and Huichen Z (2011), 'Application research on waste heat driven liquid desiccant air-conditioning system', Power and Energy Engineering Conference (APPEEC), Asia-Pacific, *IEEE* conference publications, 1: 25 – 28.

Liang ZH, Sanpasertparnich T, Tontiwachwuthikul P.PT, Gelowitz D, and Idem R (2011), 'Part 1: Design, modeling and simulation of post-combustion CO2 capture systems using reactive solvents', *Carbon Management*, 2: 265 – 288.

Liu X, Jiang Y and Qu K (2008), 'Analytical solution of combined heat and mass transfer performance in a cross-flow packed bed liquid desiccant air dehumidifier', *International Journal of Heat and Mass Transfer*, 51: 4563 – 4572.

Liu XH, Qu KY and Jiang Y (2006), 'Empirical correlations to predict the performance of the dehumidifier using liquid desiccant in heat and mass transfer', *Renewable Energy*, 31: 1627 – 639.

Liu XH, Yi XQ and Jiang Y (2011), 'Mass transfer performance comparison of two commonly used liquid desiccants: LiBr and LiCl aqueous solutions', *Energy Conversion and Management*, 52: 180 – 190.

Longo GA and Gasparella A (2005), 'Experimental and Theoretical Analysis of Heat and Mass Transfer in A Packed Column Dehumidifier/Regenerator with Liquid Desiccant', *International Journal of Heat and Mass Transfer*, 48: 5240 – 5254.

Lowenstein A (2008), 'Review of liquid desiccant technology for hvac applications', *HVAC&R Research*, 14: 819 – 839.

Lowenstein A, Slayzak S and Kozubal E (2006), 'A zero carryover liquid-desiccant air conditioner for solar applications', International Solar Energy Conference, ISEC2006, American society of mechanical engineers, pp. 397 – 407.

Lowenstein A, Slayzak S, Ryan J and Pesaran A (1998), 'Advanced commercial liquid-desiccant technology development study', Other Information: Supercedes report DE00012099; PBD: 18 Nov 1998; PBD.

Lychnos G (2010), *Feasibility of a solar-powered liquid desiccant cooling system for greenhouses*, PHD Thesis, Aston University, UK.

Ma ZJ and Wang SW (2011), 'Enhancing the performance of large primary-secondary chilled water systems by using bypass check valve', *Energy*, 36: 268 – 276.

Martin V and Goswami DY (2000), 'Effectiveness of heat and mass transfer processes in a packed bed liquid desiccant dehumidifier/regenerator', *HVAC & R Research*, 6: 21 – 39.

Martinez AT (1994), 'On the evaluation of the wet bulb temperature as a function of dry bulb temperature and relative humidity', *Atmosfera*, 7: 197 – 184.

Matlab (2013), http://www.mathworks.com.au; accessed 22 March 2013.

McDowall R (2006), *Fundamentals of HVAC systems*, Academic Press.

Mittal V, Kasana K and Thakur N (2005), 'The Study of Solar Absorption Air-Conditioning Systems', *Journal of Energy in Southern Africa*, 16: 59 – 66.

Mohammad AT, Mat SB, Sulaiman MY, Sopian K, and Al-abidi AA (2013), 'Historical review of liquid desiccant evaporation cooling technology', *Energy and Buildings*, 67: 22 – 33.

Mohan BS, Maiya MP, and Tiwari S (2008), 'Performance characterisation of liquid desiccant column for a hybrid air conditioner', *Applied Thermal Engineering*, 28: 1342 – 1355.

Munters (2012), 'Desiccant Wheels', accessed 26 March 2014, available at http://www.munters.com/upload/DocumentLibrary/MuntersDesiccantWheels.pdf.

Nauman EB (2008), *Chemical reactor design, optimization, and scaleup*, Wiley-AIChE, Hoboken, N.J.

Nayak SM, Hwang Y and Radermacher R (2009), 'Performance characterization of gas engine generator integrated with a liquid desiccant dehumidification system', *Applied Thermal Engineering*, 29: 479 – 490.

NSW Public Works Dept. State Projects (1993), *Building energy manual*, NSW, Sydney.

Öberg V and Goswami DY (1998), 'Experimental Study of the Heat and Mass Transfer in A Packed Bed Liquid Desiccant Air Dehumidifier', *Journal of Solar Energy Engineering*, 120: 289 – 297.

Oliveira AC, Afonsoa CF, Riffat SB and Doherty PS (2000), 'Thermal performance of a novel air conditioning system using a liquid desiccant', *Applied Thermal Engineering*, 20: 1213 – 1223.

ONS, http://www.overnitesupply.com, accessed July 2013.

Patanwar P and Shukla SK (2012), 'Parametric Studies of a Hybrid Desiccant Cooling', *International Journal of Energy Engineering*, 2: 253 – 258.

Patnaik S, Lenz TG, and Lof GOG (1990), 'Performance studies for an experimental solar open-cycle liquid desiccant air dehumidification system', *Solar Energy*, 44: 123 – 135.

Pesaran AA, Penny TR and Czanderna AW (1992), 'Desiccant cooling: state-of-the-art assessment', NREL/TP 254-4147 (1992), National Renewable Energy Laboratory, Golden, CO.

Piché S, Larachi F and Grandjean B.PA (2001), 'Flooding Capacity in Packed Towers: Database, Correlations, and Analysis', *Industrial & Engineering Chemistry Research*, 40: 476 – 487.

Rautenbach C (2009), *Modelling of flow through porous packing elements of a CO2 absorption tower*, Mater Thesis, Department of Mathematical Sciences, University of Stellenbosch, South Africa: Matieland.

Richards JR (2000), *Control of Gaseous Emissions: Student Manual, APTI Course 415*. North Carolina State University, USA, accessed 2 January 2014 available at www.4cleanair.org/apti/415combined.pdf.

Rishel JB (2001), 'Applying Affinity Laws For Centrifugal Pumps', *Heating/Piping/Air Conditioning Engineering : HPAC*, 73: 35 – 38.

Saman WY and Alizadeh S (2001), 'Modelling and performance analysis of a cross-flow type plate heat exchanger for dehumidification/cooling', *Solar Energy*, 70: 361 – 372.

Saman WY and Alizadeh S (2002), 'An experimental study of a cross-flow type plate heat exchanger for dehumidification/cooling', *Solar Energy*, 73: 59 – 71.

Schifftner KC (2002), 'Packed Towers' in *Air Pollution Control Equipment Selection Guide*, CRC Press, accessed 2 June 2012, available at http://uow.summon.serialssolutions.com.

SDH (2013), 'Solar district heating guidelines', accessed 1 September 2013, available at www.solar-district-heating.eu/Documents/Solar district heating guidelines.

Stine WB and Geyer M (2001), *Power from the sun*, accsessed 22 April 2013, available at http://www.powerfromthesun.net.

Wang J, Li CN, Liu JH, Liu SC and Chen J (2009), 'A new air-conditioning system of liquid desiccant and evaporation cooling', Power and Energy Engineering Conference, APPEEC 2009, Asia-Pacific, 1: 27 – 31.

Wanger W and Pruss A (1993), 'International equations for the saturation properties of ordinary water substance; revised according to the international temperature scale of 1990', Journal Of Physical And Chemestry, 22: 783 – 787.

Westerlund L and Dahl J (1994), 'Absorbers in the open absorption system', *Applied Energy*, 48: pp33-49.

Yin YG, Qian JF and Zhang XS (2014), 'Recent advancements in liquid desiccant dehumidification technology', *Renewable and Sustainable Energy Reviews*, 31: 38 – 52.

Zhai Z and McNeill JS (2014), 'Roles of building simulation tools in sustainable building design', *Building Simulation*, 7: 107 – 109.

Zhang T, Liu X and Jiang Y (2012), 'Performance optimization of heat pump driven liquid desiccant dehumidification systems', *Energy and Buildings*, 52: 132 – 144.

Zurigat YH, Abu-Arabi MK and Abdul-Wahab SA (2004), 'Air Dehumidification by Triethylene Glycol Desiccant in A Packed Column', *Energy Conversion and Management*, 45: 141 – 155.

Appendix A: the c-source code of the absorber

```
* Absorber.c
* Target selection: rsim.tlc
 * Note: GRT includes extra infrastructure and instrumentation for prototyping
 * Embedded hardware selection: 32-bit Generic
 * Emulation hardware selection:
 *    Differs from embedded hardware (MATLAB Host)
 * Code generation objectives: Unspecified
 * Validation result: Not run
#include <math.h>
#include "Absorber.h"
#include "Absorber_private.h"
#include "Absorber_dt.h"
#undef S_FUNCTION_NAME
#if !defined(RTW_GENERATED_SFCN_TUNABLE_PRMS_Absorber_sf)
#define RTW_GENERATED_SFCN_TUNABLE_PRMS_Absorber_sf
#endif
 #include "Absorber_sf.h"
 /* user code (top of parameter file) */
const int_T gblNumToFiles = 0;
const int_T gblNumFrFiles = 0;
const int_T gblNumFrWksBlocks = 0;
const char *gblSlvrJacPatternFileName =
  "Absorber_rsim_rtw\\Absorber_Jpattern.mat";
 /* Root inports information  */
const int_T gblNumRootInportBlks = 0;
const int_T gblNumModelInputs = 0;
extern rtInportTUtable *gblInportTUtables;
extern const char *gblInportFileName;
const int_T gblInportDataTypeIdx[] = { -1 };
const int_T gblInportDims[] = { -1 } ;
const int_T gblInportComplex[] = { -1 };
const int_T gblInportInterpoFlag[] = { -1 };
const int_T gblInportContinuous[] = { -1 };
#include "simstruc.h"
#include "fixedpoint.h"
const real_T Absorber_RGND = 0.0;      /* real_T ground */

/* Block signals (auto storage) */
BlockIO rtB;
/* Parent Simstruct */
```

```
static SimStruct model_S;
SimStruct *const rtS = &model_S;

/* Start for root system: '<Root>' */
void MdlStart(void)
{
  /* RTW Generated Level2 S-Function Block: '<S1>/Absorber' (Absorber_sf) */
  {
    SimStruct *rts = ssGetSFunction(rtS, 0);
    sfcnStart(rts);
    if (ssGetErrorStatus(rts) != (NULL))
      return;
  }
}

/* Outputs for root system: '<Root>' */
void MdlOutputs(int_T tid)
{
  /* RTW Generated Level2 S-Function Block: '<S1>/Absorber' (Absorber_sf) */
  {
    SimStruct *rts = ssGetSFunction(rtS, 0);
    sfcnOutputs(rts, 0);
  }

  /* tid is required for a uniform function interface.
   * Argument tid is not used in the function. */
  UNUSED_PARAMETER(tid);
}

/* Update for root system: '<Root>' */
void MdlUpdate(int_T tid)
{
  /* RTW Generated Level2 S-Function Block: '<S1>/Absorber' (Absorber_sf) */
  {
    SimStruct *rts = ssGetSFunction(rtS, 0);
    sfcnUpdate(rts, 0);
    if (ssGetErrorStatus(rts) != (NULL))
      return;
  }

  /* tid is required for a uniform function interface.
   * Argument tid is not used in the function. */
```

```
  UNUSED_PARAMETER(tid);
}

/* Termination for root system: '<Root>' */
void MdlTerminate(void)
{
  /* RTW Generated Level2 S-Function Block: '<S1>/Absorber' (Absorber_sf) */
  {
    SimStruct *rts = ssGetSFunction(rtS, 0);
    sfcnTerminate(rts);
  }
}
/* Function to initialize sizes */
void MdlInitializeSizes(void)
{
  ssSetNumContStates(rtS, 0);          /* Number of continuous states */
  ssSetNumY(rtS, 0);                   /* Number of model outputs */
  ssSetNumU(rtS, 0);                   /* Number of model inputs */
  ssSetDirectFeedThrough(rtS, 0);      /* The model is not direct feedthrough */
  ssSetNumSampleTimes(rtS, 1);         /* Number of sample times */
  ssSetNumBlocks(rtS, 1);              /* Number of blocks */
  ssSetNumBlockIO(rtS, 11);            /* Number of block outputs */
}
/* Function to initialize sample times. */
void MdlInitializeSampleTimes(void)
{
  /* task periods */
  ssSetSampleTime(rtS, 0, 0.0);

  /* task offsets */
  ssSetOffsetTime(rtS, 0, 1.0);
}

/* Function to register the model */
SimStruct * Absorber(void)
{
  static struct _ssMdlInfo mdlInfo;
  (void) memset((char *)rtS, 0,
                sizeof(SimStruct));
  (void) memset((char *)&mdlInfo, 0,
                sizeof(struct _ssMdlInfo));
  ssSetMdlInfoPtr(rtS, &mdlInfo);
```

```
/* timing info */
{
  static time_T mdlPeriod[NSAMPLE_TIMES];
  static time_T mdlOffset[NSAMPLE_TIMES];
  static time_T mdlTaskTimes[NSAMPLE_TIMES];
  static int_T mdlTsMap[NSAMPLE_TIMES];
  static int_T mdlSampleHits[NSAMPLE_TIMES];
  static boolean_T mdlTNextWasAdjustedPtr[NSAMPLE_TIMES];
  static int_T mdlPerTaskSampleHits[NSAMPLE_TIMES * NSAMPLE_TIMES];
  static time_T mdlTimeOfNextSampleHit[NSAMPLE_TIMES];

  {
    int_T i;
    for (i = 0; i < NSAMPLE_TIMES; i++) {
      mdlPeriod[i] = 0.0;
      mdlOffset[i] = 0.0;
      mdlTaskTimes[i] = 0.0;
      mdlTsMap[i] = i;
      mdlSampleHits[i] = 1;
    }
  }

  ssSetSampleTimePtr(rtS, &mdlPeriod[0]);
  ssSetOffsetTimePtr(rtS, &mdlOffset[0]);
  ssSetSampleTimeTaskIDPtr(rtS, &mdlTsMap[0]);
  ssSetTPtr(rtS, &mdlTaskTimes[0]);
  ssSetSampleHitPtr(rtS, &mdlSampleHits[0]);
  ssSetTNextWasAdjustedPtr(rtS, &mdlTNextWasAdjustedPtr[0]);
  ssSetPerTaskSampleHitsPtr(rtS, &mdlPerTaskSampleHits[0]);
  ssSetTimeOfNextSampleHitPtr(rtS, &mdlTimeOfNextSampleHit[0]);
}
ssSetSolverMode(rtS, SOLVER_MODE_SINGLETASKING);

/*
 * initialize model vectors and cache them in SimStruct
 */

/* block I/O */
{
  ssSetBlockIO(rtS, ((void *) &rtB));
  (void) memset(((void *) &rtB), 0,
```

```
            sizeof(BlockIO));
}
/* data type transition information */
{
  static DataTypeTransInfo dtInfo;
  (void) memset((char_T *) &dtInfo, 0,
            sizeof(dtInfo));
  ssSetModelMappingInfo(rtS, &dtInfo);
  dtInfo.numDataTypes = 14;
  dtInfo.dataTypeSizes = &rtDataTypeSizes[0];
  dtInfo.dataTypeNames = &rtDataTypeNames[0];

  /* Block I/O transition table */
  dtInfo.B = &rtBTransTable;
}

/* Model specific registration */
ssSetRootSS(rtS, rtS);
ssSetVersion(rtS, SIMSTRUCT_VERSION_LEVEL2);
ssSetModelName(rtS, "Absorber");
ssSetPath(rtS, "Absorber");
ssSetTStart(rtS, 1.0);
ssSetTFinal(rtS, 10.0);
/* Setup for data logging */
{
  static RTWLogInfo rt_DataLoggingInfo;
  ssSetRTWLogInfo(rtS, &rt_DataLoggingInfo);
}
/* Setup for data logging */
{
  rtliSetLogXSignalInfo(ssGetRTWLogInfo(rtS), (NULL));
  rtliSetLogXSignalPtrs(ssGetRTWLogInfo(rtS), (NULL));
  rtliSetLogT(ssGetRTWLogInfo(rtS), "tout");
  rtliSetLogX(ssGetRTWLogInfo(rtS), "");
  rtliSetLogXFinal(ssGetRTWLogInfo(rtS), "");
  rtliSetSigLog(ssGetRTWLogInfo(rtS), "");
  rtliSetLogVarNameModifier(ssGetRTWLogInfo(rtS), "rt_");
  rtliSetLogFormat(ssGetRTWLogInfo(rtS), 0);
  rtliSetLogMaxRows(ssGetRTWLogInfo(rtS), 1000);
  rtliSetLogDecimation(ssGetRTWLogInfo(rtS), 1);
  rtliSetLogY(ssGetRTWLogInfo(rtS), "");
  rtliSetLogYSignalInfo(ssGetRTWLogInfo(rtS), (NULL));
```

```
 rtliSetLogYSignalPtrs(ssGetRTWLogInfo(rtS), (NULL));
}

{
 static ssSolverInfo slvrInfo;
 ssSetStepSize(rtS, 1.0);
 ssSetMinStepSize(rtS, 0.0);
 ssSetMaxNumMinSteps(rtS, -1);
 ssSetMinStepViolatedError(rtS, 0);
 ssSetMaxStepSize(rtS, 1.0);
 ssSetSolverMaxOrder(rtS, -1);
 ssSetSolverRefineFactor(rtS, 1);
 ssSetOutputTimes(rtS, (NULL));
 ssSetNumOutputTimes(rtS, 0);
 ssSetOutputTimesOnly(rtS, 0);
 ssSetOutputTimesIndex(rtS, 0);
 ssSetZCCacheNeedsReset(rtS, 0);
 ssSetDerivCacheNeedsReset(rtS, 0);
 ssSetNumNonContDerivSigInfos(rtS, 0);
 ssSetNonContDerivSigInfos(rtS, (NULL));
 ssSetSolverInfo(rtS, &slvrInfo);
 ssSetSolverName(rtS, "VariableStepDiscrete");
 ssSetVariableStepSolver(rtS, 1);
 ssSetSolverConsistencyChecking(rtS, 0);
 ssSetSolverAdaptiveZcDetection(rtS, 0);
 ssSetSolverRobustResetMethod(rtS, 0);
 ssSetSolverStateProjection(rtS, 0);
 ssSetSolverMassMatrixType(rtS, (ssMatrixType)0);
 ssSetSolverMassMatrixNzMax(rtS, 0);
 ssSetModelOutputs(rtS, MdlOutputs);
 ssSetModelLogData(rtS, rt_UpdateTXYLogVars);
 ssSetModelUpdate(rtS, MdlUpdate);
 ssSetTNextTid(rtS, INT_MIN);
 ssSetTNext(rtS, rtMinusInf);
 ssSetSolverNeedsReset(rtS);
 ssSetNumNonsampledZCs(rtS, 0);
}

ssSetChecksumVal(rtS, 0, 2057640626U);
ssSetChecksumVal(rtS, 1, 3259018578U);
ssSetChecksumVal(rtS, 2, 1169092376U);
ssSetChecksumVal(rtS, 3, 3706155210U);
```

```
/* child S-Function registration */
ssSetNumSFunctions(rtS, 1);

/* register each child */
{
  static SimStruct childSFunctions[1];
  static SimStruct *childSFunctionPtrs[1];
  (void) memset((void *)&childSFunctions[0], 0,
                sizeof(childSFunctions));
  ssSetSFunctions(rtS, &childSFunctionPtrs[0]);
  ssSetSFunction(rtS, 0, &childSFunctions[0]);
  /* RTW Generated Level2 S-Function Block: Absorber/<S1>/Absorber (Absorber_sf) */
  {
    SimStruct *rts = ssGetSFunction(rtS, 0);
    /* timing info */
    static time_T sfcnPeriod[1];
    static time_T sfcnOffset[1];
    static int_T sfcnTsMap[1];
    (void) memset((void*)sfcnPeriod, 0,
                  sizeof(time_T)*1);
    (void) memset((void*)sfcnOffset, 0,
                  sizeof(time_T)*1);
    ssSetSampleTimePtr(rts, &sfcnPeriod[0]);
    ssSetOffsetTimePtr(rts, &sfcnOffset[0]);
    ssSetSampleTimeTaskIDPtr(rts, sfcnTsMap);

    /* Set up the mdlInfo pointer */
    ssSetMdlInfoPtr(rts, ssGetMdlInfoPtr(rtS));

    /* Allocate memory of model methods 2 */
    {
      static struct _ssSFcnModelMethods2 methods2;
      ssSetModelMethods2(rts, &methods2);
    }

    /* Allocate memory of model methods 3 */
    {
      static struct _ssSFcnModelMethods3 methods3;
      ssSetModelMethods3(rts, &methods3);
    }
```

```
/* Allocate memory for states auxilliary information */
{
 static struct _ssStatesInfo2 statesInfo2;
 ssSetStatesInfo2(rts, &statesInfo2);
}

/* inputs */
{
 static struct _ssPortInputs inputPortInfo[10];
 _ssSetNumInputPorts(rts, 10);
 ssSetPortInfoForInputs(rts, &inputPortInfo[0]);

 /* port 0 */
 {
  static real_T const *sfcnUPtrs[1];
  sfcnUPtrs[0] = (real_T*)&Absorber_RGND;
  ssSetInputPortSignalPtrs(rts, 0, (InputPtrsType)&sfcnUPtrs[0]);
  _ssSetInputPortNumDimensions(rts, 0, 1);
  ssSetInputPortWidth(rts, 0, 1);
 }
 /* port 1 */
 {
  static real_T const *sfcnUPtrs[1];
  sfcnUPtrs[0] = (real_T*)&Absorber_RGND;
  ssSetInputPortSignalPtrs(rts, 1, (InputPtrsType)&sfcnUPtrs[0]);
  _ssSetInputPortNumDimensions(rts, 1, 1);
  ssSetInputPortWidth(rts, 1, 1);
 }

 /* port 2 */
 {
  static real_T const *sfcnUPtrs[1];
  sfcnUPtrs[0] = (real_T*)&Absorber_RGND;
  ssSetInputPortSignalPtrs(rts, 2, (InputPtrsType)&sfcnUPtrs[0]);
  _ssSetInputPortNumDimensions(rts, 2, 1);
  ssSetInputPortWidth(rts, 2, 1);
 }
  /* port 3 */
 {
  static real_T const *sfcnUPtrs[1];
  sfcnUPtrs[0] = (real_T*)&Absorber_RGND;
  ssSetInputPortSignalPtrs(rts, 3, (InputPtrsType)&sfcnUPtrs[0]);
```

```
  _ssSetInputPortNumDimensions(rts, 3, 1);
  ssSetInputPortWidth(rts, 3, 1);
}

/* port 4 */
{
  static real_T const *sfcnUPtrs[1];
  sfcnUPtrs[0] = (real_T*)&Absorber_RGND;
  ssSetInputPortSignalPtrs(rts, 4, (InputPtrsType)&sfcnUPtrs[0]);
  _ssSetInputPortNumDimensions(rts, 4, 1);
  ssSetInputPortWidth(rts, 4, 1);
}
 /* port 5 */
{
  static real_T const *sfcnUPtrs[1];
  sfcnUPtrs[0] = (real_T*)&Absorber_RGND;
  ssSetInputPortSignalPtrs(rts, 5, (InputPtrsType)&sfcnUPtrs[0]);
  _ssSetInputPortNumDimensions(rts, 5, 1);
  ssSetInputPortWidth(rts, 5, 1);
}

/* port 6 */
{
  static real_T const *sfcnUPtrs[1];
  sfcnUPtrs[0] = (real_T*)&Absorber_RGND;
  ssSetInputPortSignalPtrs(rts, 6, (InputPtrsType)&sfcnUPtrs[0]);
  _ssSetInputPortNumDimensions(rts, 6, 1);
  ssSetInputPortWidth(rts, 6, 1);
}

/* port 7 */
{
  static real_T const *sfcnUPtrs[1];
  sfcnUPtrs[0] = (real_T*)&Absorber_RGND;
  ssSetInputPortSignalPtrs(rts, 7, (InputPtrsType)&sfcnUPtrs[0]);
  _ssSetInputPortNumDimensions(rts, 7, 1);
  ssSetInputPortWidth(rts, 7, 1);
}

/* port 8 */
{
  static real_T const *sfcnUPtrs[1];
```

```
    sfcnUPtrs[0] = (real_T*)&Absorber_RGND;
    ssSetInputPortSignalPtrs(rts, 8, (InputPtrsType)&sfcnUPtrs[0]);
    _ssSetInputPortNumDimensions(rts, 8, 1);
    ssSetInputPortWidth(rts, 8, 1);
  }
  /* port 9 */
  {
    static real_T const *sfcnUPtrs[1];
    sfcnUPtrs[0] = (real_T*)&Absorber_RGND;
    ssSetInputPortSignalPtrs(rts, 9, (InputPtrsType)&sfcnUPtrs[0]);
    _ssSetInputPortNumDimensions(rts, 9, 1);
    ssSetInputPortWidth(rts, 9, 1);
  }
}

/* outputs */
{
  static struct _ssPortOutputs outputPortInfo[11];
  ssSetPortInfoForOutputs(rts, &outputPortInfo[0]);
  _ssSetNumOutputPorts(rts, 11);

  /* port 0 */
  {
    _ssSetOutputPortNumDimensions(rts, 0, 1);
    ssSetOutputPortWidth(rts, 0, 1);
    ssSetOutputPortSignal(rts, 0, ((real_T *) &rtB.Absorber_o1));
  }

  /* port 1 */
  {
    _ssSetOutputPortNumDimensions(rts, 1, 1);
    ssSetOutputPortWidth(rts, 1, 1);
    ssSetOutputPortSignal(rts, 1, ((real_T *) &rtB.Absorber_o2));
  }

  /* port 2 */
  {
    _ssSetOutputPortNumDimensions(rts, 2, 1);
    ssSetOutputPortWidth(rts, 2, 1);
    ssSetOutputPortSignal(rts, 2, ((real_T *) &rtB.Absorber_o3));
  }
```

```
/* port 3 */
{
  _ssSetOutputPortNumDimensions(rts, 3, 1);
  ssSetOutputPortWidth(rts, 3, 1);
  ssSetOutputPortSignal(rts, 3, ((real_T *) &rtB.Absorber_o4));
}

/* port 4 */
{
  _ssSetOutputPortNumDimensions(rts, 4, 1);
  ssSetOutputPortWidth(rts, 4, 1);
  ssSetOutputPortSignal(rts, 4, ((real_T *) &rtB.Absorber_o5));
}

/* port 5 */
{
  _ssSetOutputPortNumDimensions(rts, 5, 1);
  ssSetOutputPortWidth(rts, 5, 1);
  ssSetOutputPortSignal(rts, 5, ((real_T *) &rtB.Absorber_o6));
}

/* port 6 */
{
  _ssSetOutputPortNumDimensions(rts, 6, 1);
  ssSetOutputPortWidth(rts, 6, 1);
  ssSetOutputPortSignal(rts, 6, ((real_T *) &rtB.Absorber_o7));
}

/* port 7 */
{
  _ssSetOutputPortNumDimensions(rts, 7, 1);
  ssSetOutputPortWidth(rts, 7, 1);
  ssSetOutputPortSignal(rts, 7, ((real_T *) &rtB.Absorber_o8));
}

/* port 8 */
{
  _ssSetOutputPortNumDimensions(rts, 8, 1);
  ssSetOutputPortWidth(rts, 8, 1);
  ssSetOutputPortSignal(rts, 8, ((real_T *) &rtB.Absorber_o9));
}
```

```
  /* port 9 */
  {
    _ssSetOutputPortNumDimensions(rts, 9, 1);
    ssSetOutputPortWidth(rts, 9, 1);
    ssSetOutputPortSignal(rts, 9, ((real_T *) &rtB.Absorber_o10));
  }

  /* port 10 */
  {
    _ssSetOutputPortNumDimensions(rts, 10, 1);
    ssSetOutputPortWidth(rts, 10, 1);
    ssSetOutputPortSignal(rts, 10, ((real_T *) &rtB.Absorber_o11));
  }
}

/* path info */
ssSetModelName(rts, "Absorber");
ssSetPath(rts, "Absorber/Absorber/Absorber");
if (ssGetRTModel(rtS) == (NULL)) {
  ssSetParentSS(rts, rtS);
  ssSetRootSS(rts, ssGetRootSS(rtS));
} else {
  ssSetRTModel(rts,ssGetRTModel(rtS));
  ssSetParentSS(rts, (NULL));
  ssSetRootSS(rts, rts);
}

ssSetVersion(rts, SIMSTRUCT_VERSION_LEVEL2);

/* registration */
Absorber_sf(rts);
sfcnInitializeSizes(rts);
sfcnInitializeSampleTimes(rts);

/* adjust sample time */
ssSetSampleTime(rts, 0, 0.0);
ssSetOffsetTime(rts, 0, 1.0);
sfcnTsMap[0] = 0;

/* set compiled values of dynamic vector attributes */
ssSetNumNonsampledZCs(rts, 0);
```

```
/* Update connectivity flags for each port */
_ssSetInputPortConnected(rts, 0, 0);
_ssSetInputPortConnected(rts, 1, 0);
_ssSetInputPortConnected(rts, 2, 0);
_ssSetInputPortConnected(rts, 3, 0);
_ssSetInputPortConnected(rts, 4, 0);
_ssSetInputPortConnected(rts, 5, 0);
_ssSetInputPortConnected(rts, 6, 0);
_ssSetInputPortConnected(rts, 7, 0);
_ssSetInputPortConnected(rts, 8, 0);
_ssSetInputPortConnected(rts, 9, 0);
_ssSetOutputPortConnected(rts, 0, 0);
_ssSetOutputPortConnected(rts, 1, 0);
_ssSetOutputPortConnected(rts, 2, 0);
_ssSetOutputPortConnected(rts, 3, 0);
_ssSetOutputPortConnected(rts, 4, 0);
_ssSetOutputPortConnected(rts, 5, 0);
_ssSetOutputPortConnected(rts, 6, 0);
_ssSetOutputPortConnected(rts, 7, 0);
_ssSetOutputPortConnected(rts, 8, 0);
_ssSetOutputPortConnected(rts, 9, 0);
_ssSetOutputPortConnected(rts, 10, 0);
_ssSetOutputPortBeingMerged(rts, 0, 0);
_ssSetOutputPortBeingMerged(rts, 1, 0);
_ssSetOutputPortBeingMerged(rts, 2, 0);
_ssSetOutputPortBeingMerged(rts, 3, 0);
_ssSetOutputPortBeingMerged(rts, 4, 0);
_ssSetOutputPortBeingMerged(rts, 5, 0);
_ssSetOutputPortBeingMerged(rts, 6, 0);
_ssSetOutputPortBeingMerged(rts, 7, 0);
_ssSetOutputPortBeingMerged(rts, 8, 0);
_ssSetOutputPortBeingMerged(rts, 9, 0);
_ssSetOutputPortBeingMerged(rts, 10, 0);

/* Update the BufferDstPort flags for each input port */
ssSetInputPortBufferDstPort(rts, 0, -1);
ssSetInputPortBufferDstPort(rts, 1, -1);
ssSetInputPortBufferDstPort(rts, 2, -1);
ssSetInputPortBufferDstPort(rts, 3, -1);
ssSetInputPortBufferDstPort(rts, 4, -1);
ssSetInputPortBufferDstPort(rts, 5, -1);
ssSetInputPortBufferDstPort(rts, 6, -1);
```

```
    ssSetInputPortBufferDstPort(rts, 7, -1);
    ssSetInputPortBufferDstPort(rts, 8, -1);
    ssSetInputPortBufferDstPort(rts, 9, -1);

    /* Instance data for generated S-Function: Absorber */
#include "Absorber_sfcn_rtw/Absorber_sid.h"

   }
  }

  return rtS;
}
```

Appendix B: the c-source code of the regenerator

```
 * Regenerator.c
* Target selection: rsim.tlc
 * Note: GRT includes extra infrastructure and instrumentation for prototyping
 * Embedded hardware selection: 32-bit Generic
 * Emulation hardware selection:
 *    Differs from embedded hardware (MATLAB Host)
 * Code generation objectives: Unspecified
 * Validation result: Not run
#include <math.h>
#include "Regenerator.h"
#include "Regenerator_private.h"
#include "Regenerator_dt.h"
#undef S_FUNCTION_NAME
#if !defined(RTW_GENERATED_SFCN_TUNABLE_PRMS_Regenerator1_sf)
#define RTW_GENERATED_SFCN_TUNABLE_PRMS_Regenerator1_sf
#endif
 #include "Regenerator1_sf.h"
/* user code (top of parameter file) */
const int_T gblNumToFiles = 0;
const int_T gblNumFrFiles = 0;
const int_T gblNumFrWksBlocks = 0;
const char *gblSlvrJacPatternFileName =
  "Regenerator_rsim_rtw\\Regenerator_Jpattern.mat";
/* Root inports information  */
const int_T gblNumRootInportBlks = 0;
const int_T gblNumModelInputs = 0;
```

```
extern rtInportTUtable *gblInportTUtables;
extern const char *gblInportFileName;
const int_T gblInportDataTypeIdx[] = { -1 };
const int_T gblInportDims[] = { -1 } ;
const int_T gblInportComplex[] = { -1 };
 const int_T gblInportInterpoFlag[] = { -1 };
const int_T gblInportContinuous[] = { -1 };
 #include "simstruc.h"
#include "fixedpoint.h"

const real_T Regenerator_RGND = 0.0;   /* real_T ground */

/* Block signals (auto storage) */
BlockIO rtB;

/* Block states (auto storage) */
D_Work rtDWork;

/* Parent Simstruct */
static SimStruct model_S;
SimStruct *const rtS = &model_S;

/* Start for root system: '<Root>' */
void MdlStart(void)
{
  /* RTW Generated Level2 S-Function Block: '<S1>/Regenerator' (Regenerator1_sf) */
  {
    SimStruct *rts = ssGetSFunction(rtS, 0);
    sfcnStart(rts);
    if (ssGetErrorStatus(rts) != (NULL))
      return;
  }
}

/* Outputs for root system: '<Root>' */
void MdlOutputs(int_T tid)
{
  /* RTW Generated Level2 S-Function Block: '<S1>/Regenerator' (Regenerator1_sf) */
  {
    SimStruct *rts = ssGetSFunction(rtS, 0);
    sfcnOutputs(rts, 0);
  }
```

```
  /* tid is required for a uniform function interface.
   * Argument tid is not used in the function. */
  UNUSED_PARAMETER(tid);
}

/* Update for root system: '<Root>' */
void MdlUpdate(int_T tid)
{
  /* RTW Generated Level2 S-Function Block: '<S1>/Regenerator' (Regenerator1_sf) */
  {
    SimStruct *rts = ssGetSFunction(rtS, 0);
    sfcnUpdate(rts, 0);
    if (ssGetErrorStatus(rts) != (NULL))
      return;
  }

  /* tid is required for a uniform function interface.
   * Argument tid is not used in the function. */
  UNUSED_PARAMETER(tid);
}

/* Termination for root system: '<Root>' */
void MdlTerminate(void)
{
  /* RTW Generated Level2 S-Function Block: '<S1>/Regenerator' (Regenerator1_sf) */
  {
    SimStruct *rts = ssGetSFunction(rtS, 0);
    sfcnTerminate(rts);
  }
}

/* Function to initialize sizes */
void MdlInitializeSizes(void)
{
  ssSetNumContStates(rtS, 0);          /* Number of continuous states */
  ssSetNumY(rtS, 0);                   /* Number of model outputs */
  ssSetNumU(rtS, 0);                   /* Number of model inputs */
  ssSetDirectFeedThrough(rtS, 0);      /* The model is not direct feedthrough */
  ssSetNumSampleTimes(rtS, 2);         /* Number of sample times */
  ssSetNumBlocks(rtS, 1);              /* Number of blocks */
  ssSetNumBlockIO(rtS, 8);             /* Number of block outputs */
```

```
}

/* Function to initialize sample times. */
void MdlInitializeSampleTimes(void)
{
  /* task periods */
  ssSetSampleTime(rtS, 0, 0.0);
  ssSetSampleTime(rtS, 1, 60.0);

  /* task offsets */
  ssSetOffsetTime(rtS, 0, 1.0);
  ssSetOffsetTime(rtS, 1, 0.0);
}

/* Function to register the model */
SimStruct * Regenerator(void)
{
  static struct _ssMdlInfo mdlInfo;
  (void) memset((char *)rtS, 0,
                sizeof(SimStruct));
  (void) memset((char *)&mdlInfo, 0,
                sizeof(struct _ssMdlInfo));
  ssSetMdlInfoPtr(rtS, &mdlInfo);

  /* timing info */
  {
    static time_T mdlPeriod[NSAMPLE_TIMES];
    static time_T mdlOffset[NSAMPLE_TIMES];
    static time_T mdlTaskTimes[NSAMPLE_TIMES];
    static int_T mdlTsMap[NSAMPLE_TIMES];
    static int_T mdlSampleHits[NSAMPLE_TIMES];
    static boolean_T mdlTNextWasAdjustedPtr[NSAMPLE_TIMES];
    static int_T mdlPerTaskSampleHits[NSAMPLE_TIMES * NSAMPLE_TIMES];
    static time_T mdlTimeOfNextSampleHit[NSAMPLE_TIMES];

    {
      int_T i;
      for (i = 0; i < NSAMPLE_TIMES; i++) {
        mdlPeriod[i] = 0.0;
        mdlOffset[i] = 0.0;
        mdlTaskTimes[i] = 0.0;
        mdlTsMap[i] = i;
```

```
      mdlSampleHits[i] = 1;
    }
  }

  ssSetSampleTimePtr(rtS, &mdlPeriod[0]);
  ssSetOffsetTimePtr(rtS, &mdlOffset[0]);
  ssSetSampleTimeTaskIDPtr(rtS, &mdlTsMap[0]);
  ssSetTPtr(rtS, &mdlTaskTimes[0]);
  ssSetSampleHitPtr(rtS, &mdlSampleHits[0]);
  ssSetTNextWasAdjustedPtr(rtS, &mdlTNextWasAdjustedPtr[0]);
  ssSetPerTaskSampleHitsPtr(rtS, &mdlPerTaskSampleHits[0]);
  ssSetTimeOfNextSampleHitPtr(rtS, &mdlTimeOfNextSampleHit[0]);
}

ssSetSolverMode(rtS, SOLVER_MODE_SINGLETASKING);

/*
 * initialize model vectors and cache them in SimStruct
 */

/* block I/O */
{
  ssSetBlockIO(rtS, ((void *) &rtB));
  (void) memset(((void *) &rtB), 0,
                sizeof(BlockIO));
}

/* states (dwork) */
{
  void *dwork = (void *) &rtDWork;
  ssSetRootDWork(rtS, dwork);
  (void) memset(dwork, 0,
                sizeof(D_Work));
}

/* data type transition information */
{
  static DataTypeTransInfo dtInfo;
  (void) memset((char_T *) &dtInfo, 0,
                sizeof(dtInfo));
  ssSetModelMappingInfo(rtS, &dtInfo);
  dtInfo.numDataTypes = 14;
```

```
  dtInfo.dataTypeSizes = &rtDataTypeSizes[0];
  dtInfo.dataTypeNames = &rtDataTypeNames[0];

  /* Block I/O transition table */
  dtInfo.B = &rtBTransTable;
}

/* Model specific registration */
ssSetRootSS(rtS, rtS);
ssSetVersion(rtS, SIMSTRUCT_VERSION_LEVEL2);
ssSetModelName(rtS, "Regenerator");
ssSetPath(rtS, "Regenerator");
ssSetTStart(rtS, 1.0);
ssSetTFinal(rtS, 10.0);

/* Setup for data logging */
{
  static RTWLogInfo rt_DataLoggingInfo;
  ssSetRTWLogInfo(rtS, &rt_DataLoggingInfo);
}

/* Setup for data logging */
{
  rtliSetLogXSignalInfo(ssGetRTWLogInfo(rtS), (NULL));
  rtliSetLogXSignalPtrs(ssGetRTWLogInfo(rtS), (NULL));
  rtliSetLogT(ssGetRTWLogInfo(rtS), "tout");
  rtliSetLogX(ssGetRTWLogInfo(rtS), "");
  rtliSetLogXFinal(ssGetRTWLogInfo(rtS), "");
  rtliSetSigLog(ssGetRTWLogInfo(rtS), "");
  rtliSetLogVarNameModifier(ssGetRTWLogInfo(rtS), "rt_");
  rtliSetLogFormat(ssGetRTWLogInfo(rtS), 0);
  rtliSetLogMaxRows(ssGetRTWLogInfo(rtS), 1000);
  rtliSetLogDecimation(ssGetRTWLogInfo(rtS), 1);
  rtliSetLogY(ssGetRTWLogInfo(rtS), "");
  rtliSetLogYSignalInfo(ssGetRTWLogInfo(rtS), (NULL));
  rtliSetLogYSignalPtrs(ssGetRTWLogInfo(rtS), (NULL));
}

{
  static ssSolverInfo slvrInfo;
  ssSetStepSize(rtS, 1.0);
  ssSetMinStepSize(rtS, 0.0);
```

```
  ssSetMaxNumMinSteps(rtS, -1);
  ssSetMinStepViolatedError(rtS, 0);
  ssSetMaxStepSize(rtS, 1.0);
  ssSetSolverMaxOrder(rtS, -1);
  ssSetSolverRefineFactor(rtS, 1);
  ssSetOutputTimes(rtS, (NULL));
  ssSetNumOutputTimes(rtS, 0);
  ssSetOutputTimesOnly(rtS, 0);
  ssSetOutputTimesIndex(rtS, 0);
  ssSetZCCacheNeedsReset(rtS, 0);
  ssSetDerivCacheNeedsReset(rtS, 0);
  ssSetNumNonContDerivSigInfos(rtS, 0);
  ssSetNonContDerivSigInfos(rtS, (NULL));
  ssSetSolverInfo(rtS, &slvrInfo);
  ssSetSolverName(rtS, "VariableStepDiscrete");
  ssSetVariableStepSolver(rtS, 1);
  ssSetSolverConsistencyChecking(rtS, 0);
  ssSetSolverAdaptiveZcDetection(rtS, 0);
  ssSetSolverRobustResetMethod(rtS, 0);
  ssSetSolverStateProjection(rtS, 0);
  ssSetSolverMassMatrixType(rtS, (ssMatrixType)0);
  ssSetSolverMassMatrixNzMax(rtS, 0);
  ssSetModelOutputs(rtS, MdlOutputs);
  ssSetModelLogData(rtS, rt_UpdateTXYLogVars);
  ssSetModelUpdate(rtS, MdlUpdate);
  ssSetTNextTid(rtS, INT_MIN);
  ssSetTNext(rtS, rtMinusInf);
  ssSetSolverNeedsReset(rtS);
  ssSetNumNonsampledZCs(rtS, 0);
}

ssSetChecksumVal(rtS, 0, 123438343U);
ssSetChecksumVal(rtS, 1, 489284708U);
ssSetChecksumVal(rtS, 2, 2432187286U);
ssSetChecksumVal(rtS, 3, 576231561U);

/* child S-Function registration */
ssSetNumSFunctions(rtS, 1);

/* register each child */
{
  static SimStruct childSFunctions[1];
```

```
static SimStruct *childSFunctionPtrs[1];
(void) memset((void *)&childSFunctions[0], 0,
            sizeof(childSFunctions));
ssSetSFunctions(rtS, &childSFunctionPtrs[0]);
ssSetSFunction(rtS, 0, &childSFunctions[0]);

/* RTW Generated Level2 S-Function Block: Regenerator/<S1>/Regenerator (Regenerator1_sf) */
{
 SimStruct *rts = ssGetSFunction(rtS, 0);

 /* timing info */
 static time_T sfcnPeriod[2];
 static time_T sfcnOffset[2];
 static int_T sfcnTsMap[2];
 (void) memset((void*)sfcnPeriod, 0,
              sizeof(time_T)*2);
 (void) memset((void*)sfcnOffset, 0,
              sizeof(time_T)*2);
 ssSetSampleTimePtr(rts, &sfcnPeriod[0]);
 ssSetOffsetTimePtr(rts, &sfcnOffset[0]);
 ssSetSampleTimeTaskIDPtr(rts, sfcnTsMap);

 /* Set up the mdlInfo pointer */
 ssSetMdlInfoPtr(rts, ssGetMdlInfoPtr(rtS));

 /* Allocate memory of model methods 2 */
 {
  static struct _ssSFcnModelMethods2 methods2;
  ssSetModelMethods2(rts, &methods2);
 }

 /* Allocate memory of model methods 3 */
 {
  static struct _ssSFcnModelMethods3 methods3;
  ssSetModelMethods3(rts, &methods3);
 }

 /* Allocate memory for states auxilliary information */
 {
  static struct _ssStatesInfo2 statesInfo2;
  ssSetStatesInfo2(rts, &statesInfo2);
 }
```

```
/* inputs */
{
 static struct _ssPortInputs inputPortInfo[19];
 _ssSetNumInputPorts(rts, 19);
 ssSetPortInfoForInputs(rts, &inputPortInfo[0]);

 /* port 0 */
 {
  static real_T const *sfcnUPtrs[1];
  sfcnUPtrs[0] = (real_T*)&Regenerator_RGND;
  ssSetInputPortSignalPtrs(rts, 0, (InputPtrsType)&sfcnUPtrs[0]);
  _ssSetInputPortNumDimensions(rts, 0, 1);
  ssSetInputPortWidth(rts, 0, 1);
 }

 /* port 1 */
 {
  static real_T const *sfcnUPtrs[1];
  sfcnUPtrs[0] = (real_T*)&Regenerator_RGND;
  ssSetInputPortSignalPtrs(rts, 1, (InputPtrsType)&sfcnUPtrs[0]);
  _ssSetInputPortNumDimensions(rts, 1, 1);
  ssSetInputPortWidth(rts, 1, 1);
 }

 /* port 2 */
 {
  static real_T const *sfcnUPtrs[1];
  sfcnUPtrs[0] = (real_T*)&Regenerator_RGND;
  ssSetInputPortSignalPtrs(rts, 2, (InputPtrsType)&sfcnUPtrs[0]);
  _ssSetInputPortNumDimensions(rts, 2, 1);
  ssSetInputPortWidth(rts, 2, 1);
 }

 /* port 3 */
 {
  static real_T const *sfcnUPtrs[1];
  sfcnUPtrs[0] = (real_T*)&Regenerator_RGND;
  ssSetInputPortSignalPtrs(rts, 3, (InputPtrsType)&sfcnUPtrs[0]);
  _ssSetInputPortNumDimensions(rts, 3, 1);
  ssSetInputPortWidth(rts, 3, 1);
 }
```

```
/* port 4 */
{
  static real_T const *sfcnUPtrs[1];
  sfcnUPtrs[0] = (real_T*)&Regenerator_RGND;
  ssSetInputPortSignalPtrs(rts, 4, (InputPtrsType)&sfcnUPtrs[0]);
  _ssSetInputPortNumDimensions(rts, 4, 1);
  ssSetInputPortWidth(rts, 4, 1);
}

/* port 5 */
{
  static real_T const *sfcnUPtrs[1];
  sfcnUPtrs[0] = (real_T*)&Regenerator_RGND;
  ssSetInputPortSignalPtrs(rts, 5, (InputPtrsType)&sfcnUPtrs[0]);
  _ssSetInputPortNumDimensions(rts, 5, 1);
  ssSetInputPortWidth(rts, 5, 1);
}

/* port 6 */
{
  static real_T const *sfcnUPtrs[1];
  sfcnUPtrs[0] = (real_T*)&Regenerator_RGND;
  ssSetInputPortSignalPtrs(rts, 6, (InputPtrsType)&sfcnUPtrs[0]);
  _ssSetInputPortNumDimensions(rts, 6, 1);
  ssSetInputPortWidth(rts, 6, 1);
}

/* port 7 */
{
  static real_T const *sfcnUPtrs[1];
  sfcnUPtrs[0] = (real_T*)&Regenerator_RGND;
  ssSetInputPortSignalPtrs(rts, 7, (InputPtrsType)&sfcnUPtrs[0]);
  _ssSetInputPortNumDimensions(rts, 7, 1);
  ssSetInputPortWidth(rts, 7, 1);
}

/* port 8 */
{
  static real_T const *sfcnUPtrs[1];
  sfcnUPtrs[0] = (real_T*)&Regenerator_RGND;
  ssSetInputPortSignalPtrs(rts, 8, (InputPtrsType)&sfcnUPtrs[0]);
```

```
  _ssSetInputPortNumDimensions(rts, 8, 1);
  ssSetInputPortWidth(rts, 8, 1);
}

/* port 9 */
{
  static real_T const *sfcnUPtrs[1];
  sfcnUPtrs[0] = (real_T*)&Regenerator_RGND;
  ssSetInputPortSignalPtrs(rts, 9, (InputPtrsType)&sfcnUPtrs[0]);
  _ssSetInputPortNumDimensions(rts, 9, 1);
  ssSetInputPortWidth(rts, 9, 1);
}

/* port 10 */
{
  static real_T const *sfcnUPtrs[1];
  sfcnUPtrs[0] = (real_T*)&Regenerator_RGND;
  ssSetInputPortSignalPtrs(rts, 10, (InputPtrsType)&sfcnUPtrs[0]);
  _ssSetInputPortNumDimensions(rts, 10, 1);
  ssSetInputPortWidth(rts, 10, 1);
}

/* port 11 */
{
  static real_T const *sfcnUPtrs[1];
  sfcnUPtrs[0] = (real_T*)&Regenerator_RGND;
  ssSetInputPortSignalPtrs(rts, 11, (InputPtrsType)&sfcnUPtrs[0]);
  _ssSetInputPortNumDimensions(rts, 11, 1);
  ssSetInputPortWidth(rts, 11, 1);
}

/* port 12 */
{
  static real_T const *sfcnUPtrs[1];
  sfcnUPtrs[0] = (real_T*)&Regenerator_RGND;
  ssSetInputPortSignalPtrs(rts, 12, (InputPtrsType)&sfcnUPtrs[0]);
  _ssSetInputPortNumDimensions(rts, 12, 1);
  ssSetInputPortWidth(rts, 12, 1);
}

/* port 13 */
{
```

```
  static real_T const *sfcnUPtrs[1];
  sfcnUPtrs[0] = (real_T*)&Regenerator_RGND;
  ssSetInputPortSignalPtrs(rts, 13, (InputPtrsType)&sfcnUPtrs[0]);
  _ssSetInputPortNumDimensions(rts, 13, 1);
  ssSetInputPortWidth(rts, 13, 1);
}

/* port 14 */
{
  static real_T const *sfcnUPtrs[1];
  sfcnUPtrs[0] = (real_T*)&Regenerator_RGND;
  ssSetInputPortSignalPtrs(rts, 14, (InputPtrsType)&sfcnUPtrs[0]);
  _ssSetInputPortNumDimensions(rts, 14, 1);
  ssSetInputPortWidth(rts, 14, 1);
}

/* port 15 */
{
  static real_T const *sfcnUPtrs[1];
  sfcnUPtrs[0] = (real_T*)&Regenerator_RGND;
  ssSetInputPortSignalPtrs(rts, 15, (InputPtrsType)&sfcnUPtrs[0]);
  _ssSetInputPortNumDimensions(rts, 15, 1);
  ssSetInputPortWidth(rts, 15, 1);
}

/* port 16 */
{
  static real_T const *sfcnUPtrs[1];
  sfcnUPtrs[0] = (real_T*)&Regenerator_RGND;
  ssSetInputPortSignalPtrs(rts, 16, (InputPtrsType)&sfcnUPtrs[0]);
  _ssSetInputPortNumDimensions(rts, 16, 1);
  ssSetInputPortWidth(rts, 16, 1);
}

/* port 17 */
{
  static real_T const *sfcnUPtrs[1];
  sfcnUPtrs[0] = (real_T*)&Regenerator_RGND;
  ssSetInputPortSignalPtrs(rts, 17, (InputPtrsType)&sfcnUPtrs[0]);
  _ssSetInputPortNumDimensions(rts, 17, 1);
  ssSetInputPortWidth(rts, 17, 1);
}
```

```
  /* port 18 */
  {
    static real_T const *sfcnUPtrs[1];
    sfcnUPtrs[0] = (real_T*)&Regenerator_RGND;
    ssSetInputPortSignalPtrs(rts, 18, (InputPtrsType)&sfcnUPtrs[0]);
    _ssSetInputPortNumDimensions(rts, 18, 1);
    ssSetInputPortWidth(rts, 18, 1);
  }
 }

 /* outputs */
 {
  static struct _ssPortOutputs outputPortInfo[8];
  ssSetPortInfoForOutputs(rts, &outputPortInfo[0]);
  _ssSetNumOutputPorts(rts, 8);

  /* port 0 */
  {
    _ssSetOutputPortNumDimensions(rts, 0, 1);
    ssSetOutputPortWidth(rts, 0, 1);
    ssSetOutputPortSignal(rts, 0, ((real_T *) &rtB.Regenerator_o1));
  }

  /* port 1 */
  {
    _ssSetOutputPortNumDimensions(rts, 1, 1);
    ssSetOutputPortWidth(rts, 1, 1);
    ssSetOutputPortSignal(rts, 1, ((real_T *) &rtB.Regenerator_o2));
  }

  /* port 2 */
  {
    _ssSetOutputPortNumDimensions(rts, 2, 1);
    ssSetOutputPortWidth(rts, 2, 1);
    ssSetOutputPortSignal(rts, 2, ((real_T *) &rtB.Regenerator_o3));
  }

  /* port 3 */
  {
    _ssSetOutputPortNumDimensions(rts, 3, 1);
    ssSetOutputPortWidth(rts, 3, 1);
```

```
  ssSetOutputPortSignal(rts, 3, ((real_T *) &rtB.Regenerator_o4));
 }

 /* port 4 */
 {
  _ssSetOutputPortNumDimensions(rts, 4, 1);
  ssSetOutputPortWidth(rts, 4, 1);
  ssSetOutputPortSignal(rts, 4, ((real_T *) &rtB.Regenerator_o5));
 }

 /* port 5 */
 {
  _ssSetOutputPortNumDimensions(rts, 5, 1);
  ssSetOutputPortWidth(rts, 5, 1);
  ssSetOutputPortSignal(rts, 5, ((real_T *) &rtB.Regenerator_o6));
 }

 /* port 6 */
 {
  _ssSetOutputPortNumDimensions(rts, 6, 1);
  ssSetOutputPortWidth(rts, 6, 1);
  ssSetOutputPortSignal(rts, 6, ((real_T *) &rtB.Regenerator_o7));
 }

 /* port 7 */
 {
  _ssSetOutputPortNumDimensions(rts, 7, 1);
  ssSetOutputPortWidth(rts, 7, 1);
  ssSetOutputPortSignal(rts, 7, ((real_T *) &rtB.Regenerator_o8));
 }
}

/* path info */
ssSetModelName(rts, "Regenerator");
ssSetPath(rts, "Regenerator/Regenerator1/Regenerator");
if (ssGetRTModel(rtS) == (NULL)) {
 ssSetParentSS(rts, rtS);
 ssSetRootSS(rts, ssGetRootSS(rtS));
} else {
 ssSetRTModel(rts,ssGetRTModel(rtS));
 ssSetParentSS(rts, (NULL));
 ssSetRootSS(rts, rts);
```

```
}

ssSetVersion(rts, SIMSTRUCT_VERSION_LEVEL2);

/* work vectors */
{
  static struct _ssDWorkRecord dWorkRecord[3];
  static struct _ssDWorkAuxRecord dWorkAuxRecord[3];
  ssSetSFcnDWork(rts, dWorkRecord);
  ssSetSFcnDWorkAux(rts, dWorkAuxRecord);
  _ssSetNumDWork(rts, 3);

  /* DWORK0 */
  ssSetDWorkWidth(rts, 0, 1);
  ssSetDWorkDataType(rts, 0,SS_INT8);
  ssSetDWorkComplexSignal(rts, 0, 0);
  ssSetDWork(rts, 0, &rtDWork.Regenerator_DWORK0);

  /* DWORK1 */
  ssSetDWorkWidth(rts, 1, 1);
  ssSetDWorkDataType(rts, 1,SS_INT8);
  ssSetDWorkComplexSignal(rts, 1, 0);
  ssSetDWork(rts, 1, &rtDWork.Regenerator_DWORK1);

  /* DWORK2 */
  ssSetDWorkWidth(rts, 2, 1);
  ssSetDWorkDataType(rts, 2,SS_DOUBLE);
  ssSetDWorkComplexSignal(rts, 2, 0);
  ssSetDWork(rts, 2, &rtDWork.Regenerator_DWORK2);
}

/* registration */
Regenerator1_sf(rts);
sfcnInitializeSizes(rts);
sfcnInitializeSampleTimes(rts);

/* adjust sample time */
ssSetSampleTime(rts, 0, 0.0);
ssSetOffsetTime(rts, 0, 1.0);
ssSetSampleTime(rts, 1, 60.0);
ssSetOffsetTime(rts, 1, 0.0);
sfcnTsMap[0] = 0;
```

```
sfcnTsMap[1] = 1;

/* set compiled values of dynamic vector attributes */
ssSetNumNonsampledZCs(rts, 0);

/* Update connectivity flags for each port */
_ssSetInputPortConnected(rts, 0, 0);
_ssSetInputPortConnected(rts, 1, 0);
_ssSetInputPortConnected(rts, 2, 0);
_ssSetInputPortConnected(rts, 3, 0);
_ssSetInputPortConnected(rts, 4, 0);
_ssSetInputPortConnected(rts, 5, 0);
_ssSetInputPortConnected(rts, 6, 0);
_ssSetInputPortConnected(rts, 7, 0);
_ssSetInputPortConnected(rts, 8, 0);
_ssSetInputPortConnected(rts, 9, 0);
_ssSetInputPortConnected(rts, 10, 0);
_ssSetInputPortConnected(rts, 11, 0);
_ssSetInputPortConnected(rts, 12, 0);
_ssSetInputPortConnected(rts, 13, 0);
_ssSetInputPortConnected(rts, 14, 0);
_ssSetInputPortConnected(rts, 15, 0);
_ssSetInputPortConnected(rts, 16, 0);
_ssSetInputPortConnected(rts, 17, 0);
_ssSetInputPortConnected(rts, 18, 0);
_ssSetOutputPortConnected(rts, 0, 0);
_ssSetOutputPortConnected(rts, 1, 0);
_ssSetOutputPortConnected(rts, 2, 0);
_ssSetOutputPortConnected(rts, 3, 0);
_ssSetOutputPortConnected(rts, 4, 0);
_ssSetOutputPortConnected(rts, 5, 0);
_ssSetOutputPortConnected(rts, 6, 0);
_ssSetOutputPortConnected(rts, 7, 0);
_ssSetOutputPortBeingMerged(rts, 0, 0);
_ssSetOutputPortBeingMerged(rts, 1, 0);
_ssSetOutputPortBeingMerged(rts, 2, 0);
_ssSetOutputPortBeingMerged(rts, 3, 0);
_ssSetOutputPortBeingMerged(rts, 4, 0);
_ssSetOutputPortBeingMerged(rts, 5, 0);
_ssSetOutputPortBeingMerged(rts, 6, 0);
_ssSetOutputPortBeingMerged(rts, 7, 0);
```

```
    /* Update the BufferDstPort flags for each input port */
    ssSetInputPortBufferDstPort(rts, 0, -1);
    ssSetInputPortBufferDstPort(rts, 1, -1);
    ssSetInputPortBufferDstPort(rts, 2, -1);
    ssSetInputPortBufferDstPort(rts, 3, -1);
    ssSetInputPortBufferDstPort(rts, 4, -1);
    ssSetInputPortBufferDstPort(rts, 5, -1);
    ssSetInputPortBufferDstPort(rts, 6, -1);
    ssSetInputPortBufferDstPort(rts, 7, -1);
    ssSetInputPortBufferDstPort(rts, 8, -1);
    ssSetInputPortBufferDstPort(rts, 9, -1);
    ssSetInputPortBufferDstPort(rts, 10, -1);
    ssSetInputPortBufferDstPort(rts, 11, -1);
    ssSetInputPortBufferDstPort(rts, 12, -1);
    ssSetInputPortBufferDstPort(rts, 13, -1);
    ssSetInputPortBufferDstPort(rts, 14, -1);
    ssSetInputPortBufferDstPort(rts, 15, -1);
    ssSetInputPortBufferDstPort(rts, 16, -1);
    ssSetInputPortBufferDstPort(rts, 17, -1);
    ssSetInputPortBufferDstPort(rts, 18, -1);

    /* Instance data for generated S-Function: Regenerator1 */
#include "Regenerator1_sfcn_rtw/Regenerator1_sid.h"

   }
  }

  return rtS;
}
```